Discrete Dynamics in Nature and Society

Recent Trends in Modelling, Bifurcation Analysis, and Control of Chaotic Systems in Bioeconomics

Lead Guest Editor: Qamar Din
Guest Editors: Hamdy N. Agiza, Abdelalim A. Elsadany, and Amr Elsonbaty

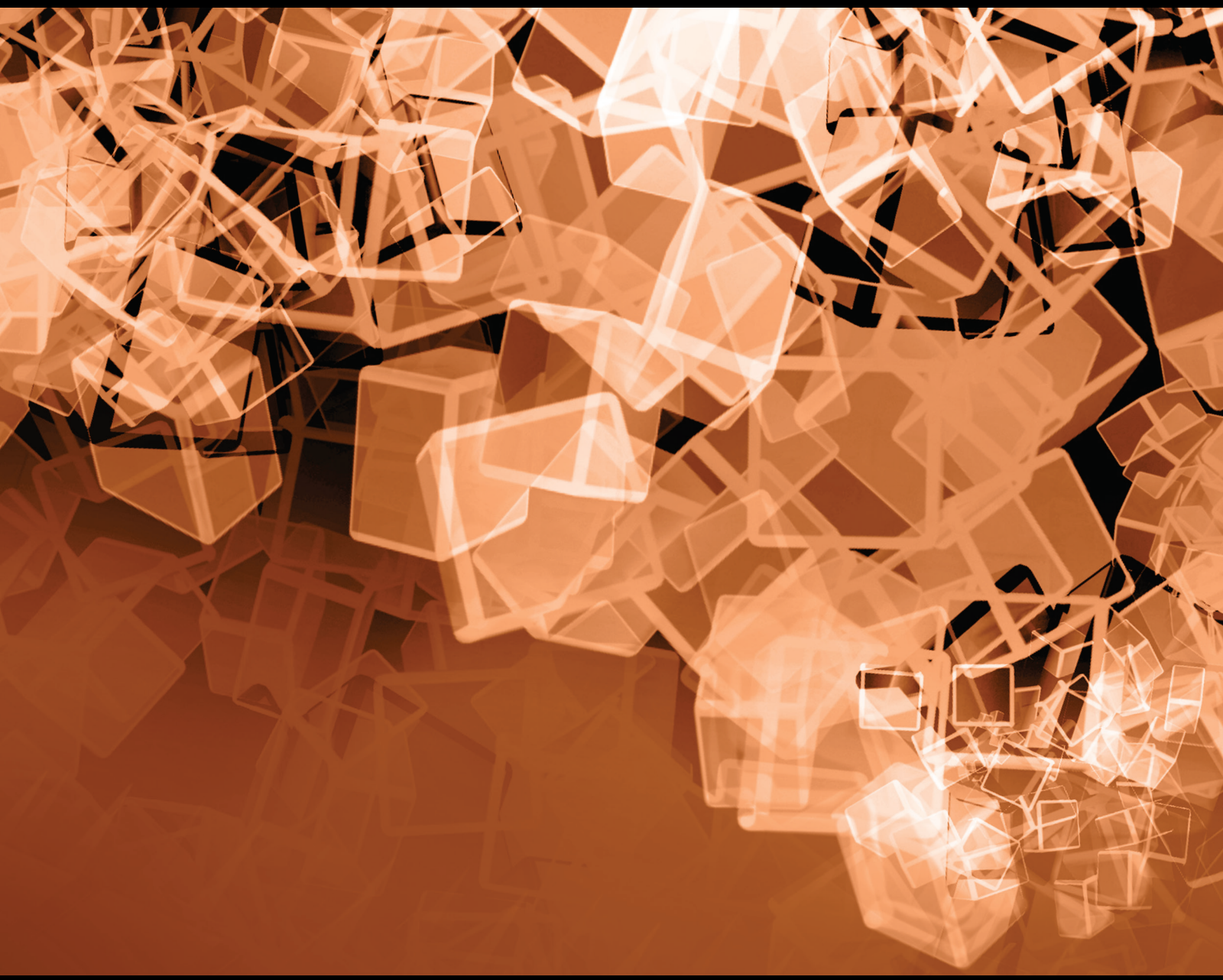

Recent Trends in Modelling, Bifurcation Analysis, and Control of Chaotic Systems in Bioeconomics

Discrete Dynamics in Nature and Society

Recent Trends in Modelling, Bifurcation Analysis, and Control of Chaotic Systems in Bioeconomics

Lead Guest Editor: Qamar Din
Guest Editors: Hamdy N. Agiza, Abdelalim A. Elsadany, and Amr Elsonbaty

Contents

Hindawi
Discrete Dynamics in Nature and Society
Volume 2021, Article ID 6679161, 22 pages
https://doi.org/10.1155/2021/6679161

Research Article

Stability and Bifurcation Analysis of a Discrete Singular Bioeconomic System

Qamar Din,[1] **A. M. Yousef**,[2] **and A. A. Elsadany**[3,4]

[1]*Department of Mathematics, University of Poonch Rawalakot, Rawalakot 12350, Pakistan*
[2]*Mathematics Department, Faculty of Science, South Valley University, Qena, Egypt*
[3]*Mathematics Department, College of Science and Humanities Studies in Al-Kharj, Prince Sattam Bin Abdulaziz University, Al-Kharj 11942, Saudi Arabia*
[4]*Department of Basic Science, Faculty of Computers and Informatics, Suez Canal University, Ismailia 41522, Egypt*

Correspondence should be addressed to Qamar Din; qamar.sms@gmail.com

Received 23 December 2020; Accepted 5 July 2021; Published 13 July 2021

Academic Editor: Douglas Anderson

The main concern of this paper is to discuss stability and bifurcation analysis for a class of discrete predator-prey interaction with Holling type II functional response and harvesting effort. Firstly, we establish a discrete singular bioeconomic system, which is based on the discretization of a system of differential algebraic equations. It is shown that the discretized system exhibits much richer dynamical behaviors than its corresponding continuous counterpart. Our investigation reveals that, in the discretized system, two types of bifurcations (i.e., period-doubling and Neimark–Sacker bifurcations) can be studied; however, the dynamics of the continuous model includes only Hopf bifurcation. Moreover, the state delayed feedback control method is implemented for controlling the chaotic behavior of the bioeconomic model. Numerical simulations are presented to illustrate the theoretical analysis. The maximal Lyapunov exponents (MLE) are computed numerically to ensure further dynamical behaviors and complexity of the model.

1. Introduction

Bioeconomics is linked closely to the early development of ideas in fisheries economics due to the pioneering work of Canadian economists Gordon [1] and Anthony Scott (in 1955). Their basic theories used recent developments in modeling of biological fisheries, initially the contributions made by Schaefer in 1954 and 1957 on introducing a systematic connection between fishing mechanism and growth of biological type through the implementation of mathematical modeling verified by experimental studies, and also associated itself to resource protection, ecology, and the environment [2]. These concepts were developed from the multifishing science environment in Canada at that time. Modeling and fishing science developed rapidly during an innovative and productive period, especially among Canadian fishing researchers of various disciplines. Fishing mortality and population modeling were launched for economists, and novel interdisciplinary methods of modeling became obtainable for the economists, which made it feasible to measure the economical and biological impacts of various fisheries management decisions and fishing activities. Modern bioeconomics related to fisheries science can furnish perception into developing methods to deal with the overexploitation and complexities of overcapacity in marine fisheries where most are affected by lack of solid governance, changing coastal ecosystem dynamics, and natural fluctuations [3].

Moreover, Gordon in [1] suggested economic theory keeping in view the common property of resource, which was based on the effect of the harvest effort on an ecosystem by taking into account an economic perspective, assuming that $x(t)$ and $e(t)$ denote the density of harvested population and the harvest effort in an ecosystem, respectively; then the total cost is equal to $ce(t)$, and the total revenue is equal to $pe(t)x(t)$, where c denotes the cost of harvest effort, and p is

used for the unit price of harvested population. Then, the economic interest μ for the harvest effort by the harvested population is given by

$$\mu = e(t)(px(t) - c). \tag{1}$$

Taking into account Gordon [1] theory, Zhang et al. [4] studied a class of bioeconomic system with implementation of theory for singular systems. Their study was consisted of bifurcation analysis and chaos control for the proposed bioeconomic model. Later on, Liu et al. [5] reported stability, bifurcation analysis, and state feedback control for a class of predator-prey interaction with harvest effort on predator and stage structure for prey. Chakraborty et al. [6] studied a bioeconomic system with implementation of theory of differential algebraic equations. They investigated stability, Hopf bifurcation, and state feedback control for a class of predator-prey interaction with time-delayed effect. Zhang et al. [7] investigated a singular bioeconomic model for prey-predator interaction with diffusion and time delay. Zhang et al. [8] carried out comprehensive study related to theory, applications, complexity, and control of singular bioeconomic systems. Zhang et al. [9] explored the Hopf bifurcation for a predator-prey type bioeconomic system with two delays and predator harvesting. Meng and Zhang [10] discussed the qualitative behavior of a delayed singular bioeconomic predator-prey model without and with stochastic fluctuation. Liu et al. [11] analyzed the local dynamics and Hopf bifurcation for a biological economic model with Holling type II functional response and harvesting effort on prey. Liu et al. [12] proposed a singular fishery model for a class of prey-predator interaction with gestation delay for predator and maturation delay for prey. Liu et al. [13] formulated and discussed a singular predator-prey model by implementing commercial harvesting on predator with gestation delay for predator and maturation delay for prey. In [14], Li et al. studied a singular bioeconomic predator-prey system with Holling type II functional response and nonlinear harvesting on prey. Meng and Wu [15] discussed a singular prey-predator system with two delays, nonlinear predator harvesting and Beddington–DeAngelis functional response. Babaei and Shafiee [16] reported stability analysis, bifurcation, chaotic behavior, and control for a singular bioeconomic model of prey-predator interaction governed by an algebraic equation and 3-dimensional differential equations.

In case of mathematical modeling of predator-prey interaction, the research concerning interspecific interactions has been numerously based on continuous predator-prey systems of two variables. On the other hand, particular species, covering several classes of insects and seasonal plants, have nonoverlapping generations successively, and consequently, their population undergoes in discrete time steps. Populations with nonoverlapping generations can be modeled suitably with difference equations, otherwise known as iterative maps or discrete dynamical systems. Several authors have shown that nonoverlapping generations governed by iterative maps reveal complex and chaotic behavior, and the dynamics in such cases may yield a much richer set of patterns than those examined in continuous-time systems (cf. [17–24]). Furthermore, discrete-time models also have been used for rich dynamics of bioeconomic systems for some classes of predator-prey interaction. For example, in [25], the authors analyzed complex dynamics of a discrete-time bioeconomic system for predator-prey interaction with the implementation of Euler approximations. Wu and Chen [26] implemented the Poincaré scheme for discretization of a singular bioeconomic model and they analyzed period-doubling bifurcation, Neimark–Sacker bifurcation, and stability behavior. Liu et al. [27] studied the chaotic behavior of a discrete singular system related to the bioeconomic model of the prey-predator type.

Taking into account predator interaction with logistic growth and Holling type II functional response for prey population, we have the following system [28]:

$$\begin{cases} \dfrac{dx}{dt} = x\left(d - kx - \dfrac{y}{a+x}\right), \\ \dfrac{dy}{dt} = y\left(\dfrac{bx}{a+x} - r\right), \end{cases} \tag{2}$$

where $x = x(t)$ and $y = y(t)$ denote state variables for the densities of prey and predator at time t, respectively. Moreover, d is the intrinsic growth rate of prey, r represents the natural death rate of the predator, a is used for half capturing saturation constant, and b represents the maximal growth rate of the predator. Furthermore, d/k denotes the environmental carrying capacity for the prey population.

Keeping in view (1) and (2), we obtain the following predator-prey biological economic model with Holling type II functional response with harvest effort:

$$\begin{cases} \dfrac{dx}{dt} = x\left(d - kx - \dfrac{y}{a+x} - e\right), \\ \dfrac{dy}{dt} = y\left(\dfrac{bx}{a+x} - r\right), \\ \mu = e(px - c). \end{cases} \tag{3}$$

Applying the forward Euler scheme to system (3), we obtain the discrete-time predator-prey biological economic model with Holling type II functional response as follows:

$$\begin{cases} x_{n+1} = x_n + hx_n\left(d - kx_n - \dfrac{y_n}{a+x_n} - e_n\right), \\ y_{n+1} = y_n + hy_n\left(\dfrac{bx_n}{a+x_n} - r\right), \\ \mu = e_n(px_n - c), \end{cases} \tag{4}$$

where h is the integral step size for the Euler approximation. In this paper, we discuss some dynamical aspects of the discrete singular model (4). For this, the first existence of

interior (positive) fixed point and local dynamics of system (4) about biologically feasible equilibrium are carried out. Secondly, it is proved that system (4) undergoes period-doubling bifurcation and Neimark–Sacker bifurcation by varying the economic profit μ as the bifurcation parameter. Thirdly, a state delayed feedback control strategy is applied to avoid bifurcating and chaotic behavior of bioeconomic model (4). At the end, numerical examples are presented for verification and illustration of our theoretical discussion.

2. Fixed Points and Stability Analysis

In order to study the qualitative behavior of the solutions of the nonlinear model (4), we study the existence of fixed points and their stability properties. From system (4), we can see that there exists a fixed point $X_0 := (x_0, y_0, e_0)$ in R_3^+ if and only if X_0 is a solution of the following equations:

$$\begin{cases} x = x + hx\left(d - kx - \dfrac{y}{a+x} - e\right), \\ y = y + hy\left(-r + \dfrac{bx}{a+x}\right), \\ \mu = e(px - c). \end{cases} \tag{5}$$

Through a simple calculation, we obtain

$$X_0 = (x_0, y_0, e_0) = \left(\frac{ar}{(b-r)}, (a+x_0)(d - kx_0 - e_0), \frac{\mu}{(px_0 - c)}\right). \tag{6}$$

For biological considerations, we focus on the dynamics of the positive fixed point of the system (4). Thus, throughout the paper, we assume the conditions for the existence of a unique positive fixed point of system (4) as follows:

$$\begin{aligned} &b > r, \\ &bc < r(ap + c), \\ &\frac{bd - r(ak + d)}{(b-r)^2} - \frac{\mu}{r(ap + c) - bc} > 0. \end{aligned} \tag{7}$$

In μk-plane, the existence of a unique positive fixed point of system (4) is depicted in Figure 1.

The generalized Jacobian matrix $J(x_0, y_0, e_0)$ of system (4) about interior (positive) fixed point (x_0, y_0, e_0) is computed as follows:

$$J(x_0, y_0, e_0) = \begin{pmatrix} 1 - hkx_0 + \dfrac{hx_0y_0}{(a+x_0)^2} & -\dfrac{hx_0}{a+x_0} & -hx_0 \\ \dfrac{abhy_0}{(a+x_0)^2} & 1 & 0 \\ e_0p & 0 & px_0 - c \end{pmatrix}. \tag{8}$$

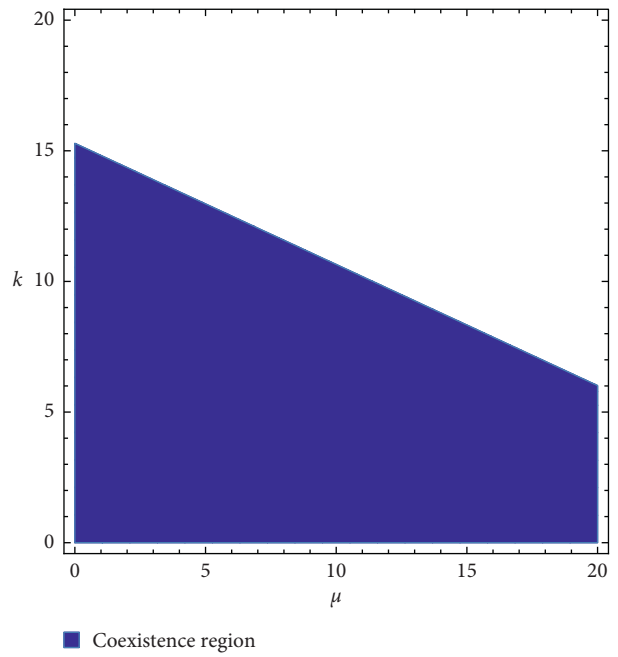

Figure 1: Coexistence region for system (4) with $a = 6.76$, $b = 9.4$, $c = 1.58$, $r = 0.74$, $p = 9.2$, and $d = 8.83$.

Then, it is easy to see that the generalized characteristic equation of the Jacobian matrix $J(x_0, y_0, e_0)$ can be written as

$$\det\begin{pmatrix} 1 - hkx_0 + \dfrac{hx_0y_0}{(a+x_0)^2} - \lambda & -\dfrac{hx_0}{a+x_0} & -hx_0 \\ \dfrac{abhy_0}{(a+x_0)^2} & 1 - \lambda & 0 \\ e_0p & 0 & px_0 - c \end{pmatrix} = 0, \tag{9}$$

which on simplification yields

$$\lambda^2 + P\lambda + Q = 0, \tag{10}$$

where

$$\begin{aligned} P &= hkx_0 - \frac{hx_0y_0}{(a+x_0)^2} - \frac{he_0px_0}{px_0 - c} - 2 \\ &= \frac{1}{((arp/(b-r)) - c)^2}\left[R_1\mu - (S_1 + 2)\left(\frac{arp}{b-r} - c\right)^2\right] = H - Q - 1, \\ Q &= 1 - hkx_0 + \frac{hx_0y_0}{(a+x_0)^2} + \frac{he_0px_0}{px_0 - c} + \frac{abh^2x_0y_0}{(a+x_0)^3} \\ &= \frac{1}{((arp/(b-r)) - c)^2}\left[R_2\mu - (S_2 - 1)\left(\frac{arp}{b-r} - c\right)^2\right], \end{aligned} \tag{11}$$

where

$$H = \frac{abx_0y_0}{(a+x_0)^3} > 0,$$

$$R_1 = -\frac{hr}{b}(ap+c),$$

$$S_1 = -\frac{hr}{b}\left(d - \frac{ak(b+r)}{b-r}\right), \tag{12}$$

$$R_2 = \frac{hr}{b}[(ap+c)(1-hr)+hcb],$$

$$S_2 = \frac{hr}{b}\left[d - \frac{ak(b+r)}{b-r} + h\,d(b-r) - hark\right].$$

Let $F(\lambda) = \lambda^2 + P\lambda + Q$, then

$$F(1) = 1 + P + Q = H > 0,$$

$$F(-1) = 1 - P + Q = \frac{2}{((arp/(b-r))-c)^2} \tag{13}$$

$$\left[R_3\mu - (S_3-2)\left(\frac{arp}{b-r} - c\right)^2\right],$$

where

$$R_3 = \frac{hr}{b}\left[(ap+c)\left(1 - \frac{hr}{2}\right) + \frac{hcb}{2}\right],$$

$$S_3 = \frac{hr}{b}\left[d - \frac{ak(b+r)}{b-r} + \frac{h\,d(b-r)}{2} - \frac{hark}{2}\right]. \tag{14}$$

In order to discuss the stability of the fixed point of (x_0, y_0, e_0), we need the following lemma.

Lemma 1 (see [23]). *Consider $S(\zeta) = \zeta^2 + P\zeta + Q$. Moreover, assuming that $S(1) > 0$ and ζ_1 and ζ_2 are two roots of $S(\zeta) = 0$, then the following hold true:*

(i) $|\zeta_1| < 1$ *and* $|\zeta_2| < 1$ *if and only if* $S(-1) > 0$, *and* $S(0) = Q < 1$

(ii) $|\zeta_1| < 1$ *and* $|\zeta_2| > 1$ *(or* $|\zeta_1| > 1$ *and* $|\zeta_2| < 1$*) if and only if* $S(-1) < 0$

(iii) $|\zeta_1| > 1$ *and* $|\zeta_2| > 1$ *if and only if* $S(-1) > 0$ *and* $S(0) > 1$

(iv) $\zeta_1 = -1$ *and* $|\zeta_2| \neq 1$ *if and only if* $S(-1) = 0$ *and* $P \neq 0, 2$

(v) ζ_1 *and* ζ_2 *are complex and* $|\zeta_1| = 1$ *and* $|\zeta_2| = 1$ *if and only if* $P^2 - 4Q < 0$ *and* $Q = 1$

Assume that ζ_1 and ζ_2 are roots for the characteristic equation of the variational matrix $J(x_0, y_0, e_0)$ about interior (positive) fixed point (x_0, y_0, e_0) which are known as eigenvalues for the equilibrium point (x_0, y_0, e_0). Taking into account the topological types related to the fixed point (x_0, y_0, e_0) of system (4), we say that the fixed point (x_0, y_0, e_0) is a sink (asymptotically stable) if $|\zeta_1| < 1$ and $|\zeta_2| < 1$; (x_0, y_0, e_0) is called a source (repeller) if $|\zeta_1| > 1$ and $|\zeta_2| > 1$; (x_0, y_0, e_0) is called a saddle if $|\zeta_1| > 1$ and $|\zeta_2| < 1$ (or $|\zeta_1| < 1$ and $|\zeta_2| > 1$; and (x_0, y_0, e_0) is called nonhyperbolic if either $|\zeta_1| = 1$ or $|\zeta_2| = 1$, on the other hand, if $\zeta_1 = -1$ and $|\zeta_2| \neq 1$ are necessary conditions for the emergence of period-doubling bifurcation and $-2 < P < 2$ with $Q = 1$ are necessary conditions for the occurrence of Neimark–Sacker bifurcation. Moreover, if $S(1) = 1 + P + Q > 0$, then all cases of Lemma 1 are depicted in Figure 2 in PQ-plane.

Keeping in view Lemma 1, the following theorem is presented for local dynamics of system (4) about its positive fixed point.

Theorem 1. *Assume that $b > r$, $bc < r(ap+c)$, and $((bd - r(ak+d))/(b-r)^2) - (\mu/(r(ap+c) - bc)) > 0$; then, there exists unique interior (positive) fixed point (x_0, y_0, e_0) for system (4) satisfying the following conditions:*

(i) (x_0, y_0, e_0) *is a sink if and only if* $R_2\mu < S_2((arp/(b-r)) - c)^2$ *and* $R_3\mu > (S_3 - 2)((arp/(b-r)) - c)^2$

(ii) (x_0, y_0, e_0) *is a source if and only* $R_2\mu > S_2((arp/(b-r)) - c)^2$ *and* $R_3\mu > (S_3 - 2)((arp/(b-r)) - c)^2$

(iii) (x_0, y_0, e_0) *is a saddle if and only if* $R_3\mu < (S_3 - 2)((arp/(b-r)) - c)^2$

(iv) (x_0, y_0, e_0) *is nonhyperbolic if one of the following conditions hold true:*

(1) $R_3\mu = (S_3 - 2)((arp/(b-r)) - c)^2$, $R_1\mu \neq (S_1 + 2)((arp/(b-r)) - c)^2, (S_1 + 4)\ ((arp/(b-r)) - c)^2$

(2) $R_2\mu = S_2((arp/(b-r)) - c)^2$ *and* $H(\mu) < 4$

Next, for $a = 3.9$, $b = 14$, $c = 3.7$, $r = 3.4$, $p = 5.8$, $d = 21.1$, and $h = 0.25$, the dynamical classification of interior equilibrium of system (4) is depicted in μk-plane (see Figure 3).

Taking into account part (iv.1) of Theorem 1, it is easily to observe that the eigenvalues about the equilibrium point (x_0, y_0, e_0) are given by $\lambda_1 = -1$ and $\lambda_2 = 1 - P$ with $|\lambda_2| \neq -1$. On the other hand, if part (iv.2) of Theorem 1 holds true, then one can obtain that the eigenvalues for the equilibrium point (x_0, y_0, e_0) are conjugate complex numbers with modulus one.

Next, we consider the following set:

$$F_B = \begin{cases} 0 < \mu = \dfrac{1}{R_3}(S_3 - 2)\left(\dfrac{arp}{b-r} - c\right)^2 < \left(d - \dfrac{kar}{b-r}\right)\left(\dfrac{par}{b-r} - c\right) \\ (a, b, c, d, k, p, r, \mu, h): \\ R_1\mu \neq (S_1 + 2)\left(\dfrac{arp}{b-r} - c\right)^2, \\ (S_1 + 4)\left(\dfrac{arp}{b-r} - c\right)^2. \end{cases} \tag{15}$$

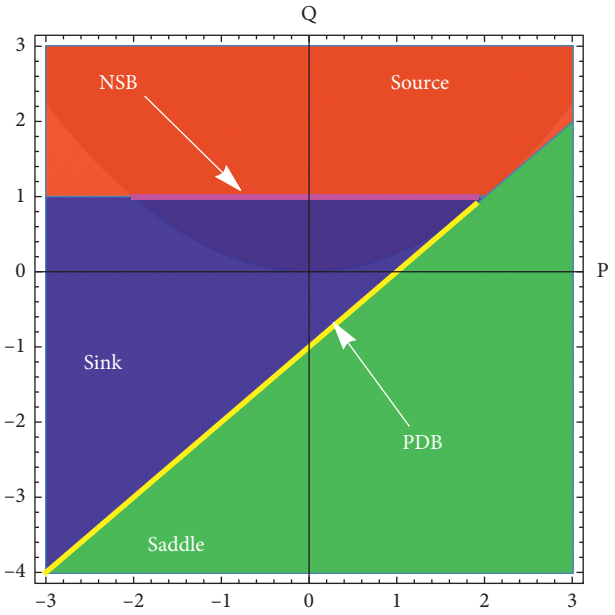

Figure 2: Dynamical classification of planar system with $S(1) > 0$.

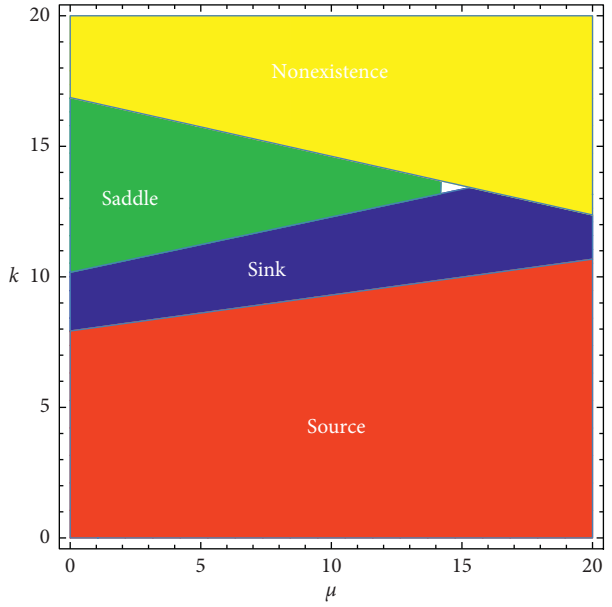

Figure 3: Dynamical classification of interior equilibrium of system (4) in μk-plane.

It is easy to see that the steady state (x_0, y_0, e_0) undergoes period-doubling (flip) bifurcation whenever parameters vary in a small neighborhood of F_B.

Next, we consider the following curve:

$$\left\{H_B = (a,b,c,d,k,p,r,\mu,h):\ 0 < \mu = \frac{S_2}{R_2}\left(\frac{arp}{b-r} - c\right)^2 < \left(d - \frac{kar}{b-r}\right)\left(\frac{par}{b-r} - c\right), H(\mu) < 4\right\}. \tag{16}$$

On the other hand, (x_0, y_0, e_0) undergoes the Neimark–Sacker (Hopf) bifurcation whenever parameters vary in a small neighborhood of H_B. In Section 3, we discuss the occurrence of period-doubling bifurcation around the

interior fixed point (x_0, y_0, e_0) with the variation of parameters in a small neighborhood of F_B, and the emergence of the Neimark–Sacker bifurcation about (x_0, y_0, e_0) with varying the parameters in a small neighborhood of H_B.

3. Bifurcation Analysis

Keeping in view the analysis of Section 3, we discuss the period-doubling bifurcation and Neimark–Sacker bifurcation about the positive fixed point (x_0, y_0, e_0) in this section. For this, choose parameter μ as bifurcation parameter for investigating the period-doubling bifurcation and Neimark–Sacker bifurcation about (x_0, y_0, e_0) by implementing the novel normal form theory of discrete singular systems, the center manifold theorem, and the bifurcation theory of discrete systems [29–35].

3.1. Period-Doubling Bifurcation. First, we start our investigation related to period-doubling bifurcation for system (4) about its equilibrium (x_0, y_0, e_0) with a variation of parameters in a small neighborhood of F_B. For this, we choose parameters $(a, b, c, d, k, p, r, \mu_1, h)$ arbitrarily from F_B, taking into account system (4) with $(a, b, c, d, k, p, r, \mu_1, h) \in F_B$. In this case, system (4) is described by the following 2-dimensional map:

$$\begin{cases} x \longrightarrow x + hx\left(d - kx - \dfrac{y}{a+x} - e\right), \\ y \longrightarrow y + hy\left(-r + \dfrac{bx}{a+x}\right), \\ \mu_1 = e(px - c). \end{cases} \tag{17}$$

It is easy to see that system (17) has a unique positive fixed point (x_0, y_0, e_0) such that the eigenvalues are given by $\lambda_1 = -1$ and $\lambda_2 = 1 - P$ with $|\lambda_2| \neq -1$. Assume that $(a, b, c, d, k, p, r, \mu_1, h) \in F_B$ with $\mu_1 = (1/R_1)(S_1 - 2)((arp/(b-r)) - c)^2$. Next, we take μ^* as a bifurcation parameter, considering a perturbation for system (17) as follows:

$$\begin{cases} x \longrightarrow x + hx\left(d - kx - \dfrac{y}{a+x} - e\right), \\ y \longrightarrow y + hy\left(-r + \dfrac{bx}{a+x}\right), \\ \mu_1 + \mu^* = e(px - c), \end{cases} \tag{18}$$

where $\mu^* \ll 1$ is taken as a small perturbation parameter.

Then, system (17) can be described in the following way:

$$\begin{cases} (x, y)^T \longrightarrow f(x, y, e), \\ g(x, y, e) = 0, \end{cases} \tag{19}$$

where

$$f(x, y, e) \coloneqq \left(f_1(x, y, e), f_2(x, y, e)\right)^T,$$

$$\begin{cases} f_1(x, y, e) = x + hx\left(d - kx - \dfrac{y}{a+x} - e\right), \\ f_2(x, y, e) = y + hy\left(-r + \dfrac{bx}{a+x}\right), \\ g(x, y, e) = e(px - c) - \mu_1. \end{cases} \tag{20}$$

Then, it is easy to see that $Dg(x_0, y_0, e) = (e_0 p, 0, px_0 - c)$ such that the rank of $Dg(x_0, y_0, e_0) = 1$. On the other hand, a local parameterization ψ for the 2-dimensional smooth manifold defined by $M_g = \{(x, y, e) \in R^3; g(x, y, e) = 0, \text{and rank } Dg(x, y, e) = 1\}$ about $(x, y, e) \in B(x_0, y_0, e_0) \subset M_g$ is given as follows: for any $(x, y, e) \in B(x_0, y_0, e_0)$, there is $Z \in A \subset R^2$ such that

$$\begin{aligned} X = \psi(Z) &= X_0 + U_0 Z + V_0 H(Z), \\ g(\psi(Z)) &= 0, \end{aligned} \tag{21}$$

where

$$\begin{aligned} U_0 &= \begin{pmatrix} 1 & 0 \\ 0 & 1 \\ 0 & 0 \end{pmatrix}, \\ V_0 &= \begin{pmatrix} 0 \\ 0 \\ 1 \end{pmatrix}, \end{aligned} \tag{22}$$

$X = (x, y, e)$, $X_0 = (x_0, y_0, e_0)$, $Z = (z_1, z_2)$, and $H: R^2 \longrightarrow R$ is a smooth mapping. For further details, the interested reader is referred to [36]. Taking into account the definition of ψ, we obtain the following:

$$D\psi(z) = \begin{pmatrix} D(g(X)) \\ U_0^T \end{pmatrix}^{-1} \begin{pmatrix} 0 & 0 \\ 1 & 0 \\ 0 & 1 \end{pmatrix}, \tag{23}$$

for arbitrarily chosen $(x, y, e) \in B(x_0, y_o, e_0)$. Then, system (19) is written as follows:

$$Z \longrightarrow f(Z), \quad Z \in A \subset R^2, \tag{24}$$

where $A = \psi^{-1} B(x_0, y_o, e_0)$.

Taking into account (24), we have

$$\begin{cases} z_1 \longrightarrow a_1 z_1 + a_2 z_2 + a_{13} z_1 \mu^* + a_{11} z_1^2 + a_{12} z_1 z_2 + a_{113} z_1^2 \mu^* \\ + a_{111} z_1^3 + a_{112} z_1^2 z_2 + O\left(\left(|z_1| + |z_2| + |\mu^*|\right)^4\right), \\ z_2 \longrightarrow b_1 z_1 + b_2 z_2 + b_{13} z_1 \mu^* + b_{11} z_1^2 + b_{12} z_1 z_2 + b_{113} z_1^2 \mu^* \\ + b_{111} z_1^3 + b_{112} z_1^2 z_2 + O\left(\left(|z_1| + |z_2| + |\mu^*|\right)^4\right). \end{cases} \tag{25}$$

In order to compute the coefficients related the normal form, we need some further computation. From the aforementioned computation, one can easily get

$$
\begin{aligned}
Df_1(X) &= \left(1 + h\left(d - 2kx - \frac{ay}{(a+x)^2} - e\right), -\frac{hx}{a+x}, -hx\right)\\
Df_2(X) &= \left(\frac{abhy}{(a+x)^2}, 1 + h\left(-r + \frac{bx}{a+x}\right), 0\right)\\
Dg(X) &= (ep, 0, px - c)\\
D\psi(z) &= \begin{pmatrix} Dg(X) \\ U_0^T \end{pmatrix}^{-1} \begin{pmatrix} 0 & 0 \\ 1 & 0 \\ 0 & 1 \end{pmatrix} = \begin{pmatrix} ep & 0 & px - c \\ 1 & 0 & 0 \\ 0 & 1 & 0 \end{pmatrix}^{-1} \begin{pmatrix} 0 & 0 \\ 1 & 0 \\ 0 & 1 \end{pmatrix}\\
&= \begin{pmatrix} 1 & 0 \\ 0 & 1 \\ -\dfrac{ep}{px - c} & 0 \end{pmatrix} = \left(D_{z_1}\psi(z), D_{z_2}\psi(z)\right),
\end{aligned}
\tag{26}
$$

and from this, it follows that

$$
\begin{aligned}
D_{z_1}\psi(z) &= \left(1, 0, -\frac{ep}{px - c}\right)^T,\\
D_{z_2}\psi(z) &= (0, 1, 0)^T.
\end{aligned}
\tag{27}
$$

Assume that $f_{iz_i}(\psi(Z))$ represents the derivative of $f_i(\psi(Z))$ with respect to z_i and taking $f_{iz_i}(X) = f_{iz_i}(\psi(Z))$. In a similar way, one can adopt notations for $f_{iz_iz_j}(\psi(Z))$ and $f_{iz_iz_jz_k}(\psi(Z))$. Next, it is easy to see that

$$
\begin{cases}
f_{1z_1}(X) = Df_1(X)D_{z_1}\psi(z) = 1 + h\left(d - 2kx - \dfrac{ay}{(a+x)^2} - e + \dfrac{epx}{px - c}\right),\\
f_{1z_2}(X) = Df_1(X)D_{z_2}\psi(z) = -\dfrac{hx}{a+x},\\
f_{2z_1}(X) = Df_2(X)D_{z_1}\psi(z) = \dfrac{abhy}{(a+x)^2},\\
f_{2z_2}(X) = Df_2(X)D_{z_2}\psi(z) = 1 + h\left(-r + \dfrac{bx}{a+x}\right).
\end{cases}
\tag{28}
$$

Putting X_0 into (28), one has the following:

$$\begin{cases} f_{1z_1}(X_0) = 1 + h\left(-kx_0 + \dfrac{e_0 p x_0}{p x_0 - c} + \dfrac{x_0(d - kx_0 - e_0)}{a + x_0}\right) = 1 + \dfrac{hr}{b}\left(d + \dfrac{ak(b+r)}{b-r}\right) \\ \quad + \dfrac{hr}{b}\dfrac{(b-r)^2(ap+c)}{(apr - cb + cr)^2}(\mu_1 + \mu^*), \\ f_{1z_2}(X_0) = -\dfrac{x_0}{a + x_0} = -\dfrac{hr}{b}, \\ f_{2z_1}(X_0) = \dfrac{abhy_0}{(a + x_0)^2} = \dfrac{abh(d - kx_0 - e_0)}{a + x_0} = h(b-r)\left(d - \dfrac{kar}{b-r} - \dfrac{(\mu_1 + \mu_*)(b-r)}{apr - cb + cr}\right), \\ f_{2z_2}(X_0) = 1 + h\left(-r + \dfrac{bx_0}{a + x_0}\right) = 1. \end{cases} \tag{29}$$

Then, from (28), it is easy to see that

$$\begin{cases} Df_{1z_1}(X) = \left(h\left(-2k + \dfrac{2ay}{(a+x)^3} - \dfrac{epc}{(px - c)^2}\right), -\dfrac{ah}{(a+x)^2}, h\left(-1 + \dfrac{px}{px - c}\right)\right), \\ Df_{1z_2}(X) = \left(-\dfrac{ah}{(a+x)^2}, 0, 0\right), \\ Df_{2z_1}(X) = \left(-\dfrac{2abhy}{(a+x)^3}, \dfrac{abh}{(a+x)^2}, 0\right), \\ Df_{2z_2}(X) = \left(\dfrac{abh}{(a+x)^2}, 0, 0\right). \end{cases} \tag{30}$$

Consequently, one has the following:

$$\begin{cases} f_{1z_1z_1}(X) = Df_{1z_1}(X)D_{z_1}\psi(z) = h\left[-2k + \dfrac{2ay}{(a+x)^3} - \dfrac{2epc}{(px - c)^2}\right], \\ f_{1z_1z_2}(X) = Df_{1z_1}(X)D_{z_2}\psi(z) = -\dfrac{ah}{(a+x)^2}, \\ f_{2z_1z_1}(X) = Df_{2z_1}(X)D_{z_1}\psi(z) = -\dfrac{2abhy}{(a+x)^3}, \\ f_{2z_1z_2}(X) = Df_{2z_1}(X)D_{z_2}\psi(z) = \dfrac{abh}{(a+x)^2}. \end{cases} \tag{31}$$

Putting the value of X_0 in (31), one has the following:

$$\begin{cases} f_{1z_1z_1}(X_0) = h\left[-2k + \dfrac{2a(d - kx_0 - e_0)}{(a + x_0)^2} - \dfrac{2e_0pc}{(px_0 - c)^2}\right] = h\left[-2k + \dfrac{2d(b-r)^2}{ab^2} - \dfrac{2kr(b-r)}{b^2}\right] \\ \quad -\dfrac{2(b-r)^3}{apr - cb + cr}\left(\dfrac{1}{ab^2} + \dfrac{pc}{(apr - cb + cr)^2}\right)(\mu_1 + \mu^*)\Big], \\ f_{1z_1z_2}(X_0) = -\dfrac{ah}{(a + x_0)^2} = -\dfrac{h(b-r)^2}{ab^2}, \\ f_{2z_1z_1}(X_0) = -\dfrac{2abh(d - kx_0 - e_0)}{(a + x_0)^2} = \dfrac{2h(b-r)^2}{ab}\left(\dfrac{akr}{b-r} - d\right) + \dfrac{2h(b-r)^3}{ab(apr - cb + cr)}(\mu_1 + \mu^*), \\ f_{2z_1z_2}(X_0) = \dfrac{abh}{(a + x_0)^2} = \dfrac{h(b-r)^2}{ab}. \end{cases} \tag{32}$$

Then, from (31), it follows that

$$\begin{cases} Df_{1z_1z_1}(X) = \left(-\dfrac{6ahy}{(a+x)^4} + \dfrac{4hep^2c}{(px - c)^3}, \dfrac{2ah}{(a+x)^3}, -\dfrac{2hpc}{(px - c)^2}\right), \\ Df_{1z_1z_2}(X) = \left(\dfrac{2ah}{(a+x)^3}, 0, 0\right), \\ Df_{2z_1z_1}(X) = \left(\dfrac{6abhy}{(a+x)^4}, -\dfrac{2abh}{(a+x)^3}, 0\right), \\ Df_{2z_1z_2}(X) = \left(-\dfrac{2abh}{(a+x)^3}, 0, 0\right). \end{cases} \tag{33}$$

Then, we get

$$\begin{cases} f_{1z_1z_1z_1}(X) = Df_{1z_1z_1}(X)D_{z_1}\psi(z) = -\dfrac{6ahy}{(a+x)^4} + \dfrac{6hep^2c}{(px-c)^3}, \\ f_{1z_1z_1z_2}(X) = Df_{1z_1z_1}(X)D_{z_2}\psi(z) = \dfrac{2ah}{(a+x)^3}, \\ f_{2z_1z_1z_1}(X) = Df_{2z_1z_1}(X)D_{z_1}\psi(z) = \dfrac{6abhy}{(a+x)^4}, \\ f_{2z_1z_1z_2}(X) = Df_{2z_1z_1}(X)D_{z_2}\psi(z) = -\dfrac{2abh}{(a+x)^3}. \end{cases} \tag{34}$$

Putting the value of X_0 into (34), we obtain that

$$\begin{cases} f_{1z_1z_1z_1}(X_0) = -\dfrac{6ah(d-kx_0-e_0)}{(a+x_0)^3} + \dfrac{6he_0p^2c}{(px_0-c)^3} = \dfrac{6hkr(b-r)^2}{ab^3} - \dfrac{6h\ d(b-r)^3}{a^2b^3} \\ +\dfrac{6h(b-r)^4}{apr-cb+cr}\left[\dfrac{1}{a^2b^3} + \dfrac{p^2c}{(apr-cb+cr)^3}\right](\mu_1+\mu^*), \\ f_{1z_1z_1z_2}(X_0) = \dfrac{2ah}{(a+x_0)^3} = \dfrac{2h(b-r)^3}{a^2b^3}, \\ f_{2z_1z_1z_1}(X_0) = \dfrac{6abh(d-kx_0-e_0)}{(a+x_0)^3} = \dfrac{6h(b-r)^3}{a^2b^2}\left(d - \dfrac{akr}{b-r}\right) - \dfrac{6h(b-r)^4}{a^2b^2(apr-cb+cr)}(\mu_1+\mu^*), \\ f_{2z_1z_1z_2}(X_0) = -\dfrac{2abh}{(a+x_0)^3} = -\dfrac{2h(b-r)^3}{a^2b^2}. \end{cases} \tag{35}$$

Consequently, it follows from (29), (32), and (35) that

$$
\begin{cases}
a_1 = 1 + \dfrac{hr}{b}\left(d + \dfrac{ak(b+r)}{b-r}\right) + \dfrac{hr}{b}\dfrac{(b-r)^2(ap+c)}{(apr-cb+cr)^2}\mu_1, \\
a_2 = -\dfrac{hr}{b}, \\
a_{13} = \dfrac{hr}{b}\dfrac{(b-r)^2(ap+c)}{(apr-cb+cr)^2}, \\
a_{11} = h\left[-2k + \dfrac{2\,d(b-r)^2}{ab^2} - \dfrac{2kr(b-r)}{b^2} - \dfrac{2(b-r)^3}{apr-cb+cr}\left(\dfrac{1}{ab^2} + \dfrac{pc}{(apr-cb+cr)^2}\right)\mu_1\right], \\
a_{12} = -\dfrac{h(b-r)^2}{ab^2}, \\
a_{113} = -\dfrac{2h(b-r)^3}{apr-cb+cr}\left[\dfrac{1}{ab^2} + \dfrac{pc}{(apr-cb+cr)^2}\right] \\
a_{111} = \dfrac{6hkr(b-r)^2}{ab^3} - \dfrac{6h\,d(b-r)^3}{a^2b^3} + \dfrac{6h(b-r)^4}{apr-cb+cr}\left[\dfrac{1}{a^2b^3} + \dfrac{p^2c}{(apr-cb+cr)^3}\right]\mu_1, \\
a_{112} = \dfrac{2h(b-r)^3}{a^2b^3}, \\
b_1 = h(b-r)\left(d - \dfrac{b-r}{apr-cb+cr}\mu_1\right) - akr, \\
b_2 = 1, \\
b_{13} = -\dfrac{h(b-r)^2}{apr-cb+cr}, \\
b_{11} = \dfrac{2h(b-r)^2}{ab}\left(\dfrac{akr}{b-r} - d\right) + \dfrac{2h(b-r)^3}{ab(apr-cb+cr)}\mu_1, \\
b_{12} = \dfrac{h(b-r)^2}{ab}, \\
b_{113} = \dfrac{2h(b-r)^3}{ab(apr-cb+cr)}, \\
b_{111} = \dfrac{6h(b-r)^3}{a^2b^2}\left(d - \dfrac{akr}{b-r}\right) - \dfrac{6h(b-r)^4}{a^2b^2(apr-cb+cr)}\mu_1, \\
b_{112} = -\dfrac{2h(b-r)^3}{a^2b^2}.
\end{cases}
\tag{36}
$$

Next, we consider the following nonsingular matrix:

$$T = \begin{pmatrix} a_2 & a_2 \\ -1-a_1 & \lambda_2 - a_1 \end{pmatrix}, \tag{37}$$

implementing the following translation:

$$\begin{pmatrix} z_1 \\ z_2 \end{pmatrix} = T \begin{pmatrix} u \\ v \end{pmatrix}. \tag{38}$$

Then, it is easy to see that system (24) can be written as follows:

$$\begin{pmatrix} u \\ v \end{pmatrix} \longrightarrow \begin{pmatrix} -1 & 0 \\ 0 & \lambda_2 \end{pmatrix} \begin{pmatrix} u \\ v \end{pmatrix} + \begin{pmatrix} f_1(u, v, \mu^*) \\ f_2(u, v, \mu^*) \end{pmatrix}, \tag{39}$$

where

$$\begin{aligned} f_1(u, v, \mu^*) &= \frac{a_{11}(\lambda_2 - a_1) - a_2 b_{11}}{a_2(1+\lambda_2)} z_1^2 + \frac{a_{12}(\lambda_2 - a_1) - a_2 b_{12}}{a_2(1+\lambda_2)} z_1 z_2 + \frac{a_{13}(\lambda_2 - a_1) - a_2 b_{13}}{a_2(1+\lambda_2)} z_1 \mu^* \\ &+ \frac{a_{113}(\lambda_2 - a_1) - a_2 b_{113}}{a_2(1+\lambda_2)} z_1^2 \mu^* + \frac{a_{111}(\lambda_2 - a_1) - a_2 b_{111}}{a_2(1+\lambda_2)} z_1^3 \\ &+ \frac{a_{112}(\lambda_2 - a_1) - a_2 b_{112}}{a_2(1+\lambda_2)} z_1^2 z_2 + O\left(\left(|z_1| + |z_2| + |\mu^*| \right)^4 \right) \\ f_2(u, v, \mu^*) &= \frac{a_{11}(1+a_1) + a_2 b_{11}}{a_2(1+\lambda_2)} z_1^2 + \frac{a_{12}(1+a_1) + a_2 b_{12}}{a_2(1+\lambda_2)} z_1 z_2 + \frac{a_{13}(1+a_1) + a_2 b_{13}}{a_2(1+\lambda_2)} z_1 \mu^* \\ &+ \frac{a_{113}(1+a_1) + a_2 b_{113}}{a_2(1+\lambda_2)} z_1^2 \mu^* + \frac{a_{111}(1+a_1) + a_2 b_{111}}{a_2(1+\lambda_2)} z_1^3 \\ &+ \frac{a_{112}(1+a_1) + a_2 b_{112}}{a_2(1+\lambda_2)} z_1^2 z_2 + O\left(\left(|z_1| + |z_2| + |\mu^*| \right)^4 \right) \end{aligned} \tag{40}$$

$$\begin{aligned} z_1 &= a_2(u+v),\ z_2 = -(1+a_1)u + (\lambda_2 - a_1)v, \\ z_1 z_2 &= a_2\left[-(1+a_1)u^2 + (\lambda_2 - 2a_1 - 1)uv + a_2(\lambda_2 - a_1)v^2 \right], \\ z_1^2 &= a_2^2\left[u^2 + uv + v^2 \right], \\ z_1^3 &= a_2^3\left[u^3 + 3u^2 v + 3uv^2 + v^3 \right], \\ z_1^2 z_2 &= a_2^2\left[-(1+a_1)u^3 + (\lambda_2 - 3a_1 - 2)u^2 v + (2\lambda_2 - 3a_1 - 1)uv^2 + (\lambda_2 - 1)v^3 \right]. \end{aligned}$$

In order to determine the center manifold $W_c(0,0,0)$ of (39) about the equilibrium point $(0,0)$ in a small neighborhood of μ^*, we implement an application of the center manifold theorem [29], and it is easy to see that there exists a center manifold of the following form:

$$W_c(0,0,0) = \left\{ (u, v, \mu^*) \in R^3, v = h(u, \mu^*), h(0,0) = 0, Dh(0,0) = 0 \right\}, \tag{41}$$

for u and μ^* sufficiently small. Furthermore, we assume that

$$h(u, \mu^*) = c_0 u^2 + c_1 u\mu^* + c_2 \mu^{*2} + O\left(\left(|u| + |\mu^*| \right)^3 \right). \tag{42}$$

Then, it is easy to see that the center manifold satisfies the following:

$$h(-u + f_1(u, h(u, \mu^*), \mu^*), \mu^*) = \lambda_2 h(u, \mu^*) + f_2(u, h(u, \mu^*), \mu^*). \tag{43}$$

Taking into account (42) and (43) and then comparing coefficients for (43), one can easily obtain that

$$\begin{aligned} c_0 &= \frac{1}{\left(1-\lambda_2^2\right)}\left[\left(1+a_1\right)\left(a_2a_{11}-a_{12}\left(1+a_1\right)-a_2b_{12}\right)+a_2^2b_{11}\right], \\ c_1 &= \frac{a_{13}\left(1+a_1\right)+a_2b_{13}}{\left(1+\lambda_2\right)^2}, \\ c_2 &= 0. \end{aligned} \tag{44}$$

Furthermore, taking into account (39), it is restricted to the center manifold $W_c(0,0,0)$ as follows:

$$F:\ u \longrightarrow\ -u+d_{11}u^2+d_{12}u\mu^*+d_{112}u^2\mu^*+d_{122}u\mu^{*2}+d_{111}u^3+O\left(\left(|u|+\left|\mu^*\right|\right)^4\right), \tag{45}$$

where

$$\begin{aligned} d_{11} &= \frac{1}{\lambda_2+1}\left[\left(\lambda_2-a_1\right)\left(a_{11}a_2-a_{12}\left(1+a_1\right)+a_{113}a_2\right)-b_{11}a_2^2+\left(1+a_1\right)b_{12}a_2-b_{113}a_2^2\right], \\ d_{12} &= \frac{1}{\lambda_2+1}\left[a_{13}\left(\lambda_2-1\right)-b_{13}a_2\right], \\ d_{112} &= \frac{1}{\lambda_2+1}\left[\left(\lambda_2-a_1\right)\left(a_{11}a_2c_1+a_{12}c_1\left(\lambda_2-2a_1-1\right)+a_{13}c_0\right)-b_{11}a_2^2c_1\right] \\ &\quad -b_{12}a_2c_1\left(\lambda_2-2a_1-1\right)-b_{13}a_2c_0], \\ d_{122} &= \frac{1}{\lambda_2+1}\left[a_{13}c_1\left(\lambda_2-1\right)-b_{13}a_2c_1\right], \\ d_{111} &= \frac{1}{\lambda_2+1}\left[\left(\lambda_2-a_1\right)\left(a_{11}a_2c_0+a_{111}a_2^2+a_{12}c_0\left(\lambda_2-2a_1-1\right)-a_{112}a_2\left(1+a_1\right)\right)-b_{11}a_2^2c_0\right] \\ &\quad -b_{12}a_2c_0\left(\lambda_2-2a_1-1\right)-b_{111}a_2^3+b_{112}a_2^2\left(1+a_1\right)\Big]. \end{aligned} \tag{46}$$

In order for system (45) to undergo a flip bifurcation, we require that two discriminatory quantities $\alpha_1$and α_2 are not zero, where

$$\begin{aligned} \alpha_1 &= \left(2\frac{\partial^2F}{\partial\mu^*\partial u}+\frac{\partial F}{\partial\mu^*}\frac{\partial F}{\partial u}\right)_{(0,0)} = 2d_{12}, \\ \alpha_2 &= \left(\frac{1}{2}\left(\frac{\partial^2F}{\partial u^2}\right)^2+\frac{1}{3}\left(\frac{\partial^3F}{\partial u^3}\right)\right)_{(0,0)} = 2\left(d_{111}+d_{11}^2\right). \end{aligned} \tag{47}$$

Keeping in view the aforementioned computation and bifurcation theory given in [36, 37], we have the following theorem.

Theorem 2. *Assume that* $(a,b,c,d,k,p,r,\mu_1)\in F_B$. *If* $\alpha_2\neq 0$, *then system (17) undergoes a flip bifurcation at the fixed point* (x_0,y_0,e_0) *when the parameter* μ *varies in a small neighborhood of* μ_1. *Moreover, if* $\alpha_2>0$ *(resp.,* $\alpha_2<0$*), then the period-2 orbits that bifurcate from* (x_0,y_0,e_0) *are stable (resp., unstable).*

In the last Section 5 related to numerical simulation, we choose some parametric values for system (4) such that it undergoes period-doubling bifurcation about positive equilibrium as μ varies in the suitable interval (see Figure 4).

3.2. Neimark–Sacker Bifurcation. Finally, we discuss the Neimark–Sacker bifurcation about equilibrium (x_0, y_0, e_0) with variation of parameters $(a, b, c, d, k, p, r, \mu_2, h)$ in a small neighborhood of H_B. For this, we choose parameters $(a, b, c, d, k, p, r, \mu_2, h)$ arbitrarily from H_B, taking into account system (4) with $(a, b, c, d, k, p, r, \mu_2, h) \in H_B$. In this case, system (4) is described by the following 2-dimensional map:

$$\begin{cases} x \longrightarrow x + x\left(d - kx - \dfrac{y}{a+x} - e\right), \\ y \longrightarrow y + y\left(-r + \dfrac{bx}{a+x}\right), \\ \mu_2 = e(px - c). \end{cases} \tag{48}$$

Then, it is easy to observe that map (48) has a unique positive fixed point (x_0, y_0, e_0). Next, we take μ^* as a bifurcation parameter and consider a perturbation corresponding to map (48) given as follows:

$$\begin{cases} x \longrightarrow x + x\left(d - kx - \dfrac{y}{a+x} - e\right), \\ y \longrightarrow y + y\left(-r + \dfrac{bx}{a+x}\right), \\ \mu_2 + \mu^* = e(px - c), \end{cases} \tag{49}$$

where $\mu^* \ll 1$ is taken as a small perturbation parameter.

Furthermore, from (24), we have

$$\begin{cases} z_1 \longrightarrow a_1 z_1 + a_2 z_2 + a_{11} z_1^2 + a_{12} z_1 z_2 + a_{111} z_1^3 + a_{112} z_1^2 z_2 + O\left(\left(|z_1| + |z_2|\right)^4\right), \\ z_2 \longrightarrow b_1 z_1 + b_2 z_2 + b_{11} z_1^2 + b_{12} z_1 z_2 + b_{111} z_1^3 + b_{112} z_1^2 z_2 + O\left(\left(|z_1| + |z_2|\right)^4\right), \end{cases} \tag{50}$$

where coefficients $a_1, a_2, a_{11}, a_{12}, a_{111}, a_{112}$ and $b_1, b_2, b_{11}, b_{12}, b_{111}, b_{112}$ given in (24) are similar to the coefficients in (36) by replacing μ_1 with $\mu_2 + \mu^*$. Moreover, it must be noted that the characteristic equation corresponding to the linearization of (50) about $(z_1, z_2) = (0, 0)$ is given as follows:

$$\lambda^2 + p(\mu^*)\lambda + q(\mu^*) = 0, \tag{51}$$

where

$$\begin{aligned} p(\mu^*) &= h(\mu^*) - q(\mu^*) - 1, \\ q(\mu^*) &= \frac{1}{((arp/(b-r)) - c)^2}\left[R_2\mu - (S_2 - 1)\left(\frac{arp}{b-r} - c\right)^2\right], \\ h(\mu^*) &= \frac{abx_0y_0}{(a+x_0)^3} > 0. \end{aligned} \tag{52}$$

Suppose that $(a, b, c, d, k, p, r, \mu_2, h) \in H_B$; then eigenvalues about $(0, 0)$ are conjugate complex numbers denoted by λ and $\overline{\lambda}$ with modulus 1 such that

$$\lambda, \overline{\lambda} = -\frac{p(\mu^*)}{2} \pm \frac{i}{2}\sqrt{4q(\mu^*) - p^2(\mu^*)}, \tag{53}$$

and, consequently, one has

$$\begin{aligned} |\lambda|_{\mu^*=0} &= \sqrt{q(0)} = 1, \\ l &= \frac{d|\lambda|}{d\mu^*}\Big|_{\mu^*=0} = \frac{R_2}{2(r_1 - c)^2} \neq 0. \end{aligned} \tag{54}$$

On the other hand, it is necessary that, at $\mu^* = 0$, one must have $\lambda^m, \overline{\lambda}^m \neq 1$, $(m = 1, 2, 3, 4)$, or equivalently one has $p(0) \neq -2, 0, 1, 2$. Next, it must be noted that $p(0) = h(0) - q(0) - 1 = H(\mu_2) - 2$ and $H(\mu_2) < 4$ because $(a, b, c, d, k, p, r, \mu_2, h) \in H_B$. As a result, one has $p(0) \neq -2, 2$. Consequently, it is required that $p(0) \neq 0, 1$, which is equivalently written as follows:

$$H(\mu_2) \neq 2, 3. \tag{55}$$

Consequently, the eigenvalues of system (50) which are given by $\lambda, \overline{\lambda}$ about fixed point $(0, 0)$ do not lie in the intersection of the unit circle with the coordinate axes at $\mu^* = 0$ whenever conditions (55) hold true. Moreover, in order to discuss the normal form for system (50) about $\mu^* = 0$, we choose $\mu^* = 0$, $\sigma = 1 - (H(\mu_2)/2)$, $\omega = (1/2)\sqrt{H(\mu_2)(4 - H(\mu_2))}$,

$$T = \begin{pmatrix} a_2 & 0 \\ \sigma - a_1 & -\omega \end{pmatrix}, \tag{56}$$

taking into account the following translation:

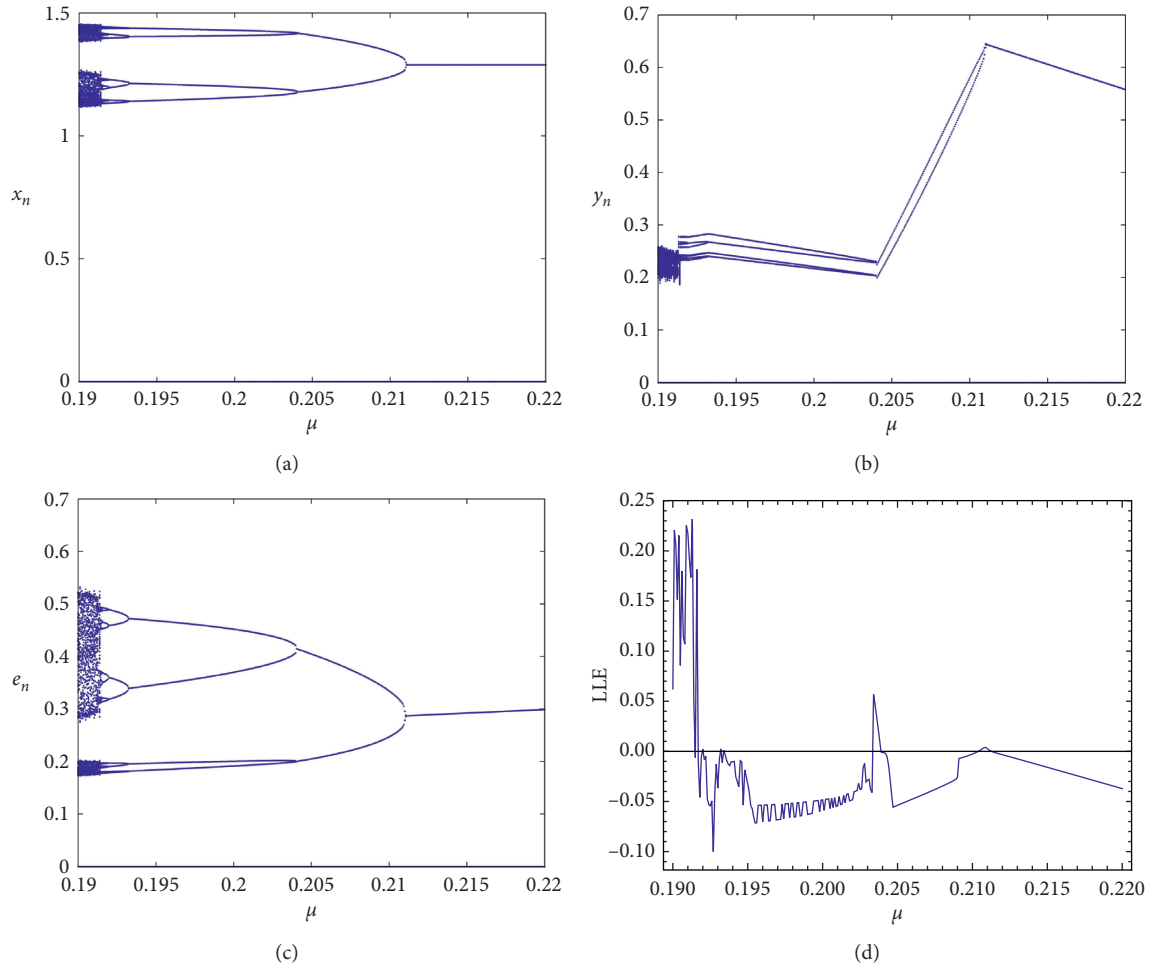

Figure 4: Bifurcation diagrams and LLE for system (3) with $a = 5.8$, $b = 8.8$, $c = 2.1$, $d = 3.6$, $k = 2.5$, $r = 1.6$, $p = 2.2$, $h = 0.98$, $\mu \in [0.19, 0.22]$, and $(x_0, y_0, e_0) = (1.28, 0.6428, 0.287)$. (a) Bifurcation diagram for x_n. (b) Bifurcation diagram for y_n. (c) Bifurcation diagram for e_n. (d) Largest Lyapunov exponents.

$$\begin{pmatrix} z_1 \\ z_2 \end{pmatrix} = T \begin{pmatrix} u \\ v \end{pmatrix}. \tag{57}$$

Then, it is easy to see that system (50) takes the following form:

$$\begin{pmatrix} u \\ v \end{pmatrix} \longrightarrow \begin{pmatrix} \sigma & -\omega \\ \omega & \sigma \end{pmatrix} \begin{pmatrix} u \\ v \end{pmatrix} + \begin{pmatrix} \overline{f_1}(u, v) \\ \overline{f_2}(u, v) \end{pmatrix}, \tag{58}$$

where

$$\overline{f_1}(u, v) = \frac{a_{11}}{a_2} z_1^2 + \frac{a_{12}}{a_2} z_1 z_2 + \frac{a_{111}}{a_2} z_1^3 + \frac{a_{112}}{a_2} z_1^2 z_2 + O\left(\left(|z_1| + |z_2| \right)^4 \right)$$

$$\overline{f_2}(u, v) = \frac{(\sigma - a_1) a_{11} - a_2 b_{11}}{a_2 \omega} z_1^2 + \frac{(\sigma - a_1) a_{12} - a_2 b_{12}}{a_2 \omega} z_1 z_2 + \frac{(\sigma - a_1) a_{111} - a_2 b_{111}}{a_2 \omega} z_1^3 + \frac{(\sigma - a_1) a_{112} - a_2 b_{112}}{a_2 \omega} z_1^2 z_2 + O\left(\left(|z_1| + |z_2| \right)^4 \right)$$

$$z_1 = a_2 u,$$

$$z_2 = (\sigma - a_1) u - \omega v,$$

$$\begin{aligned} z_1 z_2 &= a_2(\sigma - a_1)u^2 + a_2\omega uv, \\ z_1^2 &= a_2^2 u^2, \\ z_1^3 &= a_2^3 u^3, \\ z_1^2 z_2 &= a_2^2(\sigma - a_1)u^3 - \omega u^2 v. \end{aligned} \tag{59}$$

Therefore, at point $(0,0)$, we have

$$\begin{aligned} \overline{f}_{1uu} &= 2a_{11} + 2a_{12}(\sigma - a_1), \\ \overline{f}_{1uv} &= a_{12}\omega, \\ \overline{f}_{1uuu} &= 6a_{111}a_2^2, \\ \overline{f}_{1uuv} &= -\frac{a_{112}}{a_2}\omega, \\ \overline{f}_{1vv} &= \overline{f}_{1uvv} = \overline{f}_{1vvv} = 0, \\ \overline{f}_{2uu} &= \frac{2}{\omega}\left[(\sigma - a_1)(a_{11}a_2 + a_{12}(\sigma - a_1) - a_2 b_{12}) - a_2^2 b_{11}\right], \\ \overline{f}_{2uv} &= (\sigma - a_1)a_{12} - a_2 b_{12}, \\ \overline{f}_{2uuu} &= \frac{6a_2}{\omega}\left[(\sigma - a_1)(a_2 a_{111} + (\sigma - a_1)a_{112} - a_2 b_{112}) - a_2 b_{111}\right], \\ \overline{f}_{2uuv} &= \frac{2}{a_2}\left[a_2 b_{112} - (\sigma - a_1)a_{112}\right], \\ \overline{f}_{2vv} &= \overline{f}_{2uvv} = \overline{f}_{2vvv} = 0. \end{aligned} \tag{60}$$

Then, system (58) undergoes a Neimark–Sacker bifurcation, if we have the following nonzero discriminatory quantity [30, 32]:

$$\theta = \left[-\mathrm{Re}\left(\frac{(1-2\lambda)\overline{\lambda}^2}{1-\lambda}\right)L_{11}L_{12} - \frac{1}{2}|L_{11}|^2 - |L_{21}|^2 + \mathrm{Re}\left(\overline{\lambda}L_{22}\right)\right]_{\mu^*=0}, \tag{61}$$

where

$$\begin{aligned} L_{11} &= \frac{1}{4}\left(\left(\overline{f}_{1uu} + \overline{f}_{1vv}\right) + i\left(\overline{f}_{2uu} + \overline{f}_{2vv}\right)\right), \\ L_{12} &= \frac{1}{8}\left(\left(\overline{f}_{1uu} - \overline{f}_{1vv} + 2\overline{f}_{2uv}\right) + i\left(\overline{f}_{2uu} - \overline{f}_{2vv} - 2\overline{f}_{1uv}\right)\right), \\ L_{21} &= \frac{1}{8}\left(\left(\overline{f}_{1uu} - \overline{f}_{1vv} - 2\overline{f}_{2uv}\right) + i\left(\overline{f}_{2uu} - \overline{f}_{2vv} + 2\overline{f}_{1uv}\right)\right), \\ L_{22} &= \frac{1}{16}\left(\left(\overline{f}_{1uuu} + \overline{f}_{1uvv} + \overline{f}_{2uuv} + \overline{f}_{2vvv}\right) + i\left(\overline{f}_{2uuu} + \overline{f}_{2uvv} - \overline{f}_{2uuv} - \overline{f}_{2vvv}\right)\right), \end{aligned} \tag{62}$$

Keeping in mind the aforementioned computation, one has the following result.

Theorem 3. *Assume that condition (55) is satisfied and $\theta \neq 0$, then the Neimark–Sacker bifurcation exists at the fixed point (x_0, y_0, e_0) in a small neighborhood of μ_2. Further, if $\theta < 0$ (resp., $\theta > 0$), then an attracting (resp., repelling) closed invariant curve bifurcates from the fixed point for $\mu > \mu_2$ (resp., $\mu < \mu_2$).*

4. Chaos Control

Bifurcating behavior, chaos, and unstable fluctuations have always been considered as adverse criteria in biology; therefore, these are damaging for the reproduction of the biological population. Certainly, we require to take action to stabilize the biological population. For further details and applications of chaos control methods, we refer to [37–50] and the references therein.

In this section, we propose the following state delayed feedback control method for system (4):

$$\begin{cases} x_{n+1} = x_n + hx_n\left(d - kx_n - \dfrac{y_n}{a + x_n} - e_n\right) + \delta\left(x_n - x_{n-1}\right), \\ y_{n+1} = y_n + hy_n\left(\dfrac{bx_n}{a + x_n} - r\right), \\ \mu = e_n\left(px_n - c\right), \end{cases} \tag{63}$$

where δ is the feedback gain for the controlled system (63).

Next, introducing $u_n := x_n - x_{n-1}$, we obtain the following controlled system equivalent to system (63):

$$\begin{cases} x_{n+1} = x_n + hx_n\left(d - kx_n - \dfrac{y_n}{a + x_n} - e_n\right) + \delta u_n, \\ y_{n+1} = y_n + hy_n\left(\dfrac{bx_n}{a + x_n} - r\right), \\ u_{n+1} = hx_n\left(d - kx_n - \dfrac{y_n}{a + x_n} - e_n\right) + \delta u_n, \\ \mu = e_n\left(px_n - c\right). \end{cases} \tag{64}$$

The generalized variational matrix $J(x_0, y_0, u_0, e_0)$ of the controlled system (64) about its fixed point $(x_0, y_0, u_0, e_0) = ((ar/(b - r)), (a + x_0)(d - kx_0 - e_0), 0, (\mu/(px_0 - c)))$ is given as follows:

$$J\left(x_0, y_0, u_0, e_0\right) = \begin{pmatrix} m_{11} & -\dfrac{hx_0}{a + x_0} & \delta & -hx_0 \\ \dfrac{abhy_0}{\left(a + x_0\right)^2} & 1 & 0 & 0 \\ 1 - m_{11} & -\dfrac{hx_0}{a + x_0} & \delta & -hx_0 \\ pe_0 & 0 & 0 & px_0 - c \end{pmatrix}, \tag{65}$$

where

$$m_{11} := 1 + \frac{hx_0y_0}{\left(a + x_0\right)^2} - hkx_0. \tag{66}$$

Then, generalized characteristic polynomial for $J(x_0, y_0, u_0, e_0)$ is defined as follows:

$$F(\lambda) = \det\begin{pmatrix} m_{11} - \lambda & -\dfrac{hx_0}{a + x_0} & \delta & -hx_0 \\ \dfrac{abhy_0}{\left(a + x_0\right)^2} & 1 - \lambda & 0 & 0 \\ 1 - m_{11} & -\dfrac{hx_0}{a + x_0} & \delta - \lambda & -hx_0 \\ pe_0 & 0 & 0 & px_0 - c \end{pmatrix} = 0, \tag{67}$$

which, on simplification, yields

$$F(\lambda) = \lambda^3 + A\lambda^2 + B\lambda + C, \tag{68}$$

where

$$A := \frac{px_0(\delta + e_0h + m_{11} + 1) - c(\delta + m_{11} + 1)}{c - px_0},$$

$$B := \frac{c\left(\left(abh^2x_0y_0\right)/\left((a+x_0)^3\right)\right) + 2\delta m_{11} + m_{11}\right) + px_0\left(-\left(\left(abh^2x_0y_0\right)/\left((a+x_0)^3\right)\right) - e_0h - 2\delta m_{11} - m_{11}\right)}{c - px_0}, \tag{69}$$

$$C := \delta - 2\delta m_{11}.$$

Keeping in view the controllability for system (63), we have the following lemma.

Lemma 2. *Assume that* $b > r, bc < r(ap+ c)$, $((b\ d - r(ak + d))/((b-r)^2)) - (\mu/(r(ap+c) - bc)) > 0$; *then the fixed point* $(x_0, y_0, u_0, e_0) = ((ar/(b-r)), (a+x_0)(d - kx_0 - e_0), 0, (\mu/(px_0 - c)))$ *of system (63) is a sink if the following conditions are satisfied:*

$$\begin{aligned} &|A + C| < 1 + B, \\ &|A - 3C| < 3 - B, \\ &C^2 + B - AC < 1. \end{aligned} \tag{70}$$

5. Numerical Simulation and Discussion

In this section, our main purpose is to validate theoretical findings with numerical simulation. For this, first of all, the existence of the period-doubling bifurcation is illustrated through particular choice of biologically feasible parametric values. Choose $a = 5.8$, $b = 8.8$, $c = 2.1$, $d = 3.6$, $k = 2.5$, $r = 1.6$, $p = 2.2$, and $h = 0.98$ with the variation of bifurcation parameter μ in $[0.19, 0.22]$. Then, around $\mu \approx 0.211175$, system (3) undergoes period-doubling bifurcation. On the other hand, at $a = 5.8$, $b = 8.8$, $c = 2.1$, $d = 3.6$, $k = 2.5$, $r = 1.6$, $p = 2.2$, $h = 0.98$, and $\mu \equiv \mu_1 = 0.211175$, system (3) has a unique positive fixed point $(1.28889, 0.642835, 0.287096)$, and the characteristic polynomial for the Jacobian matrix of singular system (3) is given as follows:

$$P(\lambda) = \lambda^2 + 0.057005\lambda - 0.942995. \tag{71}$$

Moreover, the roots of $P(\lambda)$ are -1 and 0.942995. Consequently, $(a, b, c, d, k, p, r, \mu_1, h) \in F_B$, and it follows the correctness of Theorem 2. On the other hand, bifurcation diagrams for singular system (3) and corresponding largest Lyapunov exponents (LLE) are depicted in Figure 4.

Secondly, choose $a = 41.5$, $b = 85$, $c = 2.7$, $d = 3.4$, $k = 1.4$, $r = 3.5$, $p = 2.3$, and $h = 0.75$ with a variation of bifurcation parameter μ in $[0.4, 1.1]$ for validity of Neimark–Sacker bifurcation. Then, around $\mu \approx 0.678396$, system (3) undergoes a Neimark–Sacker bifurcation. On the other hand, at $a = 41.5$, $b = 85$, $c = 2.7$, $d = 3.4$, $k = 1.4$, $r = 3.5$, $p = 2.3$, $h = 0.75$, and $\mu \equiv \mu_2 = 0.678396$, system (3) has a unique positive fixed point $(1.78221, 18.1794, 0.484887)$, and the characteristic polynomial for the Jacobian matrix of singular system (3) is given as follows:

$$P(\lambda) = \lambda^2 - 1.20713\lambda + 1. \tag{72}$$

Moreover, the roots of $P(\lambda)$ are $0.603567 - 0.797313i$ and $0.603567 + 0.797313i$ with $|0.603567 \pm 0.797313i| = 1$. Consequently, $(a, b, c, d, k, p, r, \mu_2, h) \in H_B$, and it follows the correctness of Theorem 3. On the other hand, the bifurcation diagrams for singular system (3) and corresponding largest Lyapunov exponents (LLE) are depicted in Figure 5. Moreover, in the chaotic region, that is, for $\mu \in [0.678396, 1.1]$, some phase portraits of system (4) are depicted in Figure 6.

Finally, in order to see the efficaciousness of delayed feedback control strategy for system (4), we choose $a = 41.5$, $b = 85$, $c = 2.7$, $d = 3.4$, $k = 1.4$, $r = 3.5$, $p = 2.3$, $h = 0.75$, and $\mu = 0.95$ in the chaotic region. At these parametric values, system (4) has unique positive fixed point $(x_0, y_0, e_0) = (1.78221, 9.77703, 0.679018)$, and the complex conjugate roots of the characteristic equation for the Jacobian matrix are $0.813859 \pm 0.625908i$ with $|0.813859 \pm 0.625908i| = 1.02671 > 1$. Therefore, $(1.78221, 9.77703, 0.679018)$ is a source for system (4). Furthermore, for these parametric values, system (64) can be written as follows:

$$\begin{cases} x_{n+1} = x_n + 0.75x_n\left(3.4 - 1.4x_n - \dfrac{y_n}{41.5 + x_n} - e_n\right) + \delta u_n, \\ y_{n+1} = y_n + 0.75y_n\left(\dfrac{85x_n}{41.5 + x_n} - 3.5\right), \\ u_{n+1} = 0.75x_n\left(3.4 - 1.4x_n - \dfrac{y_n}{41.5 + x_n} - e_n\right) + \delta u_n, \\ 0.95 = e_n(2.3x_n - 2.7). \end{cases} \tag{73}$$

On the other hand, the characteristic polynomial of the Jacobian matrix of system (73) is given as follows:

$$P(\lambda) = \lambda^3 - (\delta + 1.62772)\lambda^2 + (2\delta + 1.05413)\lambda - \delta. \tag{74}$$

Taking into account the conditions of Lemma 2, we have that the positive fixed point of system (73) is a sink if $-0.920461 < \delta < -0.14539$. Consequently, system (73) is controllable in $\delta \in]-0.920461, -0.14539[$. More generally, if we take $a = 41.5$, $b = 85$, $c = 2.7$, $d = 3.4$, $k = 1.4$, $r = 3.5$, $p = 2.3$, $h = 0.75$, and $\mu \in [0.678396, 1.1]$, then the controllable region for system (64) is depicted in Figure 7.

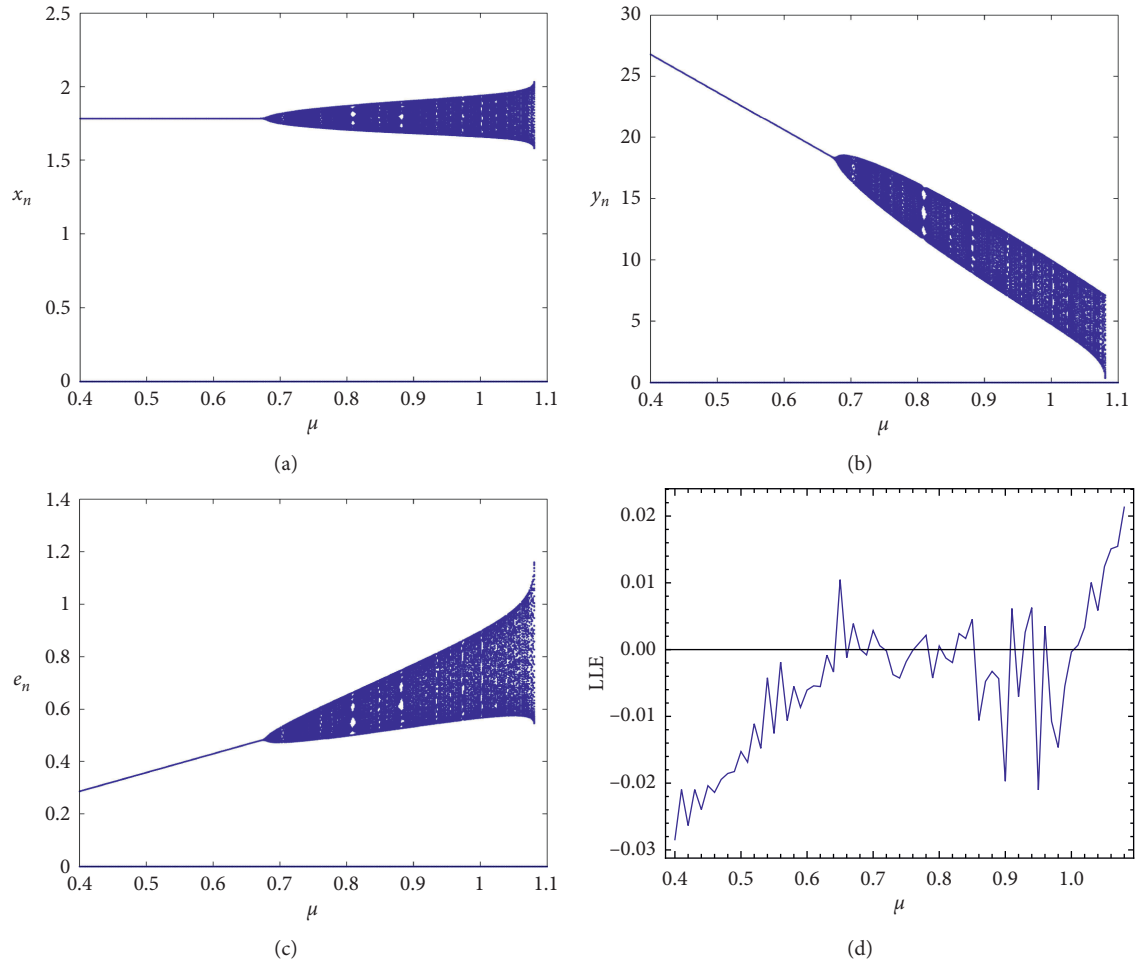

Figure 5: Bifurcation diagrams and LLE for system (3) with $a = 41.5$, $b = 85$, $c = 2.7$, $d = 3.4$, $k = 1.4$, $r = 3.5$, $p = 2.3$, $h = 0.75$, $\mu \in [0.4, 1.1]$, and $(x_0, y_0, e_0) = (1.5, 5.58, 0.775)$. (a) Bifurcation diagram for x_n. (b) Bifurcation diagram for y_n. (c) Bifurcation diagram for e_n. (d) Largest Lyapunov exponents.

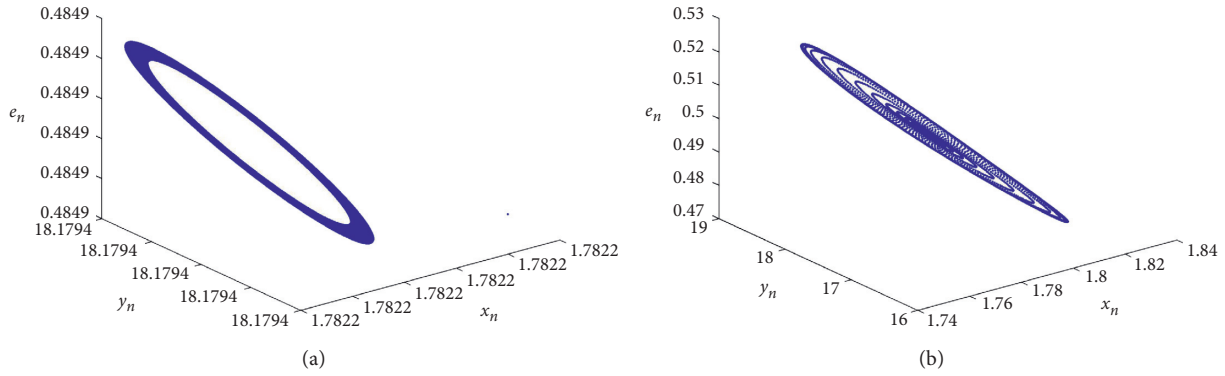

Figure 6: Continued.

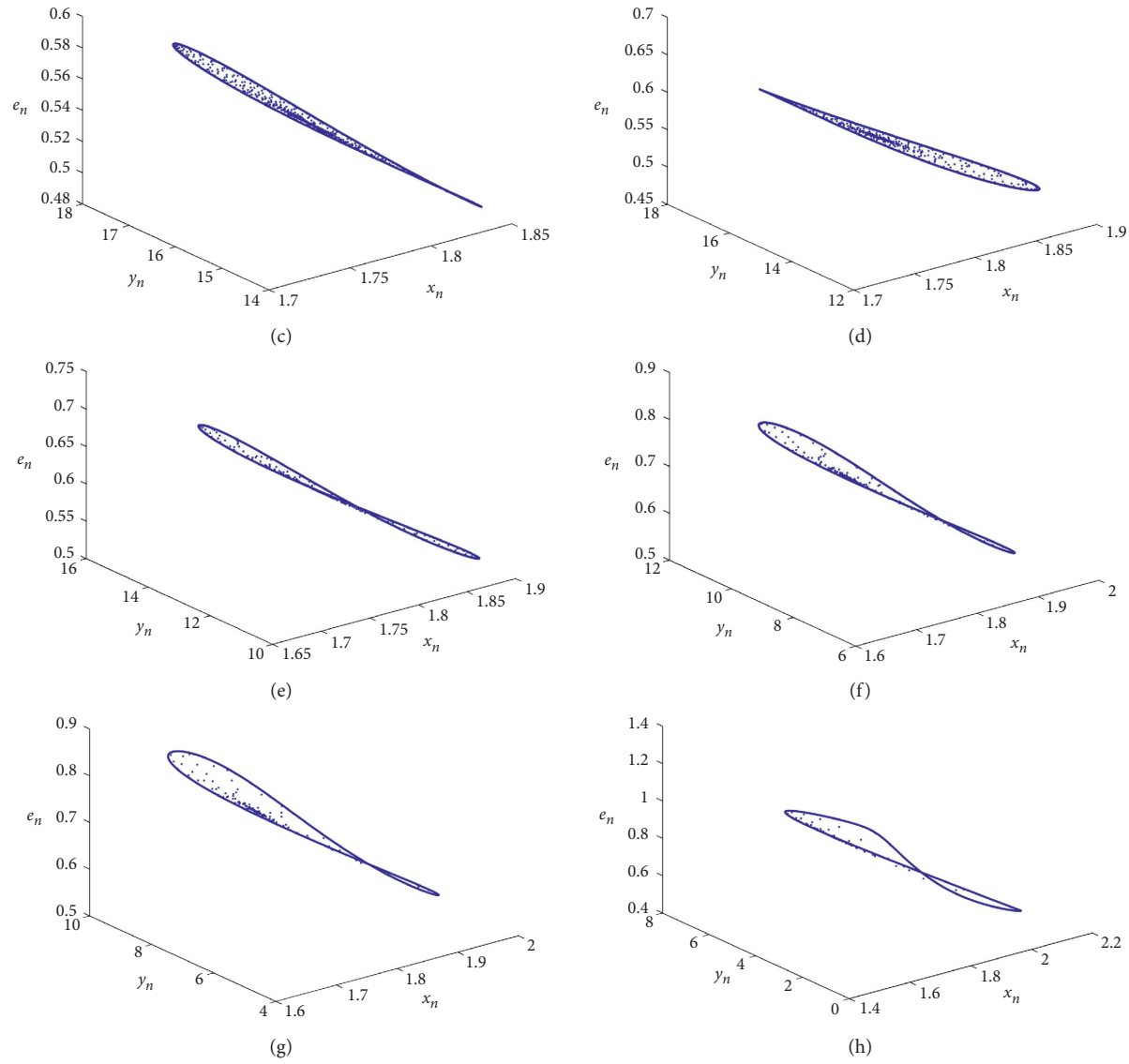

Figure 6: Phase portraits of system (4) for $a = 41.5$, $b = 85$, $c = 2.7$, $d = 3.4$, $k = 1.4$, $r = 3.5$, $p = 2.3$, and $h = 0.75$ and with different values of $\mu \in [0.678396, 1.1]$. (a) Phase portrait for $\mu = 0:678396$. (b) Phase portrait for $\mu = 0:7$. (c) Phase portrait for $\mu = 0:75$. (d) Phase portrait for $\mu = 0:8$. (e) Phase portrait for $\mu = 0:85$. (f) Phase portrait for $\mu = 0:95$. (g) Phase portrait for $\mu = 1$. (h) Phase portrait for $\mu = 1:08$.

6. Conclusion

We discuss the dynamical behavior of a discrete-time singular bioeconomic model. Moreover, Euler's approximation is implemented to a bioeconomic model governed by the differential-algebraic system proposed in [11]. The Neimark–Sacker bifurcation and period-doubling bifurcation are studied for the discrete bioeconomic model with the implementation of normal form theory, bifurcation theory, and the center manifold theorem. On the other hand, we select μ (the economic profit parameter) as a bifurcation parameter. Our investigations show richer dynamical behaviors for the discrete-time bioeconomic model compared with its continuous counterpart studied in [11]. Numerical computation for maximum Lyapunov exponents ensures further dynamical behavior and complexity of the model. Such type of complex phenomena might result from economic profit [25]. With the variation of the bifurcation parameter μ, the biologically feasible fixed point resembles the stability of economic profit, and later on, the system may sacrifice its stability by undergoing period-doubling or Neimark–Sacker bifurcation, and consequently trajectories tend to a period-doubling cascade or an invariant circle. Our theoretical discussion reveals that if the economic revenue μ increases beyond a certain threshold value μ_1 (respectively, μ_2), a phenomenon of period-doubling bifurcation (respectively, Neimark–Sacker bifurcation) occurs. From Theorem 2 (respectively, Theorem 3), if the economic revenue μ is equal to or larger than the bifurcation value μ_1 (respectively, μ_2), the predator population, the prey population, and the harvesting effort will not stay at steady states, which will result in serious biological economic

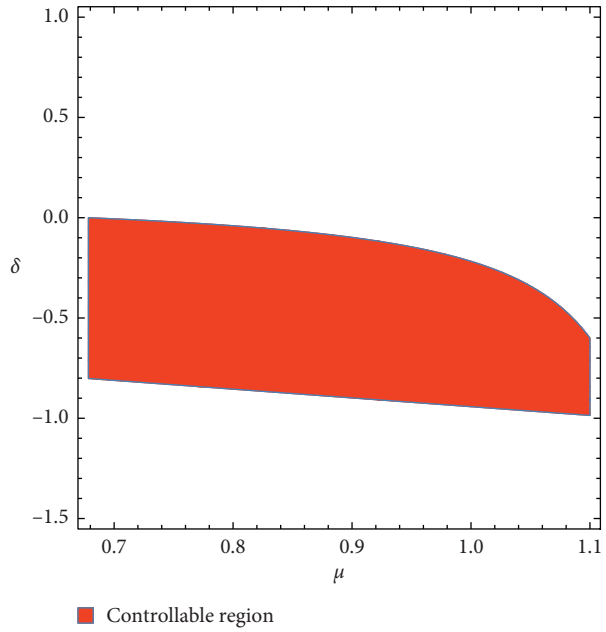

FIGURE 7: Controllability region of system (64) for $a = 41.5$, $b = 85$, $c = 2.7$, $d = 3.4$, $k = 1.4$, $r = 3.5$, $p = 2.3$, $h = 0.75$, and $\mu \in [0.678396, 1.1]$ in $\mu\delta$-plane.

environmental imbalance. Thus, it is sensible for fishermen to keep the economic revenue within a certain range for the purpose of maintaining the sustainable development of biological resources. On the other hand, the suggested state feedback control method of the delayed type vanishes such fluctuating phenomena and derives the bifurcating behavior of singular discrete-time economic prey-predator system towards a stable situation. Computation reveals that this delayed-type control strategy can be applied only by modifying the effort of harvesting for the prey population density by taking into account the present prey population density and the previous one. Consequently, economists can formulate some strategies to restrain or encourage the harvesting attempts in practical applications, for example, adjusting market price and revenue, abating pollution, making an allowance to fishermen, so that the biological populations can remain at their stable states.

Data Availability

No data were used to support this study.

Conflicts of Interest

The authors declare that they have no conflicts of interest.

References

[1] H. S. Gordon, "The economic theory of a common-property resource: the fishery," *Journal of Political Economy*, vol. 62, no. 2, pp. 124–142, 1954.

[2] M. B. Schaefer, "Some considerations of population dynamics and economics in relation to the management of the commercial marine fisheries," *Journal of the Fisheries Research Board of Canada*, vol. 14, no. 5, pp. 669–681, 1957.

[3] L. G. Anderson and J. C. Seijo, *Bioeconomics of Fisheries Management*, John Wiley & Sons, Hoboken, NJ, USA, 2010.

[4] Y. Zhang, Q. L. Zhang, and L. C. Zhao, "Bifurcations and control in singular biological economical model with stage structure," *Journal of Systems Engineering*, vol. 22, no. 3, pp. 232–238, 2007.

[5] C. Liu, Q. Zhang, and X. Duan, "Dynamical behavior in a harvested differential-algebraic prey-predator model with discrete time delay and stage structure," *Journal of the Franklin Institute*, vol. 346, no. 10, pp. 1038–1059, 2009.

[6] K. Chakraborty, M. Chakraborty, and T. K. Kar, "Bifurcation and control of a bioeconomic model of a prey-predator system with a time delay," *Nonlinear Analysis: Hybrid Systems*, vol. 5, no. 4, pp. 613–625, 2011.

[7] Q. Zhang, X. Zhang, and C. Liu, "A singular bioeconomic model with diffusion and time delay," *Journal of Systems Science and Complexity*, vol. 24, no. 2, pp. 277–290, 2011.

[8] Q. Zhang, C. Liu, and X. Zhang, *Complexity, Analysis and Control of Singular Biological Systems*, Springer, London, UK, 2012.

[9] G. Zhang, Y. Shen, and B. Chen, "Hopf bifurcation of a predator-prey system with predator harvesting and two delays," *Nonlinear Dynamics*, vol. 73, no. 4, pp. 2119–2131, 2013.

[10] X. Meng and Q. Zhang, "Complex dynamics in a singular delayed bioeconomic model with and without stochastic fluctuation," *Discrete Dynamics in Nature and Society*, vol. 2015, Article ID 302494, 15 pages, 2015.

[11] W. Liu, C. Fu, and B. Chen, "Stability and hopf bifurcation of a predator-prey biological economic system with nonlinear harvesting rate," *International Journal of Nonlinear Sciences and Numerical Simulation*, vol. 16, no. 6, pp. 249–258, 2015.

[12] C. Liu, L. Yu, and Q. Zhang, "Optimal harvest control in a singular prey-predator fishery model with maturation delay and gestation delay," *Discrete Dynamics in Nature and Society*, vol. 2016, Article ID 4398527, 9 pages, 2016.

[13] C. Liu, N. Lu, Q. Zhang, J. Li, and P. Liu, "Modeling and analysis in a prey-predator system with commercial harvesting and double time delays," *Applied Mathematics and Computation*, vol. 281, pp. 77–101, 2016.

[14] M. Li, B. Chen, and H. Ye, "A bioeconomic differential algebraic predator-prey model with nonlinear prey harvesting," *Applied Mathematical Modelling*, vol. 42, pp. 17–28, 2017.

[15] X.-Y. Meng and Y.–Q. Wu, "Bifurcation analysis in a singular Beddington-DeAngelis predator-prey model with two delays and nonlinear predator harvesting," *Mathematical Biosciences and Engineering*, vol. 16, no. 4, pp. 2668–2696, 2019.

[16] B. Babaei and M. Shafiee, "Analysis and behavior control of a modified singular prey-predator model," *European Journal of Control*, vol. 49, pp. 107–115, 2019.

[17] M. Danca, S. Codreanu, and B. Bakó, "Detailed analysis of a nonlinear prey–predator model," *Journal of Biological Physics*, vol. 23, no. 1, pp. 11–20, 1997.

[18] Z. Jing and J. Yang, "Bifurcation and chaos in discrete-time predator-prey system," *Chaos, Solitons & Fractals*, vol. 27, no. 1, pp. 259–277, 2006.

[19] X. Liu and D. Xiao, "Complex dynamic behaviors of a discrete-time predator-prey system," *Chaos, Solitons & Fractals*, vol. 32, no. 1, pp. 80–94, 2007.

[20] H. N. Agiza, E. M. Elabbasy, H. EL-Metwally, and A. A. Elsadany, "Chaotic dynamics of a discrete prey-predator model with holling type II," *Nonlinear Analysis: Real World Applications*, vol. 10, no. 1, pp. 116–129, 2009.

[21] Q. Din, "Complexity and chaos control in a discrete-time prey-predator model," *Communications in Nonlinear Science and Numerical Simulation*, vol. 49, pp. 113–134, 2017.

[22] Q. Din, "Stability, bifurcation analysis and chaos control for a predator-prey system," *Journal of Vibration and Control*, vol. 25, no. 3, pp. 612–626, 2019.

[23] Z. He and X. Jiang, "Bifurcation and chaotic behaviour of a discrete-time variable-territory predator-prey model," *IMA Journal of Applied Mathematics*, vol. 76, no. 6, pp. 899–918, 2011.

[24] Z. He and X. Lai, "Bifurcation and chaotic behavior of a discrete-time predator-prey system," *Nonlinear Analysis: Real World Applications*, vol. 12, no. 1, pp. 403–417, 2011.

[25] B. Chen and J. Chen, "Bifurcation and chaotic behavior of a discrete singular biological economic system," *Applied Mathematics and Computation*, vol. 219, no. 5, pp. 2371–2386, 2012.

[26] X. Wu and B. Chen, "Bifurcations and stability of a discrete singular bioeconomic system," *Nonlinear Dynamics*, vol. 73, no. 3, pp. 1813–1828, 2013.

[27] W. Liu, D. Cai, and J. Shi, "Dynamic behaviors of a discrete-time predator-prey bioeconomic system," *Advances in Difference Equations*, vol. 2018, no. 1, p. 133, 2018.

[28] W. F. Lucas, *Modules in Applied Mathematics: Differential Equation Models*, Springer, New York, NY, USA, 1983.

[29] J. Carr, *Application of Center Manifold Theory*, Springer-Verlag, New York, NY, USA, 1981.

[30] J. Guckenheimer and P. Holmes, *Nonlinear Oscillations, Dynamical Systems, and Bifurcations of Vector Fields*, Springer-Verlag, New York, NY, USA, 1983.

[31] C. Robinson, *Dynamical Systems: Stability*, Symbolic Dynamics and Chaos, Boca Raton, NY, USA, 1999.

[32] S. Wiggins, *Introduction to Applied Nonlinear Dynamical Systems and Chaos*, Springer-Verlag, New York, NY, USA, 2003.

[33] Y.-H. Wan, "Computation of the stability condition for the hopf bifurcation of diffeomorphisms on $\mathbb{R}^2 $," *SIAM Journal on Applied Mathematics*, vol. 34, no. 1, pp. 167–175, 1978.

[34] Y. A. Kuznetsov, *Elements of Applied Bifurcation Theory*, Springer-Verlag, New York, NY, USA, 1997.

[35] X. Sun and Y. Xiao, "Multiscale system for environmentally-driven infectious disease with threshold control strategy," *International Journal of Bifurcation and Chaos*, vol. 28, no. 5, Article ID 1850064, 2018.

[36] B. S. Chen, X. X. Liao, and Y. Q. Liu, "Normal forms and bifurcations for the difference–algebraic systems," *Acta Mathematicae Applicatae Sinica*, vol. 23, no. 3, pp. 429–433, 2000, In Chinese.

[37] E. Ott, C. Grebogi, and J. A. Yorke, "Controlling chaos," *Physical Review Letters*, vol. 64, no. 11, pp. 1196–1199, 1990.

[38] F. J. Romeiras, C. Grebogi, E. Ott, and W. P. Dayawansa, "Controlling chaotic dynamical systems," *Physica D: Nonlinear Phenomena*, vol. 58, no. 1–4, pp. 165–192, 1992.

[39] E. H. Abed, H. O. Wang, and R. C. Chen, "Stabilization of period doubling bifurcations and implications for control of chaos," *Physica D: Nonlinear Phenomena*, vol. 70, no. 1-2, pp. 154–164, 1994.

[40] K. Ogata, *Modern Control Engineering*, Prentice-Hall, Englewood, NJ, USA, 2nd edition, 1997.

[41] G. Chen and X. Yu, "On time-delayed feedback control of chaotic systems," *IEEE Transactions on Circuits and Systems I: Fundamental Theory and Applications*, vol. 46, no. 6, pp. 767–772, 1999.

[42] G. Chen, J.-Q. Fang, Y. Hong, and H. Qin, "Controlling hopf bifurcations: discrete-time systems," *Discrete Dynamics in Nature and Society*, vol. 5, no. 1, pp. 29–33, 2000.

[43] X. S. Luo, G. Chen, B. Hong Wang, and J. Qing Fang, "Hybrid control of period-doubling bifurcation and chaos in discrete nonlinear dynamical systems," *Chaos, Solitons & Fractals*, vol. 18, no. 4, pp. 775–783, 2003.

[44] G. Wen, D. Xu, and J. Xie, "Controlling Hopf bifurcations of discrete-time systems in resonance," *Chaos, Solitons & Fractals*, vol. 23, no. 5, pp. 1865–1877, 2005.

[45] X. Zhang, Q.-l. Zhang, and V. Sreeram, "Bifurcation analysis and control of a discrete harvested prey-predator system with Beddington-DeAngelis functional response," *Journal of the Franklin Institute*, vol. 347, no. 7, pp. 1076–1096, 2010.

[46] L.-G. Yuan and Q.-G. Yang, "Bifurcation, invariant curve and hybrid control in a discrete-time predator-prey system," *Applied Mathematical Modelling*, vol. 39, no. 8, pp. 2345–2362, 2015.

[47] Q. Din, "A novel chaos control strategy for discrete-time brusselator models," *Journal of Mathematical Chemistry*, vol. 56, no. 10, pp. 3045–3075, 2018.

[48] Q. Din, N. Saleem, and M. S. Shabbir, "A class of discrete predator-prey interaction with bifurcation analysis and chaos control," *Mathematical Modelling of Natural Phenomena*, vol. 15, p. 60, 2020.

[49] Q. Din and K. Haider, "Discretization, bifurcation analysis and chaos control for Schnakenberg model," *Journal of Mathematical Chemistry*, vol. 58, no. 8, pp. 1615–1649, 2020.

[50] Q. Din and M. I. Khan, "A discrete–time model for consumer–resource interaction with stability, bifurcation and chaos control," *Qualitative Theory of Dynamical Systems*, vol. 20, no. 2, pp. 1–35, 2021.

Hindawi
Discrete Dynamics in Nature and Society
Volume 2021, Article ID 2400073, 5 pages
https://doi.org/10.1155/2021/2400073

Research Article

An Algorithm to Compute the H-Bases for Ideals of Subalgebras

Rabia,[1] Muhammad Ahsan Binyamin,[1] Nazia Jabeen,[2] Adnan Aslam,[3] and Kraidi Anoh Yannick[4]

[1]*Department of Mathematics, GC University, Faisalabad, Pakistan*
[2]*Department of Mathematical Sciences, Institute of Business Administration, Karachi, Pakistan*
[3]*Department of Natural Sciences, University of Engineering and Technology (RCET), Lahore, Pakistan*
[4]*UFR of Mathematics and Informatics, University Félix Houphouët Boigny, Abidjan, Côte d'Ivoire*

Correspondence should be addressed to Kraidi Anoh Yannick; kayanoh2000@yahoo.fr

Received 24 April 2021; Accepted 16 June 2021; Published 7 July 2021

Academic Editor: Qamar Din

The concept of H-bases, introduced long ago by Macauly, has become an important ingredient for the treatment of various problems in computational algebra. The concept of H-bases is for ideals in polynomial rings, which allows an investigation of multivariate polynomial spaces degree by degree. Similarly, we have the analogue of H-bases for subalgebras, termed as SH-bases. In this paper, we present an analogue of H-bases for finitely generated ideals in a given subalgebra of a polynomial ring, and we call them "HSG-bases." We present their connection to the SAGBI-Gröbner basis concept, characterize HSG-basis, and show how to construct them.

1. Introduction

The concept of H-bases, introduced long ago by Macaulay [1], is based solely on homogeneous terms of a polynomial. In [2], an extension of Buchberger's algorithm is presented to construct H-bases algorithmically. Some applications of H-bases are given in [3]; in addition, many of the problems in applications which can be solved by the Gröbner technique can also be treated successfully with H-bases. The concept of H-basis for ideals of a polynomial ring over a field K can be adopted in a natural way to K-subalgebras of a polynomial ring. In [4], SH-basis (Subalgebra Analogue to H-basis for Ideals) for the K-subalgebra of $K[x_1, \ldots, x_n]$ is defined. The properties of SH-bases are typically similar to H-basis results [3]. Like H-bases, the concept of SH-basis is also tied to homogeneous polynomials. In this paper, we will present an analogue to H-bases for ideals in a given subalgebra of a polynomial ring, and we call them "HSG-bases."

The paper is organized as follows. In Section 2, we briefly describe the underlying concept of grading which leads to SAGBI-Gröbner bases and HSG-basis. Then, we give the notion of *si*-reduction, which is one of the key ingredients for the characterization and construction of HSG-basis. After setting up the necessary notation, we present the *si*-reduction algorithm (see Algorithm 1). Also, here we present some properties characterizing HSG-basis (Theorem 1). In Section 3, we present a criterion through which we can check that the given system of polynomials is an HSG-basis of the subalgebra it generates (Theorem 2), and further on the basis of this theorem, we present an algorithm for the construction of HSG-basis (Algorithm 2).

2. HSG-Bases and SAGBI-Gröbner Bases

Here and in the following sections we consider polynomials in n variables $x_1, \ldots, x_n$ with coefficients from a field K. For short, we write

$$\mathrm{P} \coloneqq K[x_1, \ldots, x_n]. \tag{1}$$

If G is a subset of subalgebra $\mathscr{A}$ in $K[x_1, \ldots, x_n]$, then the set

$$I \coloneqq \left\{ \sum_{g \in G} h_g g | h_g \in \mathscr{A} \text{ and only finitely many } h_g \neq 0 \right\} \tag{2}$$

Input: a subalgebra $\mathscr{A}$, a finite subset $G \subset \mathscr{A}$, and a polynomial $f \in \mathscr{A}$.
Output: a polynomial h such that $f \longrightarrow_{G_A,*} h$.
(1) $h := f$.
(2) While $(h \neq 0$ and $G_h = \{\sum_i a_i g_i | M^{(H)}(\sum_i a_i g_i) = M^{(H)}(h)\} \neq \varnothing)$; where $a_i \in \mathscr{A}$ and $g_i \in G$.
(3) Choose $\sum_i a_i g_i \in G_h$.
(4) $h := h - \sum_i a_i g_i$ and continue at 2.

Algorithm 1: Algorithm to compute si-reduction

Input: a subalgebra $\mathscr{A}$ and a finite subset $G \subset \mathscr{A}$.
Output: HSG-basis H for $\langle G \rangle_{\mathscr{A}}$.
(1) $H := G$, $\mathrm{Old}(H) := \varnothing$.
(2) $H = \{h_1, \ldots, h_s\}$.
(3)While $(H \neq \mathrm{Old}(H))$ do
(4) Compute Q, an $M^{(H)}$–generating set for $syz(M^{(H)}(H))$.
(5) Compute P: $= \{\sum_{i=1}^{s} q_i h_i | (q_i)_{i=1}^{s} \in Q\}$.
(6) Compute $\mathrm{red}(P)$: $= \{$final si–reduction via H of every element of $P\} - \{0\}$.
(7) $\mathrm{Old}(H) := H \cup \mathrm{red}(P)$.

Algorithm 2: Algorithm for the construction of HSG basis.

is the ideal of A in P generated by G and we write it shortly as $\langle G \rangle_{\mathscr{A}}$. In this section, we want to introduce HSG-bases and discuss some of their properties. This concept is very similar to the concept of SAGBI-Gröbner bases. Therefore, we will briefly explain the underlying common structure. Let Γ denote an ordered monoid, i.e., an abelian semigroup under an operation $+$, equipped with a total ordering $>$ such that, for all $\alpha, \beta, \gamma \in \Gamma$,

$$\alpha > \beta \Rightarrow \alpha + \gamma > \beta + \gamma. \tag{3}$$

A direct sum,

$$\mathrm{P} = \bigoplus_{\gamma \in \Gamma} \mathrm{P}_{\gamma}^{(\Gamma)}, \tag{4}$$

is called grading (induced by Γ) or briefly a Γ-grading if for all $\alpha, \beta \in \Gamma$,

$$f \in \mathrm{P}_{\alpha}^{(\Gamma)}, g \in \mathrm{P}_{\beta}^{(\Gamma)} \Rightarrow f \cdot g \in \mathrm{P}_{\alpha+\beta}^{(\Gamma)}. \tag{5}$$

Since the decomposition above is a direct sum, each polynomial $f \neq 0$ has a unique representation.

$$f = \sum_{i=1}^{s} f_{\gamma_i}, \quad 0 \neq f_{\gamma_i} \in \mathrm{P}_{\gamma_i}^{(\Gamma)}. \tag{6}$$

Assuming that $\gamma_1 > \gamma_2 > \cdots > \gamma_s$, the Γ-homogeneous term f_{γ_1} is called the maximal part of f, denoted by $M^{(\Gamma)}(f) := f_{\gamma_1}$, and $f - M^{(\Gamma)}(f)$ is called the d-reductum of f. For $G \subset \mathscr{A}$, $M^{(\Gamma)}(G) := \{M^{(\Gamma)}(g) | g \in G\}$.

There are two major examples of gradings. The first one is grading by degrees:

$$\mathrm{P}_d^{(\Gamma)} = \{p \in \mathrm{P} | p \text{ is homogeneous of degree } d\}, \quad \forall d \in \mathbb{N}. \tag{7}$$

Here, $\Gamma = \mathbb{N}$ with the natural total ordering. This grading is called the H-grading because of the homogeneous polynomials. Therefore, we also write H in place of this Γ. The space of all polynomials of degree at most d can now be written as

$$\mathrm{P}_d := \oplus_{k=0}^{d} \mathrm{P}_k^{(H)}. \tag{8}$$

The maximal part of a polynomial $f \neq 0$ is its homogeneous form of highest degree, $M^{(H)}(f)$. For simplicity, let $M^{(H)}(0) := 0$.

Definition 1. A subset $G = \{g_1, \ldots, g_s\} \subset \mathscr{A}$ (subalgebra) is called HSG-basis for the ideal $I_{\mathscr{A}} \subset \mathscr{A}$, if for all $0 \neq f \in I_{\mathscr{A}}$,

$$\exists h_1, \ldots, h_s \in \mathscr{A}: f = \sum_{i=1}^{s} h_i g_i, \deg(f) = \max_{i=1}^{s} \{\deg(h_i g_i)\} \Big(\text{Note that this condition is not obvious, } -x^3 y^3 + x^4$$
$$= \left(x^2\right)\left(x^3 y + x^2\right) + (-xy)\left(x^4 + x^2 y^2\right) \text{ see in } K\left[x^2, xy\right]\Big). \tag{9}$$

The representation for f in (9) is also called its HSG representation with respect to G.

Note that HSG-basis for ideal in a subalgebra is also a generating set of it. To obtain more insights into HSG-bases, we will give some equivalent definitions. First, we need a more technical notion.

Definition 2. For given $f, f_1, \ldots, f_m$, we say that f si–reduces to $\tilde{f}$ with respect to $F = \{f_1, \ldots, f_m\}$ in $\mathscr{A}$ if

$$\widetilde{f} = f - \sum_{i=1}^{m} a_i f_i, \deg(\widetilde{f}) < \deg(f) \tag{10}$$

holds with polynomials $a_i \in \mathscr{A}$ satisfying $\deg(a_i f_i) \leq \deg(f)$. We write it as $f \longrightarrow_{F_{\mathscr{A}}} \widetilde{f}$. By $\longrightarrow_{F_{\mathscr{A}},*}$ we denote the transitive closure of the binary relation $\longrightarrow_{F_{\mathscr{A}}}$ 1.

The concept of *si*−reduction plays an important role in the characterization and construction of HSG-basis. For $f \in \mathscr{A}$ and $G \subset \mathscr{A}$, the following algorithm computes h such that $f \longrightarrow_{G_{\mathscr{A}},*} h$ (i.e., f reduces to h completely).

We note that such an element a_i in the subalgebra $\mathscr{A}$ can easily be determined as in the case of reduction in polynomial ring. We also note that $\deg(h - \sum_i a_i g_i)$ is strictly smaller than the $\deg(h)$ (by the choice of $\sum_i a_i g_i$). This shows that Algorithm 1 always terminates.

Theorem 1. *Let $G = \{g_1, \ldots, g_s\} \subset \mathscr{A}$ (subset of subalgebra $\mathscr{A}$) and $I_{\mathscr{A}}$ be an ideal of $\mathscr{A}$. Then, the following conditions are equivalent:*

(1) G is an HSG-basis for the ideal $I_{\mathscr{A}}$.

(2) $\langle M^{(H)}(g_1), \ldots, M^{(H)}(g_s) \rangle_{K[M(H)]} = \langle M^{(H)}(f) | f \in I_{\mathscr{A}} \rangle_{K[M(H)]}$.

(3) For all $f \in I$, $f \longrightarrow_{G_{\mathscr{A}},*} 0$.

Proof. (1)⇒(2). Let $M^{(H)}(p) \in \langle M^{(H)}(f) | f \in I_{\mathscr{A}} \rangle$ for some $p \in I_{\mathscr{A}}$. Since G is an HSG-basis, by (9), there are some $h_1, \ldots, h_s \in \mathscr{A}$ so that $p = \sum_{i=1}^{s} h_i g_i$ and $M^{(H)}(p) = M^{(H)}(\sum_{i=1}^{s} h_i g_i) = \sum_{i \in J} M^{(H)}(h_i) M^{(H)}(g_i) \in \langle M^{(H)}(g_1), \ldots, M^{(H)}(g_s)) \rangle$, where $J = \{i | \deg(h_i g_i) = \deg(p)\}$.

(2)⇒(3). Let $0 \neq f \in I_{\mathscr{A}}$. By using Algorithm 1, we get $f \longrightarrow_{F_{\mathscr{A}}} h_1 \longrightarrow_{F_{\mathscr{A}}} h_2 \ldots \longrightarrow_{F_{\mathscr{A}}} h$, where h is *si*−reduced any further with respect to F. $M^{(H)}(f) \in \langle M^{(H)}(g_1), \ldots, M^{(H)}(g_s) \rangle$ implies $M^{(H)}(f) = \sum_{i \in J} M^{(H)}(h_i) M^{(H)}(g_i)$; then, $f \longrightarrow_{G_{\mathscr{A}}} \widetilde{f} = f - \sum h_i g_i \in I_{\mathscr{A}}$. If we follow the above process inductively, then $f \longrightarrow_{G_{\mathscr{A}},*} 0$.

(3)⇒(1). Let

$$f_0 \longrightarrow_{G_{\mathscr{A}}} f_1 \longrightarrow_{G_{\mathscr{A}}} \cdots \longrightarrow_{G_{\mathscr{A}}} f_d = 0, \tag{11}$$

where $M^{(H)}(f_{i-1}) = \sum_{j=1}^{s} M^{(H)}(h_{ij}) M^{(H)}(g_j)$, $i = 1, 2, \ldots, d$, $\deg(f_{i-1}) > \deg(f_i)$. Then,

$$f = \sum_{j=1}^{s} \sum_{i=1}^{d} M^{(H)}(h_{ij}) M^{(H)}(g_j). \tag{12}$$

Note that

$$\deg(f) = \deg(f_\circ) = \deg\left(\sum_{j=1}^{s} M^{(H)}(h_{1j}) M^{(H)}(g_j) \right), \tag{13}$$

and

$$\deg\left(\sum_{j=1}^{s} M^{(H)}(h_{ij}) M^{(H)}(g_j) \right) > \deg\left(\sum_{j=1}^{s} M^{(H)}(h_{i+1,j}) M^{(H)}(g_j) \right), \; i = 1, 2, \ldots, d. \tag{14}$$

Hence,

$$\deg(f) = \max_i \left(\deg\left(\sum_{j=1}^{s} M^{(H)}(h_{ij}) M^{(H)}(g_j) \right) \right). \tag{15}$$

(11) and (15) give the HSG representation. □

The second major example of gradings leads to the SAGBI-Gröbner basis concept. Here, $\Gamma = \mathbb{N}^n$ with component-wise addition equipped with a total ordering satisfying (11). In addition, $\gamma \geq 0$, $\forall \gamma \in \Gamma$. For arbitrary $\gamma = (\gamma_1, \ldots, \gamma_n) \in \Gamma$, the space $\mathrm{P}_\gamma^{(\Gamma)}$ is a vector space of dimension 1, namely,

$$\mathrm{P}_\gamma^{(\Gamma)} = \{c \cdot x^{\gamma_1} \ldots x^{\gamma_n} | c \in K\}. \tag{16}$$

The maximal part $M^{(\Gamma)}(f)$ of a polynomial f is a product of a leading coefficient $\mathrm{LC}(f)$ and a leading monomial $\mathrm{LM}(f)$, that is $M^{(\Gamma)}(f) = \mathrm{LC}(f) \cdot \mathrm{LM}(f)$, where $\mathrm{LC}(f) \in K$. The si-reduction $f \longrightarrow_{G_{\mathscr{A}}} \widetilde{f}$ is defined if there exists a polynomial $g \in G$ and $a \in \mathscr{A}$ such that $\mathrm{LM}(f) = \mathrm{LM}(g)\mathrm{LM}(a)$ and then we set $\widetilde{f} := (f - (M^{(\Gamma)}(f))/(M^{(\Gamma)}(g) M^{(\Gamma)}(a)) a g)$. The relation $\longrightarrow_{G_{\mathscr{A}},*}$ is constructed as above.

A SAGBI-Gröbner basis G (with respect to a given monomial ordering and a given ideal $I_{\mathscr{A}}$ in a subalgebra $\mathscr{A}$) is a set of polynomials generating $I_{\mathscr{A}}$ and satisfying one of the following equivalent conditions:

(i) Every $f \in I_{\mathscr{A}}$ has a representation:

$$f = \sum_{i=1}^{s} h_i g_i, \qquad \mathrm{LM}(f) = \max_{i=1}^{s} \{\mathrm{LM}(h_i)\mathrm{LM}(g_i)\}, \tag{17}$$

where $h_i \in \mathscr{A}$ and $g_i \in G$.

(ii) $\langle M^{(\Gamma)}(g) | g \in G \rangle = \langle M^{(\Gamma)}(f) | f \in I_{\mathscr{A}} \rangle$.

(iii) Every $f \in I_{\mathscr{A}}$ *si*-reduces to 0 with respect to G.

The proof of this equivalence and many other equivalent conditions can be found in [5]. If a monomial ordering is compatible with the semiordering by degrees,

$$\deg(x^\gamma) > \deg(x^\beta) \Rightarrow \gamma > \beta, \gamma, \beta \in \mathbb{N}^n, \tag{18}$$

then any SAGBI-Gröbner representation as given in (i) is an HSG representation; in other words, a SAGBI-Gröbner basis with respect to a degree compatible ordering is an HSG-basis as well. The converse is false, as the following example shows.

Example 1. Let $f_1 = x^4 + 2x^2y^2 + y^4 - 1$, $f_2 = x^2y^2 + y^4 - 2$, $f_3 = 2x^2 + y^2$. These polynomials belong to the subalgebra $\mathscr{A} = \mathbb{Q}[x^2, y^2]$. Then, we can see that f_1, f_2, and f_3 already constitute an HSG-basis for ideal $I_{\mathscr{A}} = \langle f_1, f_2, f_3\rangle$ in $\mathscr{A}$. If we order the monomials by degree lexicographical ordering, then $\langle M^{(H)}(f) | f \in I_{\mathscr{A}}\rangle_{\mathbb{Q}[M^{(H)}(\mathscr{A})]} = \langle x^4, x^2y^2, x^2\rangle_{\mathbb{Q}[M^{(H)}(\mathscr{A})]}$. Every SAGBI-Gröbner basis G with respect to this ordering contains at least four elements, for instance, $G = \{g_1, g_2, g_2, g_4\}$ with $g_1 = x^4 + 2x^2y^2 + y^4 - 1 = f_1$, $g_2 = x^2y^2 + y^4 - 2 = f_2$, $g_3 = 2x^2 + y^2 = f_3$, and $g_4 = y^4 - 4$. Obviously, this SAGBI-Gröbner basis is an HSG-basis as well.

3. Construction of HSG-Bases

In this section, we present an HSG-basis criterion, through which we can construct HSG-basis. For this purpose, we fix some notations which are necessary for this construction. Let $\mathscr{A}$ be a K−subalgebra of $K[x_1, \ldots, x_n]$.

(i) We denote $\mathscr{A} \oplus \ldots \oplus \mathscr{A}$ (s − times) by $\oplus_S \mathscr{A}$.

(ii) For a subset $G \subseteq \mathscr{A}$, we denote $\{M^{(H)}(\overset{S}{g_i}) | g_i \in G\}$ by $M^{(H)}(G)$.

Definition 3. For K−subalgebra $\mathscr{A}$ of $K[x_1, \ldots, x_n]$ and a subset $G = \{g_1, \ldots, g_s\} \subseteq \mathscr{A}$,

(1) $syz_{\mathscr{A}}(G) = \{\overrightarrow{a} = (a_i)_{i=1}^s \in \oplus_S \mathscr{A} | \sum_{i=1}^s a_i g_i = 0\}$. We call an element of $syz_{\mathscr{A}}(G)$ an $\mathscr{A}$−syzygy of G.

(2) For $\overrightarrow{a} = (a_i)_{i=1}^s \in \oplus_S \mathscr{A}$, let $M^{(H)}(\overrightarrow{a})$ represent the vector $(M^{(H)}(a_i))_{i=1}^s$.

Definition 4. We call a subset $Q = \{\overrightarrow{q_1}, \overrightarrow{q_2}, \ldots, \overrightarrow{q_m}\}$ a $M^{(H)}$-generating set for $syz(M^{(H)}(G))$ if $\{M^{(H)}(\overrightarrow{q_i}) | 1 \le i \le m\}$ generates the $K[M^{(H)}(\mathscr{A})]$-module $syz[M^{(H)}(G)]$, i.e., for $\overrightarrow{a} \in syz[M^{(H)}(G)]$, there are some $h_1, h_2, \ldots h_m \in M^H(\mathscr{A})$ such that

$$M^{(H)}(a_i)_{i=1}^s = \sum_{j=1}^m M^{(H)}(h_j) M^{(H)}(q_{ij})_{i=1}^s. \tag{19}$$

In the case of SAGBI-Gröbner bases, there is an algorithm for computing SAGBI-Gröbner bases by means of syzygies (see [6]) where syzygies and their connection to SAGBI-Gröbner bases are studied in detail. The analogue for constructing HSG-bases by means of syzygies is connected to the following result [7].

Theorem 2 *(HSG-basis criterion). Let $G = \{g_1, \ldots, g_s\}$ be the subset of a subalgebra $\mathscr{A}$. Let Q be $M^{(H)}$−generating set for the $syz(M^{(H)}(G))$. Then, G is an HSG-basis for $\langle G\rangle_{\mathscr{A}}$ if and only if for every $\overrightarrow{q_j} = (q_{j,1}, \ldots, q_{j,s}) \in Q$, we have $\sum_{i=1}^s q_{j,i} g_i \longrightarrow_{G_{\mathscr{A},*}} 0$.*

Proof. $\Rightarrow$: The statement is a direct result of Theorem 1.

$\Leftarrow$: Take $f \in \langle G\rangle_{\mathscr{A}}$. We need to show that $M^{(H)}(f) \in \langle M^{(H)}(G)\rangle_{K[M^{(H)}(\mathscr{A})]}$. For this, we write $f = \sum_{i=1}^m a_i g_i$ such that $p_0 = \max[M^{(H)}(a_i g_i)]$ (degree wise) is minimal among all such representations of f. We have $M^{(H)}(f) \le p_0$. Suppose that $M^{(H)}(f) < p_0$. Assume that $a_1 g_1, \ldots, a_{m_0} g_{m_0}$ are contributing to p_0, i.e., $M^{(H)}(a_i g_i) = p_0$ for all $1 \le i \le m_0$. If we set $\overrightarrow{a} = (a_1, \ldots, a_{m_0}, 0, \ldots, 0)$, we can see that $M^{(H)}(\overrightarrow{a}) \in syz(M^{(H)}(G))$. This implies that there are $b_1, \ldots, b_n \in \mathscr{A}$ and $\overrightarrow{Q_1}, \ldots, \overrightarrow{Q_n} \in \overrightarrow{Q}$ such that $M^{(H)}(\overrightarrow{a}) = \sum_{j=1}^n M^{(H)}(b_j) M^{(H)}(\overrightarrow{Q_j})$. We may assume that $M^{(H)}(b_j) M^{(H)}(q_{j,i}) M^{(H)}(g_i) = p_0$ for each j by homogeneity of the syzygies. Now,

$$\begin{aligned} f &= \sum_{i=1}^m a_i g_i - \sum_{i=1}^m \left(\sum_{j=1}^n b_j q_{j,i}\right) g_i + \sum_{j=1}^n b_j \left(\sum_{i=1}^m q_{j,i} g_i\right) \\ &= \sum_{i=1}^m \left(a_i - \sum_{j=1}^n b_j q_{j,i}\right) g_i + \sum_{j=1}^n b_j \left(\sum_{i=1}^m p_{j,i} g_i\right), \end{aligned} \tag{20}$$

where $\sum_{i=1}^m p_{j,i} g_i$ is an HSG representation for $\sum_{i=1}^m q_{j,i} g_i$ since $\sum_{i=1}^m q_{j,i} g_i \longrightarrow^G 0$. If we define $H_j = \max(M^{(H)}(p_{j,i} g_i))$, then

$$H_j = M^{(H)}\left(\sum q_{j,i} g_i\right) < \max\left(M^{(H)}\left(q_{j,i} g_i\right)\right), \quad \text{for all } j, \tag{21}$$

because $M^{(H)}(\overrightarrow{Q_j}) \in syz(M^{(H)}(G))$.

Consider the first sum of equation (20). For $i \le m_0$, we have $M^{(H)}(a_i) = M^{(H)}(\sum_{j=1}^n b_j q_{j,i})$, so by the cancellation of highest terms,

$$M^{(H)}\left[\left(a_i - \sum_{j=1}^n b_j q_{j,i}\right) g_i\right] < M^{(H)}(a_i g_i) = p_0. \tag{22}$$

For $i > m_0$, $M^{(H)}(a_i g_i) < p_0$ and $\sum_{j=1}^n M^{(H)}(b_j) M^{(H)}(q_{j,i}) = 0$ implies that

$$M^{(H)}\left(\sum_{j=1}^n b_j q_{j,i} g_i\right) < \max_j\left(M^{(H)}\left(b_j q_{j,i} g_i\right)\right) = p_0. \tag{23}$$

Since

$$M^{(H)}\left[\left(a_i - \sum_{j=1}^n b_j q_{j,i}\right) g_i\right] \le \max\left\{M^{(H)}(a_i g_i), M^{(H)}\left(\sum_{j=1}^n b_i q_{j,i} g_i\right)\right\} < p_0 \,(\forall i). \tag{24}$$

So, first sum of equation (20) is less than p_0. For the second sum of equation (20), we have

$$\begin{aligned} M^{(H)}\left(\sum_{j=1}^{n} b_j \sum_{i=1}^{m} p_{j,i} g_i\right) &\leq \max_{i,j} M^{(H)}\left(b_j p_{j,i} g_i\right) \\ &\leq \max_j \left[M^{(H)}\left(b_j\right) H_j\right] \\ &< \max_{i,j}\left(M^{(H)}\left(b_j q_{j,i} g_i\right)\right) = p_0. \end{aligned} \tag{25}$$

Hence, equation (20) does provide a new representation for f such that $\max(M^{(H)}(a_i g_i)) < p_0$, a contradiction. Therefore, $M^{(H)}(f) = p_0$ and $M^{(H)}(f) = \sum_{i=1}^{m_0} M^{(H)}(a_i g_i) \in \langle M^{(H)}(G)\rangle$. □

On the basis of Theorem 2, now we present an algorithm which computes HSG-basis from a given set of generators. This algorithm is not necessarily terminating but does terminate, if and only if, the considered ideal in the subalgebra has a finite HSG-basis.

Now we present some examples which show the computation of HSG-basis through Algorithm 2.

Example 2. Let the subalgebra $\mathscr{A} = Q[x^2, xy]$ and $G = \{x^3y + x^2, xy + 2\} \subseteq \mathscr{A}$. Consider $H = G$; then, $M^{(H)}(H) = \{x^3y, xy\}$.

First pass through the while loop:

(i) $M^{(H)}(q_1)(x^3y) + M^{(H)}(q_2)(xy) = 0$ implies $Q = \{(-1, x^2)\}$. Then, $(-1)(x^3y + x^2) + (x^2)(xy + 2) = -x^3y - x^2 + x^3y + 2x^2 = x^2$ gives $P = \{x^2\}$.
(ii) As x^2 is *si*-reduced with respect to H, $\mathrm{red}(P) = \{x^2\}$.
(iii) Define: $\mathrm{Old}(H) = H \cup \{x^2\}$.
As $H \neq \mathrm{Old}(H)$, we repeat the whole process. Now we have $M^{(H)}(H) = \{x^3y, xy, x^2\}$.

Second pass through the while loop:

(i) $M^{(H)}(q_1)(x^3y) + M^{(H)}(q_2)(xy) + M^{(H)}(q_3)(x^2) = 0$ implies $(-1)(x^3y) + (0)(xy) + (xy)(x^2) = 0$. Therefore, $Q = \{(-1, x^2, 0), (-1, 0, xy)\}$. Then, $(-1)(x^3y + x^2) + (0)(xy + 2) + (xy)(x^2) = -x^3y - x^2 + 0 + x^3y = -x^2$ gives $P = \{x^2, -x^2\}$.
(ii) Now, $\mathrm{red}(P) = \varnothing$.

Since $\mathrm{Old}(H) = H$, we stop here. The HSG-basis for $\langle G\rangle_{\mathscr{A}}$ is $\{x^3y + x^2, xy + 2, x^2\}$.

Example 3. Let $\mathscr{A} = Q[x^2, xy]$ and $G = \{x^3y + x^2y^2 + x^2, xy + 2\} \subseteq \mathscr{A}$. Consider $H = G$; then, $M^{(H)}(H) = \{x^3y + x^2y^2, xy\}$.

First pass through the while loop:

(i) $M^{(H)}(q_1)(x^3y + x^2y^2) + M^{(H)}(q_2)(xy) = 0$ gives $Q = \{(-1, x^2 + xy)\}$. Then, from $(-1)(x^3y + x^2y^2 + x^2) + (x^2 + xy)(xy + 2) = -x^3y - x^2y^2 - x^2 + x^3y + x^2y^2 + 2x^2 + 2xy = x^2 + 2xy$,
(ii) $\mathrm{red}(P) = \{x^2 - 4\}$.
(iii) Define: $\mathrm{Old}(H) = H \cup \{x^2 - 4\}$.

As $H \neq \mathrm{Old}(H)$, we repeat the whole process. Now we have $M^{(H)}(H) = \{x^3y + x^2y^2, xy, x^2\}$.

Second pass through the while loop:

(i) From the equation $M^{(H)}(q_1)(x^3y + x^2y^2) + M^{(H)}(q_2)(xy) + M^{(H)}(q_3)(x^2) = 0$, we have $Q = \{(-1, xy, xy), (-1, x^2 + xy, 0)\}$. We can compute P from $(-1)(x^3y + x^2y^2 + x^2) + (xy)(xy + 2) + (xy)(x^2 - 4) = -x^3y - x^2y^2 - x^2 + x^2y^2 + 2xy + x^3y - 4xy = -x^2 - 2xy$.
(ii) Now, $\mathrm{red}(P) = \varnothing$.

Since $\mathrm{Old}(H) = H$, we stop here. The HSG-basis for $\langle G\rangle_{\mathscr{A}}$ is $\{x^3y + x^2y^2 + x^2, xy + 2, x^2 - 4\}$.

4. Conclusion

In this paper, we presented the theory of HSG-bases, which are a good basis of an ideal in a subalgebra of a polynomial ring. We can further develop this theory for an arbitrary grading for which HSG-bases would be a special case for degree-based grading.

Data Availability

No data are required to support the study.

Conflicts of Interest

The authors declare that they have no conflicts of interest.

References

[1] F. S. Macaulay, "The algebraic theory of modular systems," *Cambridge Tracts in Mathematics and Mathematical Physics*, Cambridge University Press, Cambridge, UK, 1916.
[2] T. Sauer, "Gröbner bases, H-bases and interpolation," *Transactions of the American Mathematical Society*, vol. 353, no. 6, pp. 2293–2308, 2000.
[3] H. M. Möller and T. Sauer, "H-bases for polynomial interpolation and system solving," *Advances in Computational Mathematics*, vol. 12, no. 4, pp. 335–362, 2000.
[4] J. A. Khan, M. A. Binyamin, and S. Rabia, "Subalgebra analogue to H-basis for ideals," *Hacettepe Journal of Mathematics and Statistics*, vol. 6, no. 45, pp. 1685–1692, 2016.
[5] L. Robbiano and M. Sweedler, *Subalgebra Bases in Commutative Algebra*, Springer, Berlin, Germany, 1990.
[6] J. L. Miller, *Effective Algorithms for Intrinsically Computing SAGBI-Gröbner Bases in a Polynomial Ring over a Field*, pp. 421–433, Cambridge University Press, Cambridge, UK, 1998.
[7] J. L. Miller, "Analogs of gröbner bases in polynomial rings over a ring," *Journal of Symbolic Computation*, pp. 139–153, 2008.

Hindawi
Discrete Dynamics in Nature and Society
Volume 2021, Article ID 6629074, 8 pages
https://doi.org/10.1155/2021/6629074

Research Article

Exact Solutions of the Two-Dimensional Cattaneo Model Using Lie Symmetry Transformations

Khudija Bibi[1] **and Khalil Ahmad**[2]

[1]*Department of Mathematics, Faculty of Basic and Applied Sciences, International Islamic University, Islamabad 44000, Pakistan*
[2]*Department of Mathematics, Faculty of Basic and Applied Sciences, Air University, PAF Complex E-9, Islamabad 44000, Pakistan*

Correspondence should be addressed to Khudija Bibi; khudija.bibi@iiu.edu.pk

Received 17 December 2020; Revised 14 February 2021; Accepted 26 March 2021; Published 10 April 2021

Academic Editor: Paolo Renna

In this article, symmetry technique is utilized to obtain new exact solutions of the Cattaneo equation. The infinitesimal symmetries, linear combinations of these symmetries, and corresponding similarity variables are determined, which lead to many exact solutions of the considered equation. By applying similarity transformations, the mentioned partial differential equation is reduced to some ordinary differential equations of second order. Solutions of these ordinary differential equations have yielded many exact solutions of the Cattaneo equation.

1. Introduction

In the diffusion phenomenon, considered by the traditional Fick law and Fourier law, the moment a point passes by that is disturbed at a great distance, and the propagation speed of the disturbance appears infinite. However, this property is nonphysical. To handle this problem, Cattaneo proposed a model [1], in which he modified the constitutive equation by presenting a relaxation parameter which plays the role of relaxation time, where this relaxation parameter is small and depends on the thermodynamic properties of the material. From the mathematical aspect, Cattaneo model transforms the traditional diffusion equation into a hyperbolic equation, the speed of propagation is finite, and it improves the property of infinite propagation speed. On the contrary, because of the hyperbolic nature of the Cattaneo model, it can possess oscillatory solutions and negative values.

From the physical aspect, the Cattaneo model describes a physical phenomenon of heat waves. Although this phenomenon can only be observed under special states [2], circumstances, or materials, it is still gradually accepted by the community. It can be used to describe not only heat pulse propagation in some pure nonmetallic crystals [3] but also ultrasonic wave propagation in certain diluted gases. Straughan [4] considered thermal convection with the Cattaneo–Christov model in horizontal layers of an incompressible Newtonian fluid. Haddad [5] applied the theory of Cattaneo–Christov to study Brinkman's porous media. Cattaneo model is mostly used in crystalline solids [6–8], extended irreversible thermodynamics, and cosmological models.

Because of many advantages of the fractional differential equations, many scholars have introduced numerous analytical and numerical methods to study various fractional models. As Cattaneo model has wide applications in physics and theoretical analysis, so many researchers devoted themselves for the solution and generalization of the Cattaneo model. Compte and Metzler [9] generalized the Cattaneo model from three aspects which are continuous-time random walks, delayed flux-force relation, and nonlocal transport theory. Ferrillo et al. [10] compared the Cattaneo model and fractional Cattaneo model and investigated the

asymptotic behavior of solutions to the Cattaneo equations. Su et al. [11] compared the solution of a phase-lagging heat transport equation with the solution of the classical Cattaneo equation.

There exist many well-known techniques for obtaining exact solutions of the partial differential equations [12–15], but one of them is a powerful Lie group method. By using Lie group analysis, one can also find the similarity solutions of the partial differential equations. These similarity solutions lead to the exact solutions of partial differential equations. Many researchers have used this method to find solutions of partial differential equations, e.g., see in [16–20]. In the current article, exact solutions of the Cattaneo equation via the similarity transformations are obtained.

This paper is arranged into four sections as follows: in Section 2, Lie symmetry generators of the Cattaneo equation are presented. In Section 3, the considered equation is converted into some ODEs by considering the similarity variables which are obtained by taking different linear combinations of the symmetry generators, while in Section 4, the graphical representations of solutions which are obtained in Section 3 are presented. Finally, in Section 5, the summary of the present work is discussed.

2. Lie Symmetries of the Cattaneo Equation

The main goal of this paper is to investigate the exact solutions of the following Cattaneo model [21],

$$C^2 w_{tt} + w_t - D\left(w_{xx} + w_{yy}\right) = 0, \tag{1}$$

by using its symmetry analysis. In the above model, C is a relaxation parameter, and D is a diffusion coefficient.

The method to obtain the Lie symmetries of the partial differential equations has been discussed in many books, e.g., see in [22–25]. Let

$$X = \phi_1(x, y, t, w)\partial_x + \phi_2(x, y, t, w)\partial_y + \phi_3(x, y, t, w)\partial_t + \eta(x, y, t, w)\partial_w \tag{2}$$

be the vector field that generates the symmetry group of equation (1). By applying the second-order prolongation of X to equation (1), the following determining equations are obtained:

$$\begin{aligned}
\eta_{t,t} &= \frac{D\eta_{y,y} + D\eta_{x,x} - \eta_t}{C^2},\\
\eta_{t,w} &= 0,\\
\eta_{w,w} &= 0,\\
\eta_{w,x} &= -\frac{1}{2}\frac{(\phi_1)_t}{D},\\
(\phi_1)_w &= 0,\\
(\phi_1)_x &= 0,\\
(\phi_1)_{t,t} &= 0,\\
(\phi_1)_{t,y} &= 0,\\
(\phi_1)_{y,y} &= 0,\\
(\phi_2)_w &= 0,\\
(\phi_2)_x &= -(\phi_1)_y,\\
(\phi_2)_y &= 0,\\
(\phi_2)_{t,t} &= 0,\\
(\phi_3)_t &= 0,\\
(\phi_3)_w &= 0,\\
(\phi_3)_x &= \frac{(\phi_1)_t C^2}{D},\\
(\phi_3)_y &= \frac{(\phi_2)_t C^2}{D}.
\end{aligned} \tag{3}$$

The infinitesimals obtained by solving the above system are

$$\begin{aligned}
\eta &= C_4 w - \frac{1}{2}C_6\frac{wx}{D} - \frac{1}{2}C_7\frac{wy}{D},\\
\phi_1 &= C_5 y + C_6 t + C_1,\\
\phi_2 &= -C_5 x + C_7 t + C_2,\\
\phi_3 &= C_6\frac{C^2 x}{D} + C_7\frac{C^2 y}{D} + C_3.
\end{aligned} \tag{4}$$

Thus, Cattaneo equation (1), is spanned by the following vector fields:

$$
\begin{aligned}
X_1 &= \partial_x,\\
X_2 &= \partial_y,\\
X_3 &= \partial_t,\\
X_4 &= w\partial_w,\\
X_5 &= y\partial_x - x\partial_y,\\
X_6 &= t\partial_x + \frac{C^2 x}{D}\partial_t - \frac{1}{2}\frac{wx}{D}\partial_w,\\
X_7 &= t\partial_y + \frac{C^2 y}{D}\partial_t - \frac{1}{2}\frac{wy}{D}\partial_w,
\end{aligned}
\tag{5}
$$

which form a seven-dimensional Lie algebra.

3. Exact Solutions of the Cattaneo Model Obtained by considering Similarity Transformations

In this section, some group-invariant solutions of Cattaneo equation (1) by considering different linear combinations of the Lie symmetry generators which have been obtained in Section 2 are presented.

(1) The similarity variables corresponding to

$$X_1 + X_2 + X_3 + X_4 = \partial_x + \partial_y + \partial_t + w\partial_w, \tag{6}$$

are

$$
\begin{aligned}
\nu &= y - x,\\
\gamma &= t - x,\\
\mu(\nu,\gamma) &= \frac{w}{\exp(x)}.
\end{aligned}
\tag{7}
$$

The dependent variable μ given in (7) indicates that the solution of (1) is in the form

$$w = \mu\ \exp(x). \tag{8}$$

Now, we consider the independent variables given in (7) one by one to seek the solution of (1).

First, if we consider the following similarity variables,

$$
\begin{aligned}
\nu &= y - x,\\
\mu(\nu) &= \frac{w}{\exp(x)},
\end{aligned}
\tag{9}
$$

then equation (1) is reduced into the following linear ODE:

$$2\mu_{\nu\nu} - 2\mu_\nu + \mu = 0, \tag{10}$$

with the solution

$$\mu(\nu) = C_1 \exp\left(\frac{1}{2}\nu\right)\sin\left(\frac{1}{2}\nu\right) + C_2 \exp\left(\frac{1}{2}\nu\right)\cos\left(\frac{1}{2}\nu\right). \tag{11}$$

Now, by considering the similarity variables

$$
\begin{aligned}
\gamma &= t - x,\\
\mu(\gamma) &= \frac{w}{\exp(x)},
\end{aligned}
\tag{12}
$$

equation (1) is converted into the following ODE:

$$C^2\mu_{\gamma\gamma} + \mu_\gamma - D\left(\mu - 2\mu_\gamma + \mu_{\gamma\gamma}\right) = 0, \tag{13}$$

with the solution

$$\mu(\gamma) = C_3 \exp\left(\frac{-(1/2)\left(-1 - 2\ D - \sqrt{1 + 4\ D + 4\ DC^2}\right)\gamma}{C^2 - D}\right) + C_4 \exp\left(\frac{-(1/2)\left(-1 - 2\ D + \sqrt{1 + 4\ D + 4\ DC^2}\right)\gamma}{C^2 - D}\right). \tag{14}$$

Since both solutions of (1) given in (11) and (14) are linearly independent,

$$w(x, y, t) = \exp(x)(\mu(\nu) + \mu(\gamma)), \tag{15}$$

i.e.,

$$w(x,y,t)=\exp(x)\left(\begin{array}{c} C_1\exp\left(\frac{1}{2}\nu\right)\sin\left(\frac{1}{2}\nu\right)+C_2\exp\left(\frac{1}{2}\nu\right)\cos\left(\frac{1}{2}\nu\right)+C_3\exp\left(\frac{-(1/2)\left(-1-2\ D-\sqrt{1+4\ D+4\ DC^2}\right)\gamma}{C^2-D}\right)+ \\ C_4\exp\left(\frac{-(1/2)\left(-1-2\ D+\sqrt{1+4\ D+4\ DC^2}\right)\gamma}{C^2-D}\right) \end{array}\right). \tag{16}$$

Putting values of ν and γ in the above equation, we obtain that

$$w(x,y,t)=\exp(x)\left(\begin{array}{c} C_1\exp\left(\frac{1}{2}(y-x)\right)\sin\left(\frac{1}{2}(y-x)\right)+C_2\exp\left(\frac{1}{2}(y-x)\right)\cos\left(\frac{1}{2}(y-x)\right) \\ +C_3\exp\left(\frac{-(1/2)\left(-1-2\ D-\sqrt{1+4\ D+4\ DC^2}\right)(t-x)}{C^2-D}\right)+ \\ C_4\exp\left(\frac{-(1/2)\left(-1-2\ D+\sqrt{1+4\ D+4\ DC^2}\right)(t-x)}{C^2-D}\right) \end{array}\right), \tag{17}$$

is a solution of (1).

(2) The similarity variables corresponding to

$$X_5=y\partial_x-x\partial_y, \tag{18}$$

are

$$\begin{aligned} \nu&=t,\\ \gamma&=x^2+y^2,\\ \mu(\nu,\gamma)&=w. \end{aligned} \tag{19}$$

The dependent variable μ given in (19) indicates that the solution of (1) is in the form

$$w=\mu. \tag{20}$$

Again, we consider the independent variables one by one given in (19) to seek solutions of (1). Thus, by using $\nu=t$ and $\mu(\nu)=w$, equation (1) is transformed into an ODE

$$\mu_\nu+C^2\mu_{\nu\nu}=0, \tag{21}$$

with the solution

$$\mu(\nu)=C_1\exp\left(\frac{-\nu}{C^2}\right)+C_2. \tag{22}$$

And by considering

$$\begin{aligned} \gamma&=x^2+y^2,\\ \mu(\gamma)&=w, \end{aligned} \tag{23}$$

equation (1) is transformed into the following ODE:

$$\mu_\gamma+\gamma\mu_{\gamma\gamma}=0, \tag{24}$$

with the solution

$$\mu(\gamma)=C_3\ln(\gamma)+C_4. \tag{25}$$

By combining solutions given in (22) and (25), we get that

$$w(x,y,t)=C_1\exp\left(\frac{-\gamma}{C^2}\right)+C_3\ln(\gamma)+C_2+C_4, \tag{26}$$

i.e.,

$$w(x,y,t)=C_1\exp\left(\frac{-t}{C^2}\right)+C_3\ln\left(x^2+y^2\right)+C_5, \tag{27}$$

is a solution of (1).

(3) The similarity variables corresponding to

$$X_4+X_5=y\partial_x-x\partial_y+\partial_w, \tag{28}$$

are

$$\nu = x^2 + y^2,$$
$$\gamma = t, \tag{29}$$
$$\mu(\nu,\gamma) = \frac{w}{\exp(\arctan(x/y))}.$$

The dependent variable μ given in (29) indicates that the solution of (1) is in the form

$$w = \mu \exp\left(\arctan\left(\frac{x}{y}\right)\right). \tag{30}$$

By considering

$$\nu = x^2 + y^2,$$
$$\mu(\nu) = \frac{w}{\exp(\arctan(x/y))}, \tag{31}$$

equation (1) is transformed into the following ODE:

$$\nu^2\mu_{\nu\nu} + \nu\mu_\nu + \frac{1}{4}\mu = 0, \tag{32}$$

with the solution

$$\mu(\nu) = C_1 \sin\left(\frac{1}{2}\ln(\nu)\right) + C_2 \cos\left(\frac{1}{2}\ln(\nu)\right). \tag{33}$$

Thus,

$$w(x,y,t) = \exp\left(\arctan\left(\frac{x}{y}\right)\right)\mu(\nu) \text{ or } w(x,y,t) = \exp\left(\arctan\left(\frac{x}{y}\right)\right)\left(C_1 \sin\left(\frac{1}{2}\ln(\nu)\right) + C_2 \cos\left(\frac{1}{2}\ln(\nu)\right)\right), \tag{34}$$

i.e.,

$$w(x,y,t) = \exp\left(\arctan\left(\frac{x}{y}\right)\right)\left(C_1 \sin\left(\frac{1}{2}\ln\left(x^2+y^2\right)\right) + C_2 \cos\left(\frac{1}{2}\ln\left(x^2+y^2\right)\right)\right), \tag{35}$$

is a solution of (1).

Here, we neglect the similarity variables $\gamma = t$ and $\mu(\gamma) = (w/\exp(\arctan(x/y)))$ because corresponding to these variables, equation (1) is not transformed into an ODE.

(4) The similarity variables corresponding to

$$X_6 = t\partial_x + \frac{C^2 x}{t}\partial_t - \frac{1}{2}\frac{wx}{D}\partial_w \tag{36}$$

are

$$\nu = y,$$
$$\gamma = \frac{-C^2x^2 + t^2D}{D}, \tag{37}$$
$$\mu(\nu,\gamma) = \frac{w}{\exp\left(-(1/2)\left(t/C^2\right)\right)}.$$

By considering $\nu = y$ and $\mu(\nu) = (w/\exp(-(1/2)(t/C^2)))$, equation (1) is transformed into an ODE

$$D\mu_{\nu\nu} + \frac{1}{4C^2}\mu = 0, \tag{38}$$

with the solution

$$\mu(\nu) = C_1 \sin\left(\frac{1}{2}\frac{\nu}{C\sqrt{D}}\right) + C_2 \cos\left(\frac{1}{2}\frac{\nu}{C\sqrt{D}}\right). \tag{39}$$

Now, by considering

$$\gamma = \frac{-C^2x^2 + t^2D}{D},$$
$$\mu(\gamma) = \frac{w}{\exp\left(-(1/2)\left(t/C^2\right)\right)}, \tag{40}$$

equation (1) is transformed into the following ODE:

$$16C^4\gamma\mu_{\gamma\gamma} + 16C^4\mu_\gamma - \mu = 0, \tag{41}$$

with the solution

$$\mu(\gamma) = C_3 I\left(\frac{1}{2}\frac{\sqrt{\gamma}}{C^2}\right) + C_4 K\left(\frac{1}{2}\frac{\sqrt{\gamma}}{C^2}\right), \tag{42}$$

where $I((1/2)(\sqrt{\gamma}/C^2))$ and $K((1/2)(\sqrt{\gamma}/C^2))$ are the modified Bessel functions of the first and second

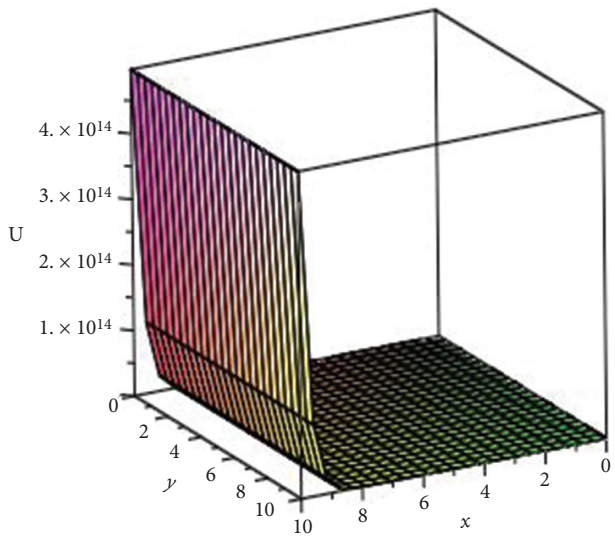

Figure 1: Graph of w given by (17) for $C = 0.1$, $D = 1$, and $C_1 = C_2 = C_3 = C_4 = 1$.

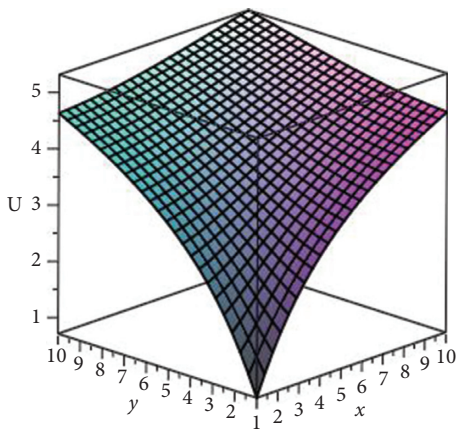

Figure 2: Graph of w given by (27) for $C = 0.5$, $C_1 = C_3 = 1$, and $C_5 = 0$.

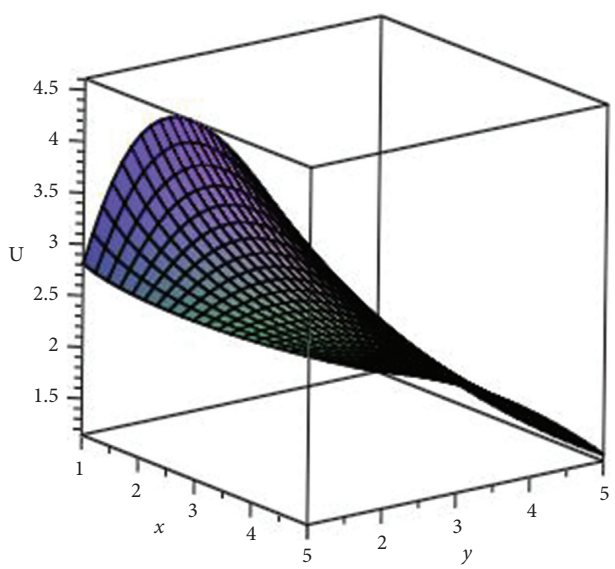

Figure 3: Graph of w given by (35) for $C_1 = C_2 = 1$.

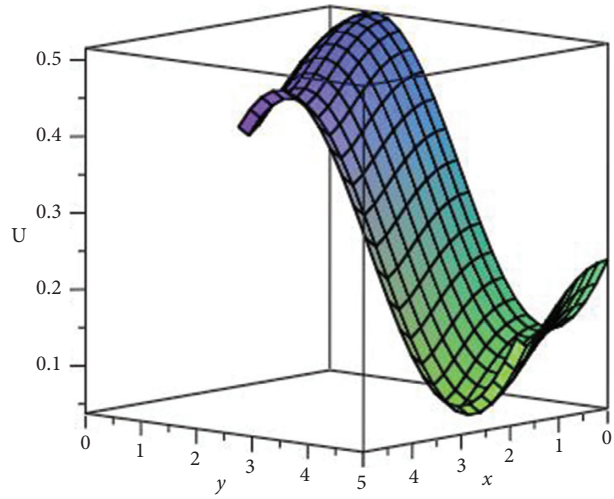

Figure 4: Graph of w given by (44) for $C = 0.5$, $D = 1$, and $C_1 = C_2 = C_3 = C_4 = 1$.

kinds, respectively. By combining (39) and (42), we have

$$w(x,y,t) = \exp\left(-\frac{1}{2}\frac{t}{C^2}\right)(\mu(\nu) + \mu(\gamma)),$$
$$w(x,y,t) = \exp\left(-\frac{1}{2}\frac{t}{C^2}\right)\left(C_1 \sin\left(\frac{1}{2}\frac{\nu}{C\sqrt{D}}\right) + C_2 \cos\left(\frac{1}{2}\frac{\nu}{C\sqrt{D}}\right) + C_3 I\left(\frac{1}{2}\frac{\sqrt{\gamma}}{C^2}\right) + C_4 K\left(\frac{1}{2}\frac{\sqrt{\gamma}}{C^2}\right)\right), \tag{43}$$

i.e.,

$$w(x,y,t) = \exp\left(-\frac{1}{2}\frac{t}{C^2}\right)\left(C_1 \sin\left(\frac{1}{2}\frac{y}{C\sqrt{D}}\right) + C_2 \cos\left(\frac{1}{2}\frac{y}{C\sqrt{D}}\right) + C_3 I\left(\frac{1}{2}\frac{\sqrt{\left(-C^2x^2 + t^2D/D\right)}}{C^2}\right) + C_4 K\left(\frac{1}{2}\frac{\sqrt{\left(-C^2x^2 + t^2D/D\right)}}{C^2}\right)\right), \tag{44}$$

is a solution of (1).

4. Surface Graphs of the Obtained Solutions

In this section, the surface graphs of the exact solutions of the Cattaneo model which are calculated in the previous section are presented. Figures 1–4 show the surface graphs of the exact solutions of the considered model given in equations (17), (27), (35), and (44), respectively.

5. Summary and Conclusions

In this paper, the authors have applied the Lie symmetry method to the Cattaneo equation for obtaining its exact solutions. On achieving the similarity variables, equation (1) is reduced to some ODEs of second order. Finally, the authors have obtained some solutions of undergone ODEs including Bessel functions, which lead to many exact solutions of the considered equation. The surface graphs of solutions are presented to show different behaviors of the considered model. This paper has an interesting application of the Lie group method in a manner that a PDE with three independent variables is directly converted into an ODE by considering its different Lie symmetry generators.

Abbreviations

μ:	A similarity dependent variable which is a function of two independent variables
ν:	A similarity independent variable
γ:	A similarity independent variable
C_1, C_2, C_3, C_4, C_5:	Constants of integration
I and K:	I and K presented in equations (42) and (44) are the modified Bessel functions of the first and second kinds, respectively.

Data Availability

No data were used to support this study.

Conflicts of Interest

The authors declare that they have no conflicts of interest.

References

[1] C. Cattaneo, "Sulla conduzione del calore," *Atti del Seminario Matematico e Fisico dell'Universit di Modena*, vol. 3, pp. 83–101, 1948.

[2] B. Straughan, *Heat Waves*, Springer Science Business, New York, NY, USA, 2011.

[3] K. V. Zhukovsky and H. M. Srivastava, "Analytical solutions for heat diffusion beyond Fourier law," *Applied Mathematics and Computation*, vol. 293, pp. 423–437, 2017.

[4] B. Straughan, "Thermal convection with the Cattaneo christov model," *International Journal of Heat and Mass Transfer*, vol. 53, no. 1–3, pp. 95–98, 2010.

[5] S. A. M. Haddad, "Thermal instability in Brinkman porous media with Cattaneo-Christov heat flux," *International Journal of Heat and Mass Transfer*, vol. 68, no. 4, pp. 659–668, 2014.

[6] D. Jou, J. Casas-Vazquez, and G. Lebon, "Extended irreversible thermodynamics," *Reports on Progress in Physics*, vol. 51, no. 8, pp. 1105–1179, 1988.

[7] M. Zakari and D. Jou, "Equations of state and transport equations in viscous cosmological models," *Physical Review D*, vol. 48, no. 4, pp. 1597–1601, 1993.

[8] S. Godoy and L. S. García-Colín, "From the quantum random walk to classical mesoscopic diffusion in crystalline solids," *Physical Review E*, vol. 53, no. 6, pp. 5779–5785, 1996.

[9] A. Compte and R. Metzler, "The generalized Cattaneo equation for the description of anomalous transport processes," *Journal of Physics A: Mathematical and General*, vol. 30, no. 21, pp. 7277–7289, 1997.

[10] F. Ferrillo, R. Spigler, and M. Concezzi, "Comparing Cattaneo and fractional derivative models for heat transfer processes," *SIAM Journal on Applied Mathematics*, vol. 78, no. 3, pp. 1450–1469, 2018.

[11] S. Su, W. Dai, P. M. Jordan, and R. E. Mickens, "Comparison of the solutions of a phase-lagging heat transport equation and damped wave equation," *International Journal of Heat and Mass Transfer*, vol. 48, no. 11, pp. 2233–2241, 2005.

[12] A. Yusuf, "Symmetry analysis, invariant subspace and conservation laws of the equation for fluid flow in porous media," *International Journal of Geometric Methods in Modern Physics*, vol. 17, no. 12, 2020.

[13] M. Alquran, I. Jaradat, and A. Yusuf, "Heart-cusp and bell-shaped-cusp optical solitons for an extended two-mode version of the complex Hirota model: application in optics," *Optical and Quantum Electronics*, vol. 53, no. 26, 2021.

[14] A. Yusuf, T. Abdulkadir Sulaiman, E. M. Khalil, M. Bayram, and H. Ahmad, "Construction of multi-wave complexiton solutions of the Kadomtsev-Petviashvili equation via two efficient analyzing techniques," *Results in Physics*, vol. 21, 2021.

[15] M. Alquran, F. Yousef, F. Alquran, T. A. Sulaiman, and A. Yusuf, "Dual-wave solutions for the quadratic-cubic conformable-Caputo time-fractional Klein-Fock-Gordon equation," *Mathematics and Computers in Simulation*, vol. 185, pp. 62–76, 2021.

[16] K. Sakkaravarthi, A. G. Johnpillai, A. Durga Devi, T. Kanna, and M. Lakshmanan, "Lie symmetry analysis and group invariant solutions of the nonlinear Helmholtz equation," *Applied Mathematics and Computation*, vol. 331, p. 457, 2018.

[17] C. Li and J. Zhang, "Lie symmetry analysis and exact solutions of generalized fractional zakharov-kuznetsov equations," *Symmetry*, vol. 11, no. 5, 2019.

[18] H. Liu, J. Li, and Q. Zhang, "Lie symmetry analysis and exact explicit solutions for general Burgers' equation," *Journal of Computational and Applied Mathematics*, vol. 228, no. 1, p. 19, 2009.

[19] P. J. Olver, *Applications of Lie Groups to Differential Equations*, Springer-Verlag, New York, NY, USA, 1986.

[20] K. Bibi and K. Ahmad, "Exact solutions of newell whitehead-segel equations using symmetry transformations," *Journal of Function Spaces*, vol. 2021, Article ID 6658081, 8 pages, 2021.

[21] Y. Huang and Z. Yin, "The compact finite difference method of two-dimensional Cattaneo model," *Journal of Function Spaces*, vol. 2020, 12 pages, 2020.

[22] N. H. Ibragimov, *CRC Handbook of Lie Group Analysis of Differential Equations*, CRC Press, Boca Raton, FL, USA, 1996.

[23] H. Stephani, *Differential Equations: Their Solutions Using Symmetries*, Cambridge University Press, Cambridge, UK, 1989.

[24] G. W. Bluman and S. Kumei, *Symmetries and Differential Equations*, Springer-Verlag, New York, NY, USA, 1989.

[25] P. J. Olver, *Equivalnce, Invariants and Symmetry*, Cambridge University Press, Cambridge, UK, 1995.

Hindawi
Discrete Dynamics in Nature and Society
Volume 2021, Article ID 8886056, 12 pages
https://doi.org/10.1155/2021/8886056

Research Article

Fractals via Generalized Jungck–S Iterative Scheme

Zhihua Chen,[1] Muhammad Tanveer,[2] Waqas Nazeer,[3] and Jing Wu[4]

[1]*Institute of Computing Science and Technology, Guangzhou University, Guangzhou 510006, China*
[2]*Department of Mathematics and Statistics, The University of Lahore, Lahore, Pakistan*
[3]*Department of Mathematics, GC University, Lahore, Pakistan*
[4]*School of Science, Xijing University, Xian 710123, China*

Correspondence should be addressed to Jing Wu; specialwujing@sina.com

Received 8 September 2020; Revised 24 September 2020; Accepted 9 February 2021; Published 1 March 2021

Academic Editor: Paolo Renna

The purpose of this research is to introduce a Jungck–S iterative method with (m, h_1, h_2)–convexity and hence unify different comparable iterative schemes existing in the literature. A Jungck–S orbit is constructed, and escape radius is derived with our scheme. A new escape radius is also obtained for generating the fractals. Julia and Mandelbrot set are visualized with the help of proposed algorithms based on our iterative scheme. Moreover, we present some complex graphs of Julia and Mandelbrot sets using the derived orbit and discuss their nature in detail.

1. Introduction

The word fractal originating from Latin language means to divide or break. This is tantamount to self-similar patterns in the complex graphics. The fractal theory has many applications in mathematics and different related disciplines. In biological sciences, this theory is being applied successfully to understand certain biologic phenomena, for example, growth culture for the microorganism, like bacteria or amoeba, and to study and analyze the fibre pattern of nerve and so forth. In physical sciences, fractals are used to determine and understand the turbulent flows in fluid mechanics. In telecommunication, fractals are used to manufacture antennae. Moreover, computer networking, radar system, and architectural models also fall into the domain of applications of fractals theory.

In 1975, Mandelbrot generated a sequence of iterates for a complex polynomial $z^2 + c$ [1] under some restrictions. He observed a chain of self-similar patterns on a graph and hence named it fractal. He claimed that the obtained image was the sequence of connected Julia sets. After his valuable work, the researcher generalized the fractals in many different ways. It is worth mentioning that complex graphical shapes, fractals, were discovered as the fixed points of certain set maps. So, the fixed point theory plays a vital role in the investigation of fractals. Different iterative schemes, mainly used to approximate the fixed points of certain mappings, can be employed to sketch some beautiful natural scenes of sunset, lighting, rainbow, galaxies, deserts, mountains, and so forth. These aesthetic patterns depend on the iterative algorithms and hence provide a good source of motivation to apply mathematical models in art and designs. The generalized form of the Mandelbrot set was given in [2].

Some logarithmic, rational, exponential, and trigonometric functions were investigated in [3]. The bicomplex, tricomplex, and quaternions functions were utilized in [4–6] to create some generalized versions of fractals. The study of fractals using fixed point theory attracted the attention of several researchers after the work of Rani et al. in [7, 8]. Some types of fractals via different explicit iterations were analyzed in [9–13].

In this paper, we define the orbit of generalized Jungck-S iterative scheme with (m, h_1, h_2)–convexity for fractals. We derive a new escape radius for complex polynomials and develop the algorithms for fractals visualization and draw some complex graphs of Julia and Mandelbrot sets using computer software. The paper is organized as follows: in Section 2, some known concepts and iterative schemes are

given. Section 3 contains the Jungck–S orbit with (m, h_1, h_2)–convexity (JSOmhh) and the derivation of escape radius for Jungck–S iterative scheme with (m, h_1, h_2)–convexity for general complex polynomial. In Section 4, we visualize some quadratic and cubic complex graphs of Julia and Mandelbrot sets. Characteristics of Julia and Mandelbrot sets are also discussed in this section. In Section 5, the summary of our present work and the plan of our future work are presented.

2. Preliminaries

Consistent with [14, 15], the following definitions will be needed in the sequel.

Definition 1 (see [14]). Let $f: \mathbb{C} \longrightarrow \mathbb{C}$ be a complex polynomial of degree ≥2 with complex coefficients and $f^p(x)$ the p^{th} iterate of x. The behavior of the iterate $f^p(x)$ for large p determines the Julia set. The set F_f, called filled Julia set, is the set of all those points of $\mathbb{C}$ for which the orbits $|f^p(z)|\}_{p=0}^{\infty} \nrightarrow \infty$ are as $p \longrightarrow \infty$; that is,

$$F_f = \left\{ z \in \mathbb{C}: \left\{ \left| f^p(z) \right| \right\}_{p=0}^{\infty} \text{is bounded} \right\}. \tag{1}$$

The boundary of the filled Julia set is called simply Julia set.

Mandelbrot [15] extended the concept of a Julia set and presented the notion of fractals. He investigated the graphical behavior of connected Julia sets and plotted them for complex function, $f_c(x) = x^2 + c$, where $x \in \mathbb{C}$ is a variable and $c \in \mathbb{C}$ is the input.

Definition 2 (see [15]). The set which consists of all those points (parameters) of $\mathbb{C}$ for which the Julia sets are connected is called Mandelbrot set M; that is,

$$M = \left\{ c \in \mathbb{C}: F_f \text{ is connected} \right\}. \tag{2}$$

Equivalently, the Mandelbrot set can be defined as follows [16]:

$$M = \{ c \in \mathbb{C}: \{ f^p(0) \} \text{ does not tend to } \infty \text{ as } p \longrightarrow \infty \}. \tag{3}$$

Different algorithms have been employed to generate Julia sets. Some popular algorithms to visualize the Julia sets are distance estimator [17], escape time [18], and potential function algorithms [19]. The escape time algorithms have been used in this paper.

We established escape time algorithms, namely, Algorithms 1 and 2 with derived escape radius to generate the fractals.

Let us refer to some iterative algorithms: the Jungck iteration was studied in [20], the Jungck–Mann iteration with s-convexity was studied in [21], the Jungck–Ishikawa iteration with s-convexity was studied in [21], the following Jungck-S iteration was studied in [20] and Kwun et al.[22] used a convex combination to define the Jungck-S iterative scheme with s-convexity. We define the Jungck-S iterative scheme with (m, h_1, h_2)-convexity (JSOmhh) in the following manner:

Definition 3 (JSOmhh)**.** Suppose that $P, Q: \mathbb{C} \longrightarrow \mathbb{C}$, where P is one to one. Let $z_0 \in \mathbb{C}$ be an initial point. The Jungck–S iterative scheme with (m, h_1, h_2)–convexity is defined as follows:

$$\begin{cases} P(z_{k+1}) = mh_1(\alpha)Q(z_k) + h_2(\alpha)Q(y_k), \\ P(y_k) = mh_1(\beta)P(z_k) + h_2(\beta)Q(z_k), \end{cases} \tag{4}$$

where $h_1(t) = (1-t)^{-s}$ and $h_2(t) = t^{-s}$, also $\alpha, \beta, s, m \in (0, 1]$, and $k = 0, 1, 2, \ldots$.

It is important to mention here that our scheme generalizes many of the above-mentioned schemes.

3. Main Results

In this section, we first introduce the Jungck–S iterative scheme with (m, h_1, h_2)–convexity (JSOmhh) and then prove escape criteria to determine the escape radius induced by (JSOmhh).

In the following theorem, we use (JSOmhh) to establish the escape criteria for $f(z) = \sum_{i=0}^{p} a_i z^i$, where $p \geq 2$, $a_i \in \mathbb{C}$, for $i = 0, 1, 2, \ldots, p$ and $|a_p| > \sum_{i=2}^{p-1} |a_i|$ with choices $Q(z) = \sum_{i=2}^{p} a_i z^i + a_0$ and $P(z) = a_1 z$ to generate fractals.

Theorem 1. *Suppose that* $|z| \geq |a_0| > (2(1 + m|a_1|)/s\alpha(\phi - \varphi))^{1/(p-1)}$ *and* $|z| \geq |a_0| > (2(1 + m|a_1|)/s\beta(\phi - \varphi))^{1/(p-1)}$ *where* $\phi = |a_p|, \varphi = \sum_{2}^{p-1} |a_i|$, *where* $\alpha, \beta, s \in (0, 1]$, *and* $\{z_k\}_{k \in \mathbb{N}}$ *is defined as*

$$\begin{cases} P(z_{k+1}) = mh_1(\alpha)P(z_k) + h_2(\alpha)Q(y_k), \\ P(y_k) = mh_1(\beta)P(z_k) + h_1(\beta)Q(z_k), \end{cases} \tag{5}$$

where $s, t, m \in (0, 1], h_1(t) = (1-t)^{-s}, h_2(t) = t^{-s}$ *and* $k = 0, 1, 2, \ldots$. *Then,* $|z_k| \longrightarrow \infty$ *as* $k \longrightarrow \infty$.

Proof. Since $f(z) = \sum_{i=0}^{p} a_i z^i$, where $a_i \in \mathbb{C}$ for $i = 0, 1, 2, \ldots, p$, $z_0 = z$, and $y_0 = y$. Handling f as $f = Q - P$ with choice $Q(z) = \sum_{i=2}^{p} a_i z^i + a_0$ and $P(z) = a_1 z$, then

$$\begin{aligned} \left| P(y_0) \right| &= \left| mh_1(\beta)P(z) + h_2(\beta)Q(z) \right| \\ &= \left| m(1-\beta)^{-s} a_1 z + \beta^{-s} \left(\sum_{i=2}^{p} a_i z^i + a_0 \right) \right| |a_1 y_0| \\ &\geq \left| s\beta \left(\sum_{i=2}^{p} a_i z^i + a_0 \right) \right| - |ma_1 z|. \end{aligned} \tag{6}$$

Because $(1-\beta)^{-s} = 1 + \beta s + \cdots > 1$ and $\beta^{-s} = 1 + s(1-\beta) + \cdots > \beta s$ for all $s, m, \beta \in (0, 1]$, therefore

$$|a_1 y_0| \geq \left| s\beta \left(\sum_{i=2}^{p} a_i z^i + a_0 \right) \right| - s\beta|a_0| - |ma_1 z|. \tag{7}$$

Since $|z| \geq |a_0|$ and $s\beta < 1$, we have

Input: $f(z) = \sum_{i=0}^{p} a_i z^i$ where $p \geq 2$, $a_i \in \mathbb{C}$ for $i = 0, 1, 2, \ldots, p$–polynomial of complex variable, $\phi, \varphi, \alpha, \beta, s, m$ – involved parameters, $A = [x_{\min}, x_{\max}] \times [y_{\min}, y_{\max}]$ –occupied area, K – fixed number of iterates, colourfunction $[0..n-1]$ – colour function with n colours.
Output: a Julia set.

(1) **for** $a_0 \in \mathbb{C}$ **do**
(2) $R = \mathrm{Max}[|a_0|, (2(1 + m|d_1|)/s\alpha(\phi - \varphi))^{1/(p-1)}, (2(1 + m|d_1|)/s\beta(\phi - \varphi))^{1/(p-1)}]$ the escape radius
(3) $k = 0$
(4) $z_0 = a_0$–initial guess for f
(5) **while** $k \leq K$ **do**
(6) $z_{k+1} = f_c(z_k)$
(7) **if** $|z_{k+1}| > R$ **then**
(8) break
(9) $k = k + 1$
(10) $c = \lfloor (n-1)(k/K) \rfloor$
(11) colour z_0 with colourfunction $[c]$.

Algorithm 1: Complex graph of Julia set.

Input: $f(z) = \sum_{i=0}^{p} a_i z^i$ where $p \geq 2$, $a_i \in \mathbb{C}$ for $i = 0, 1, 2, \ldots, p$– polynomial of complex variable, $\phi, \varphi, \alpha, \beta, s, m$ – involved parameters, $A = [x_{\min}, x_{\max}] \times [y_{\min}, y_{\max}]$ –occupied area, K – fixed number of iterates, colourfunction $[0..n-1]$ – colour function with n colours.
Output: a Mandelbrot set.

(1) **for** $a_0 \in \mathbb{C}$ **do**
(2) $R = \mathrm{Max}[|a_0|, (2(1 + m|d_1|)/s\alpha(\phi - \varphi))^{1/(p-1)}, (2(1 + m|d_1|)/s\beta(\phi - \varphi))^{1/(p-1)}]$–the escape radius
(3) $k = 0$
(4) $z_0 = 0$–initial guess for f
(5) **while** $k \leq K$ **do**
(6) $z_{k+1} = f(z_k)$
(7) **if** $|z_{k+1}| > R$ **then**
(8) break
(9) $k = k + 1$
(10) $c = \lfloor (n-1)(k/K) \rfloor$
(11) colour a_0 with colourfunction $[c]$.

Algorithm 2: Complex graph of Mandelbrot.

$$\begin{aligned}
|a_1 y_0| &\geq s\beta\left|\sum_{i=2}^{p} a_i z^i\right| - |z| - m|a_1||z| \\
&= |z|\left(s\beta\left|\sum_{i=2}^{p} a_i z^{i-1}\right| - \left(1 + m|a_1|\right)\right)|y_0| \\
&= \frac{1}{|a_1|}\left\{|z|\left(s\beta\left|\sum_{i=2}^{p} a_i z^{i-1}\right| - \left(1 + m|a_1|\right)\right)\right\}.
\end{aligned} \tag{8}$$

Since $(1 + m|a_1|) > |a_1|$, then

$$\begin{aligned}
|y_0| &\geq |z|\left(\frac{s\beta\left|\sum_{i=2}^{p} a_i z^{i-1}\right|}{1 + m|a_1|} - 1\right) \\
&\geq |z|\left(\frac{s\beta|z^{p-1}|\left(|a_p| - \sum_{i=2}^{p-1}|a_i|\right)}{1 + m|a_1|} - 1\right) \\
&= |z|\left(\frac{s\beta|z^{p-1}|(\phi - \varphi)}{1 + m|a_1|} - 1\right)|y_0| \\
&\geq s\beta|z|.
\end{aligned} \tag{9}$$

Because $|z| \geq |a_0| > (2(1 + m|a_1|)/s\beta(\phi - \varphi))^{1/(p-1)}$ where $\phi = |a_p|, \varphi = \sum_{2}^{p-1}|a_i|$, this produced the situation $|z|((|z|^{p-1}(s\beta(\phi - \varphi))/(1 + m|a_1|)) - 1) > |z| \geq s\beta|z|$. For the last step, we have

$$\begin{aligned}
|P(z_1)| &= |mh_1(\alpha)Q(z_0) + h_2(\alpha)Q(y_0)||a_1 z_1| \\
&= |m(1 - \alpha)^{-s}(z^p + d_2) + \alpha^{-s}(y^p + d_2)| \\
&\geq \left|m\left(\sum_{i=2}^{p} a_i z^i + a_0\right) + s\alpha\left(\sum_{i=2}^{p} a_i y^i + a_0\right)\right|.
\end{aligned} \tag{10}$$

Since $m > 0$, then we get

$$\begin{aligned}
|a_1 z_1| &\geq s\alpha\left|\sum_{i=2}^{p} a_i y^i + a_0\right| \\
&\geq s\alpha\left|\sum_{i=2}^{p} a_i y^i\right| - |a_0| \\
&\geq |z|\left\{s^2\alpha\beta|z^{p-1}|\left(|a_p| - \sum_{i=2}^{p-1}|a_i|\right) - 1\right\}.
\end{aligned} \tag{11}$$

Hence,

$$|z_1| \geq |z|\left(\frac{s^2\alpha\beta|z^{p-1}|(\phi-\varphi)}{1+m|a_1|}-1\right). \tag{12}$$

Since $|z| > (2(1+m|a_1|)/s\alpha(\phi-\varphi))^{1/(p-1)}$ and $|z| > (2(1+m|a_1|)/s\beta(\phi-\varphi))^{1/(p-1)}$, so $|z|^{p-1} > 2(1+m|d_1|)/s^2\alpha\beta$ and this implies $((s^2\alpha\beta(\phi-\varphi)|z|^{p-1})/(1+m|d_1|))-1>1$. Therefore, there exists $\delta>0$ such that $(s^2\alpha\beta(\phi-\varphi)|z|^{p-1}/(1+m|d_1|))-1>1+\delta$. Consequently, $|z_1|>(1+\delta)|z|$. In particular, $|z_1|>|z|$. So, we may iterate to find $|z_i|>(1+\delta)^i|z|$. Hence, the orbit of z tends to infinity and this completes the proof. □

Theorem 2. *Suppose that $\{z_i\}_{i\in\mathbb{N}}$ is a sequence of points in JSOmhh for complex polynomial $f(z)=\sum_{i=0}^{p}a_iz^i$, where $p\geq 2$, $a_i\in\mathbb{C}$, for $i=0,1,2,\ldots,p$, $\phi=|a_p|$, and $\varphi=\sum_{i=2}^{p-1}|a_i|$ with $\phi>\varphi$ such that $|z_i|\longrightarrow\infty$ as $i\longrightarrow\infty$; then $|z|\geq|a_0|>(2(1+m|d_1|)/s\alpha(\phi-\varphi))^{1/(p-1)}$ and $|z|\geq|a_0|>(2(1+m|d_1|)/s\beta(\phi-\varphi))^{1/(p-1)}$ where $\alpha,\beta,s\in(0,1]$.*

Proof. Since $\{z_i\}_{i\in\mathbb{N}}$ is the sequence of points in JSOmhh for complex polynomial $f(z)=\sum_{i=0}^{p}a_iz^i$ where $p\geq 2$, $a_i\in\mathbb{C}$ for $i=0,1,2,\ldots,p$, $\phi=|a_p|$ and $\varphi=\sum_{i=2}^{p-1}|a_i|$ with $\phi>\varphi$ such that $|z_i|\longrightarrow\infty$ as $i\longrightarrow\infty$, therefore there exists $\delta>0$ such that

$$|z_i|>(1+\delta)^i|z|. \tag{13}$$

For $i=1$, we get

$$|z_1|\geq(1+\delta)|z|. \tag{14}$$

Since $f(z)=\sum_{i=0}^{p}a_iz^i$, where $a_i\in\mathbb{C}$ for $i=0,1,2,\ldots,p$, $z_0=z$ and $y_0=y$. Handling f as $f=Q-P$ with choice $Q(z)=\sum_{i=2}^{p}a_iz^i+a_0$ and $P(z)=a_1z$, then

$$\begin{aligned}|P(y_0)|&=|mh_1(\beta)P(z)+h_2(\beta)Q(z)|\\&=\left|m(1-\beta)^{-s}a_1z+\beta^{-s}\left(\sum_{i=2}^{p}a_iz^i+a_0\right)\right||a_1y_0|\\&\geq\left|s\beta\left(\sum_{i=2}^{p}a_iz^i+a_0\right)\right|-|ma_1z|.\end{aligned} \tag{15}$$

Because $(1-\beta)^{-s}=1+\beta s+\cdots>1$ and $\beta^{-s}=1+s(1-\beta)+\cdots>\beta s$ for all $s,m,\beta\in(0,1]$, therefore

$$|a_1y_0|\geq\left|s\beta\left(\sum_{i=2}^{p}a_iz^i+a_0\right)\right|-s\beta|a_0|-|ma_1z|. \tag{16}$$

Since for fractal generation it must be true $|z|\geq|a_0|$. Also, $s\beta<1$, and we obtain

$$\begin{aligned}|a_1y_0|&\geq s\beta\left|\sum_{i=2}^{p}a_iz^i\right|-|z|-m|a_1||z|\\&=|z|\left(s\beta\left|\sum_{i=2}^{p}a_iz^{i-1}\right|-\left(1+m|a_1|\right)\right)|y_0|\\&=\frac{1}{|a_1|}\left\{|z|\left(s\beta\left|\sum_{i=2}^{p}a_iz^{i-1}\right|-\left(1+m|a_1|\right)\right)\right\}.\end{aligned} \tag{17}$$

Since $(1+m|a_1|)>|a_1|$, then

$$\begin{aligned}|y_0|&\geq|z|\left(\frac{s\beta\left|\sum_{i=2}^{p}a_iz^{i-1}\right|}{1+m|a_1|}-1\right)\geq|z|\left(\frac{s\beta|z^{p-1}|\left(|a_p|-\sum_{i=2}^{p-1}|a_i|\right)}{1+m|a_1|}-1\right)\\&=|z|\left(\frac{s\beta|z^{p-1}|(\phi-\varphi)}{1+m|a_1|}-1\right)|y_0|\\&\geq s\beta|z|.\end{aligned} \tag{18}$$

Since fractals are bounded, therefore $((sb|z^{p-1}|/(1+|d_1|))-1)\geq 1$. For the last step, we have

$$\begin{aligned}|P(z_1)|&=|mh_1(\alpha)Q(z_0)+h_2(\alpha)Q(y_0)||a_1z_1|\\&=|m(1-\alpha)^{-s}(z^p+d_2)+\alpha^{-s}(y^p+d_2)|\\&\geq\left|m\left(\sum_{i=2}^{p}a_iz^i+a_0\right)+sa\left(\sum_{i=2}^{p}a_iy^i+a_0\right)\right|.\end{aligned} \tag{19}$$

Since $m>0$, then we get

$$\begin{aligned}|a_1z_1|&\geq s\alpha\left|\sum_{i=2}^{p}a_iy^i+a_0\right|\\&\geq s\alpha\left|\sum_{i=2}^{p}a_iy^i\right|-|a_0|\\&\geq|z|\left\{s^2\alpha\beta|z^{p-1}|\left(|a_p|-\sum_{i=2}^{p-1}|a_i|\right)-1\right\}.\end{aligned} \tag{20}$$

Hence,

$$|z_1| \geq |z|\left(\frac{s^2\alpha\beta|z^{p-1}|(\phi-\varphi)}{1+m|a_1|}-1\right). \tag{21}$$

Comparing (14) and (21), we have

$$\frac{s^2\alpha\beta(\phi-\varphi)|z^{p-1}|}{1+m|a_1|}-1 = 1+\delta\frac{s^2\alpha\beta(\phi-\varphi)|z^{p-1}|}{1+m|a_1|}-1 > 1, \tag{22}$$

because $\delta > 0$. This implies

$$|z| > \left(\frac{2\left(1+m|a_1|\right)}{s^2\alpha\beta(\phi-\varphi)}\right)^{1/(p-1)}. \tag{23}$$

As a result, we obtain $|z| > (2(1+m|a_1|)/s\alpha(\phi-\varphi))^{1/(p-1)}$ and $|z| > (2(1+m|a_1|)/s\beta(\phi-\varphi))^{1/(p-1)}$ where $p \geq 2$ and $\alpha, \beta, m, s \in (0, 1]$. To visualize complex fractal, $|z| \geq |a_0|$ must exist because, for any given point $|z| < |a_0|$, we have to compute the JSOmhh of z. If, for some i, $|z_i|$ lies outside the circle of radius $\max\{|a_0|, (2(1+m|a_1|)/s\alpha(\phi-\varphi))^{1/(p-1)}, (2(1+m|a_1|)/s\beta(\phi-\varphi))^{1/(p-1)}\}$, we observed that JSOmhh escapes. Hence, z is neither in Julia sets nor in Mandelbrot sets, but $|z_i|$ is bounded to obey $|z| \geq |a_0|$; then $|z_i|$ lies in JSOmhh. Hence, it is the desired result. □

4. Application of Fractals

In this section, we use our developed algorithms and derived escape radius for JSOmhh to draw some attractive and inspiring Julia and Mandelbrot sets using the framework of Mathematica. Throughout this section, we use $K = 100$ (for maximum iterates).

4.1. Julia Sets. Figures 1–6 are quadratic Julia sets at different involved parameters. We obverse that each graph of quadratic Julia set is different from the other. We use the same complex polynomial and involved parameters except for a_0 for Figures 1 and 2 and analyze that due to a very small change in a_0, the nature of graphs changes drastically. Also, for Figures 3–6, we have the same arguments. We also observe that the correspondence between the points of quadratic Julia sets creates the artful patterns and self-similarity in points of quadratic Julia sets show that the drawn graphs are the fractals. The involved parameters for complex graphs of quadratic Julia sets 1–6 were as follows:

Figure 1: $p = 2$, $a_0 = 0.0248 + 0.0084\mathbf{i}$, $a_1 = 1/2, a_2 = 2$, $a, b, s, m = 0.1$, $A = [-0.27, 0.27] \times [-0.37, 0.37]$.

Figure 2: $p = 2$, $a_0 = -0.084$, $a_1 = 1/2, a_2 = 2$, $a, b, s, m = 0.1$, $A = [-0.37, 0.37] \times [-0.2, 0.2]$.

Figure 3: $p = 2$, $a_0 = 0.0015 + 0.00007\mathbf{i}$, $a_1 = 1/2, a_2 = 100$, $a, b, s, m = 0.5$, $A = [-0.007, 0.005] \times [-0.0025, 0.0025]$.

Figure 4: $p = 2$, $a_0 = 0.0015 + 0.00001\mathbf{i}$, $a_1 = 1/2, a_2 = 100$, $a, b, s, m = 0.5$, $A = [-0.007, 0.005] \times [-0.0025, 0.0025]$.

Figure 5: $p = 2$, $a_0 = 0.0071 + 0.0014\mathbf{i}$, $a_1 = 2, a_2 = 1$, $a, b, s, m = 0.9$, $A = [-0.053, 0.053] \times [-0.035, 0.035]$.

Figure 6: $p = 2$, $a_0 = 0.006\mathbf{i}$, $a_1 = 2, a_2 = 1$, $a, b, s, m = 0.9$, $A = [-0.053, 0.053] \times [-0.037, 0.037]$.

In Figures 7–12, cubic Julia sets are presented. Again, we use the same complex cubic polynomial and involved parameters except for a_0 for Figures 7 and 8. We observe that, due to a very small change in a_0, the nature of cubic Julia graphs also changes drastically. We have made the same augments for Figures 9–12, respectively. Furthermore, we observe that the correspondence between the points of cubic Julia sets creates the aesthetic patterns and self-similarity in points of cubic Julia sets show that the drawn graphs of cubic Julia sets are also fractals. The involved parameters for complex graphs of cubic Julia sets 7–12 were as follows:

Figure 7: $p = 3$, $a_0 = 0.00122$, $a_1 = 1 + \mathbf{i}, a_2 = 1, a_3 = 50$, $a, b, s, m = 0.9$, $A = [-0.01, 0.01] \times [-0.01, 0.01]$.

Figure 8: $p = 3$, $a_0 = 0.001019$, $a_1 = 1 + \mathbf{i}, a_2 = 1, a_3 = 50$, $a, b, s, m = 0.9$, $A = [-0.012, 0.01] \times [-0.012, 0.01]$.

Figure 9: $p = 3, a_0 = 0.000085\mathbf{i}$, $a_1 = 1 + \mathbf{i}, a_2 = 45, a_3 = 50$, $a, b, s, m = 0.9$, $A = [-0.00007, 0.00007] \times [-0.00007, 0.00007]$.

Figure 10: $p = 3,$, $a_1 = 1 + \mathbf{i}, a_2 = 45, a_3 = 50$, $a, b, s, m = 0.9$, $A = [-0.00009, 0.00009] \times [-0.00004, 0.00004]$.

Figure 11: $p = 3$, $a_0 = 0.09956 + 0.27\mathbf{i}$, $a_1 = 2, a_2 = 1$, $a_3 = 3$, $a = 0.1, b = 0.9, s, m = 0.5$, $A = [-0.8, 0.6] \times [-0.6, 0.7]$.

Figure 12: $p = 3$, $a_0 = 0.0489 + 0.366\mathbf{i}$, $a_1 = 2, a_2 = 1$, $a_3 = 3$, $a = 0.1, b = 0.9, s, m = 0.5$, $A = [-0.8, 0.6] \times [-0.6, 0.7]$.

4.2. Mandelbrot Sets. Figures 13–24 execute the quadratic complex polynomial for different involved parameters in JSOmhh. Figures 13–16 represent the quadratic Mandelbrot sets. Each quadratic Mandelbrot set has a main cardioid type body, one large bulb, and two small bulbs are seen on cardioid type body. The bulbs are self-similar and contain a large number of more small bulbs. Due to a small change in the involved parameters, the size of bulbs and main cardioid changes. Figures 17 and 18 are Mandelbrot sets for quadratic polynomial, but both figures are not like the usual quadratic Mandelbrot set. Some parts of both images are like the quadratic, cubic, and quadric Mandelbrot sets. It is observed that the values of a_i's are in the inverse proportion to the area A; that is, the larger the values of a_i's, the smaller the area A. The involved parameters for quadratic Mandelbrot sets were taken as follows:

Figure 13: $p = 2$, $a_1 = 1/2, a_2 = 2$, $a, b, s, m = 0.1$, $A = [-0.17, 0.05] \times [-0.1, 0.1]$.

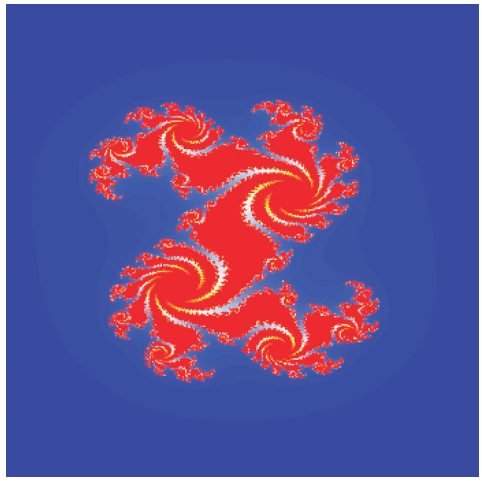

Figure 1: Quadratic Julia set in JSOmhh.

Figure 2: Quadratic Julia set in JSOmhh.

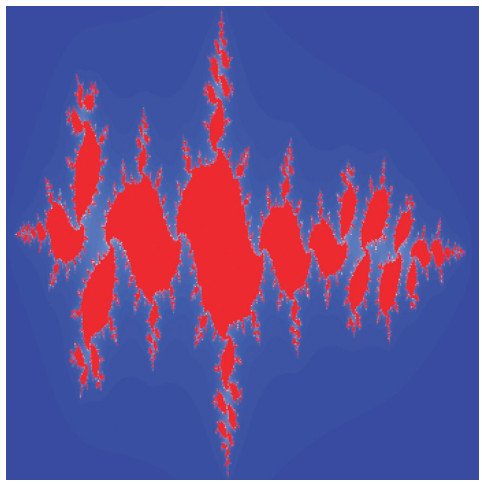

Figure 3: Quadratic Julia set in JSOmhh.

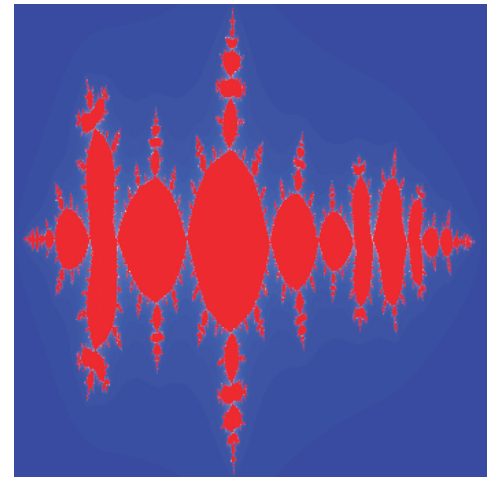

Figure 4: Quadratic Julia set in JSOmhh.

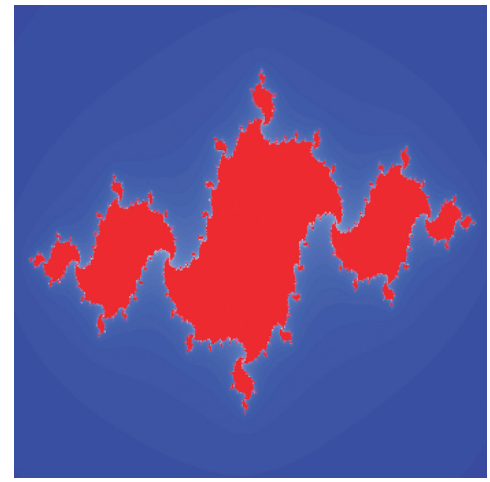

Figure 5: Quadratic Julia set in JSOmhh.

Figure 14: $p = 2$, $a_1 = 3, a_2 = 10$, $a, m = 0.5$, $b = 0.9, s = 0.8$, $A = [-0.17, 0.05] \times [-0.07, 0.07]$.

Figure 15: $p = 2$, $a_1 = 2, a_2 = 100$, $a = 0.5, b = 0.9$, $s = 0.8, m = 0.9$, $A = [-0.0081, 0.0005] \times [-0.001, 0.001]$.

Figure 16: $p = 2$, $a_1 = 100, a_2 = 1$, $a, b = 0.5, s = 0.9$, $m = 0.7$, $A = [-4200, 501] \times [-1201, 1201]$.

Figure 17: $p = 2$, $a_1 = 1, a_2 = (a_0 - 1)$, $a, b = 0.5$, $s = 0.9, m = 0.7$, $A = [-0.15, 0.7] \times [-0.4, 0.4]$.

Figure 18: $p = 2$, $a_1 = 2/3, a_2 = 1$, $a, b, s, m = 0.9$, $A = [-0.001, 0.002] \times [-0.001, 0.001]$.

Some Mandelbrot sets for cubic complex polynomial are presented here. In Figures 19–24, the graphs for cubic Mandelbrot sets are analyzed in JSOmhh. Figures 21 and 24 demonstrate the usual cubic while Figure 23 reflects the quadratic Mandelbrot sets for cubic complex polynomial.

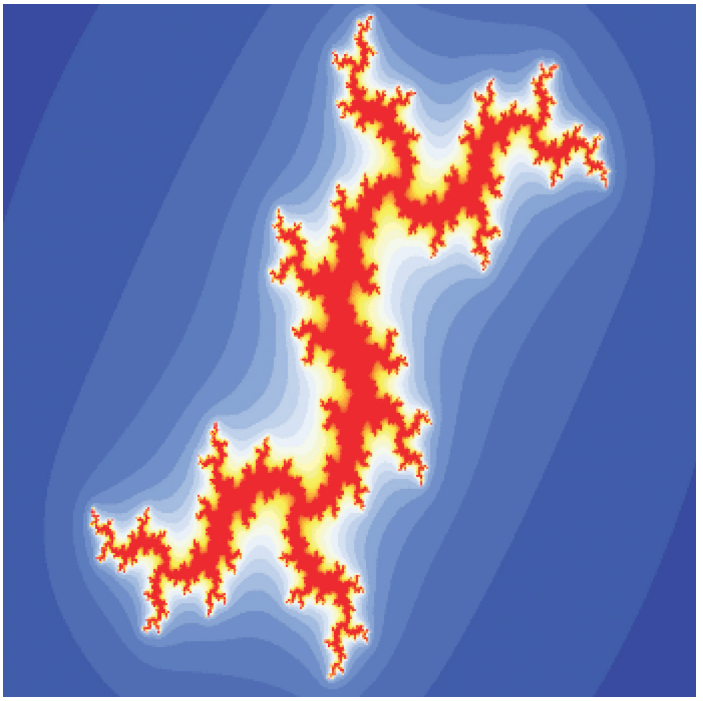

Figure 6: Quadratic Julia set in JSOmhh.

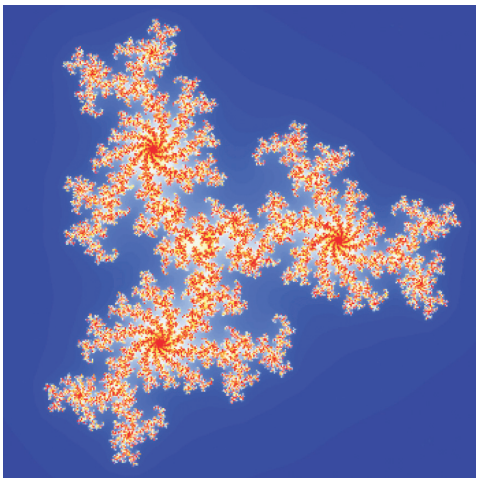

Figure 7: Cubic Julia set in JSOmhh.

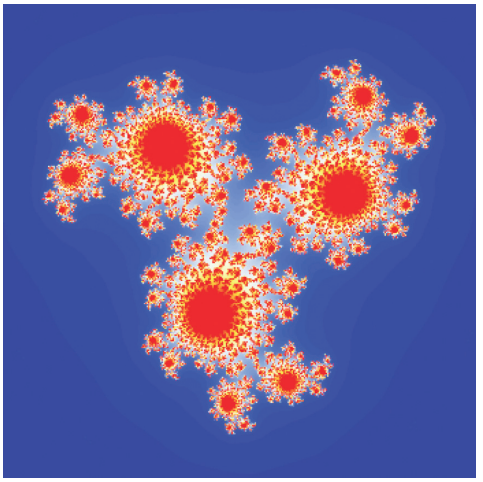

Figure 8: Cubic Julia set in JSOmhh.

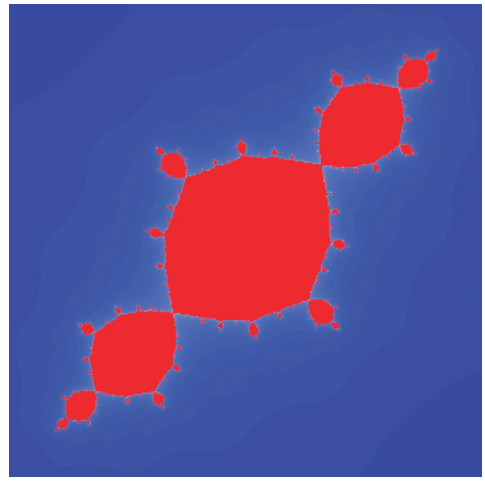

Figure 9: Cubic Julia set in JSOmhh.

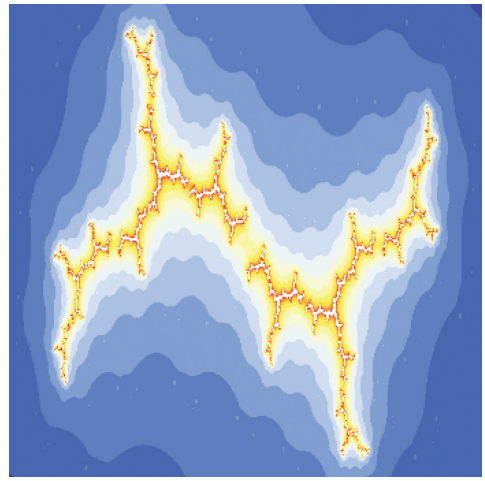

Figure 10: Cubic Julia set in JSOmhh.

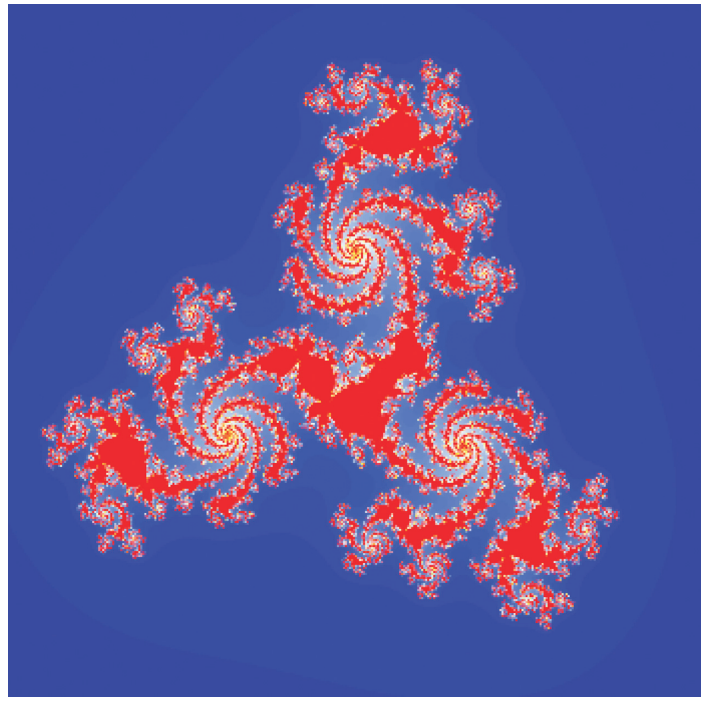

Figure 11: Cubic Julia set in JSOmhh.

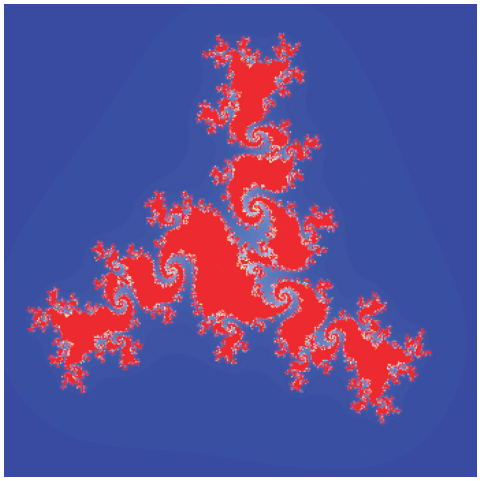

Figure 12: Cubic Julia set in JSOmhh.

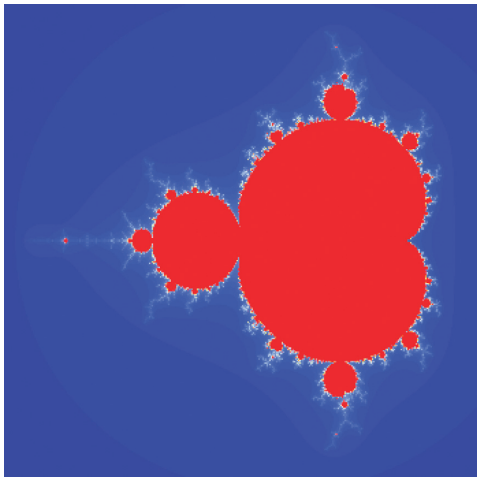

Figure 13: Quadratic Mandelbrot set in JSOmhh.

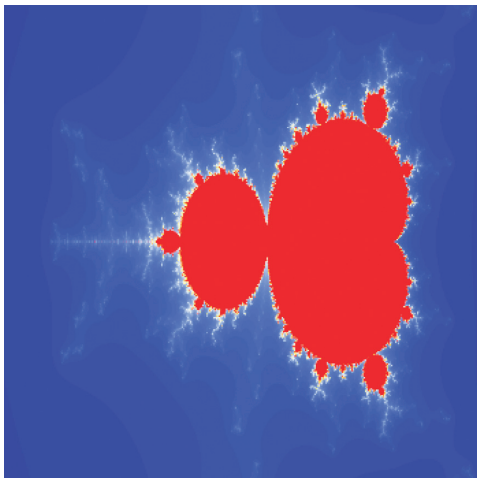

Figure 14: Quadratic Mandelbrot set in JSOmhh.

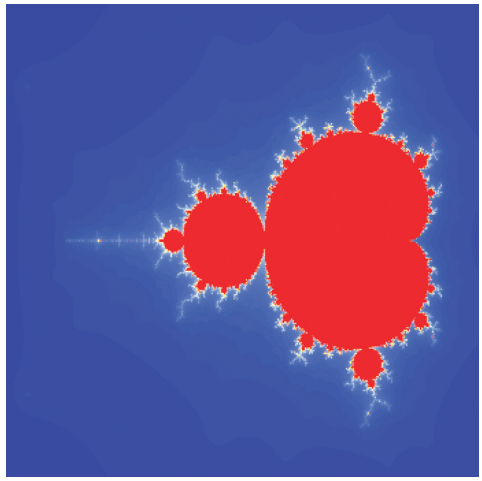

Figure 15: Quadratic Mandelbrot set in JSOmhh.

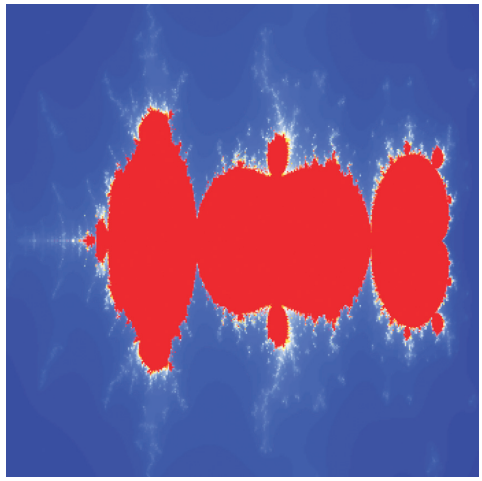

Figure 16: Quadratic Mandelbrot set in JSOmhh.

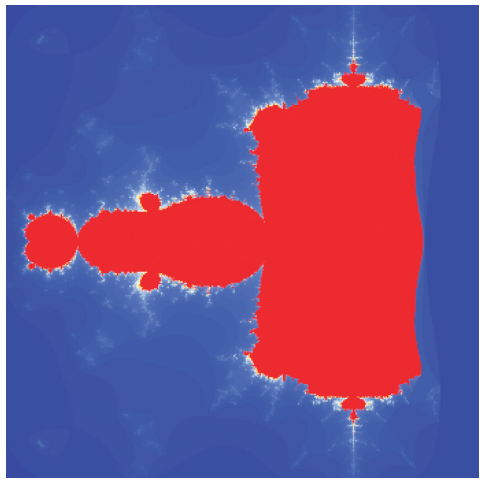

Figure 17: Quadratic Mandelbrot set in JSOmhh.

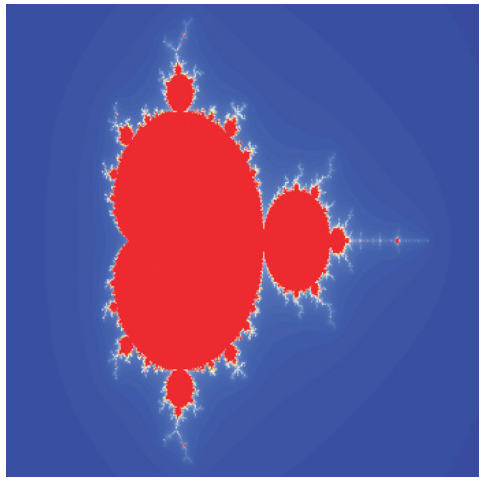

Figure 18: Quadratic Mandelbrot set in JSOmhh.

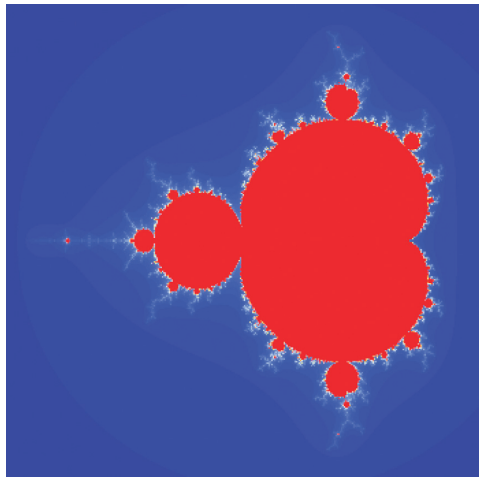

Figure 19: Cubic Mandelbrot set in JSOmhh.

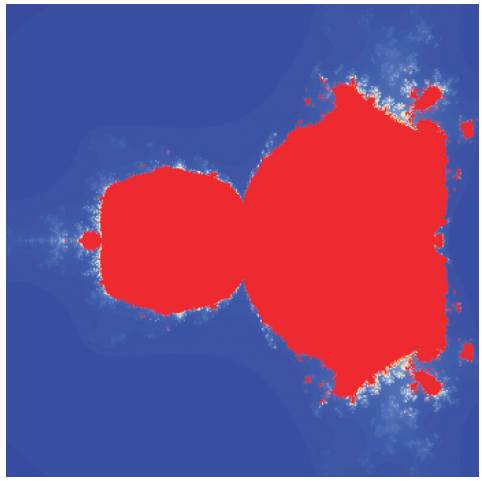

Figure 20: Cubic Mandelbrot set in JSOmhh.

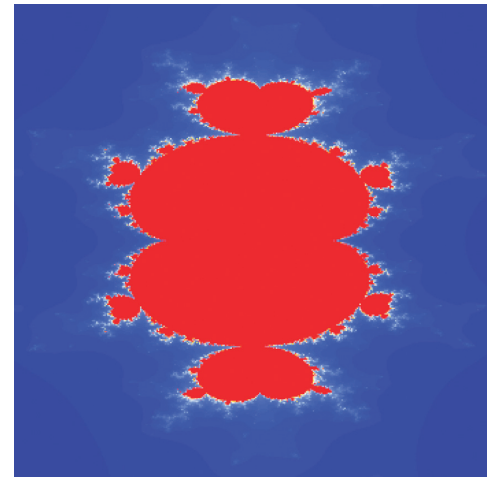

Figure 21: Cubic Mandelbrot set in JSOmhh.

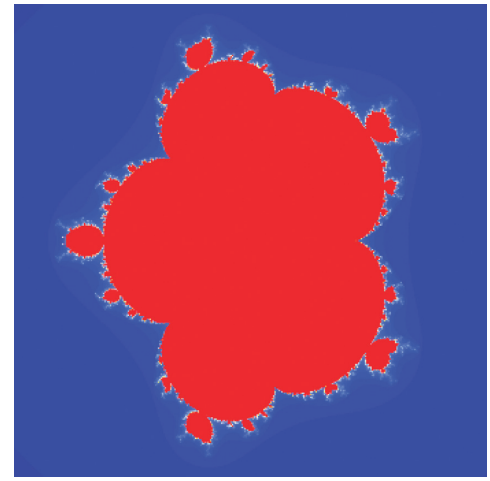

Figure 22: Cubic Mandelbrot set in JSOmhh.

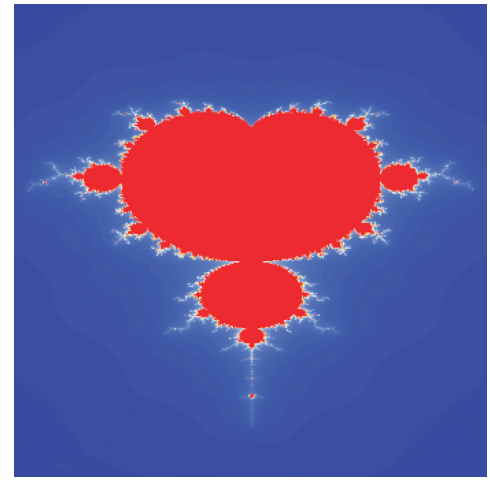

Figure 23: Quadratic Biomorph generated in Jungck-S orbit with s-convexity.

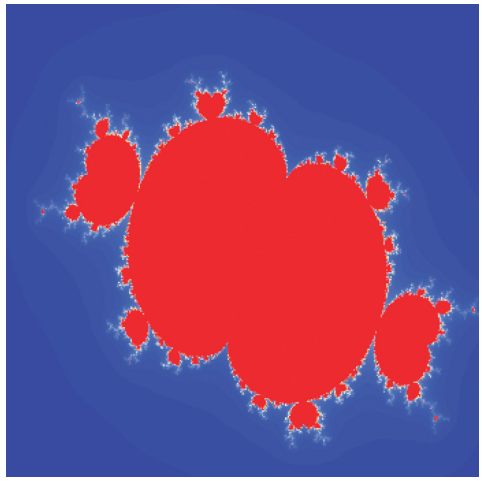

Figure 24: Cubic Mandelbrot set in JSOmhh.

Figure 19 is multishaped, Figure 20 is like semiquadratic semicubic, and Figure 23 is like Hexic Mandelbrot sets, respectively. The involved parameters were as follows:

Figure 19: $p = 3$, $a_1 = 2/3$, $a_2 = 1, a_3 = 3$, a, b, s, $m = 0.9$, $A = [-0.001, 0.0045] \times [-0.0015, 0.0015]$.

Figure 20: $p = 3$, $a_1 = 2, a_2 = 1, a_3 = 3(a_0 - 1)$, a, b, $m, s = 0.5$, $A = [-0.9, 1.05] \times [-0.9, 0.9]$.

Figure 21: $p = 3$, $a_1 = 1, a_2 = 1, a_3 = 30$, $a, b = 0.9$, $m, s = 0.5$, $A = [-0.03, 0.025] \times [-0.045, 0.045]$.

Figure 22: $p = 3$, $a_1 = 1/2, a_2 = 3a_0^2, a_3 = 3a_0^3$, a, b, $m = 0.9, s = 0.5$, $A = [-0.2, 0.2] \times [-0.2, 0.2]$.

Figure 23: $p = 3$, $a_1 = 1 + \mathbf{i}$, $a_2 = 45, a_3 = 50$, a, b, s, $m = 0.9$, $A = [-0.0001, 0.0001] \times [-0.0002, 0.0001]$.

Figure 24: $p = 3$, $a_1 = 1 + \mathbf{i}$, $a_2 = 1, a_3 = 50$, a, b, s, $m = 0.9$, $A = [-0.0022, 0.0017] \times [-0.0015, 0.0015]$.

5. Conclusions

Fractals can be used to capture images of these complex structures. In addition, fractals are used to predict or analyze various biological processes or phenomena such as the growth pattern of bacteria and the pattern of situations such as nerve dendrites. We established the Jungck–S orbit with (m, h_1, h_2)–convexity and derived the new escape criteria for the execution of fractals. We introduced two algorithms in this paper for Julia and Mandelbrot sets. Some examples of quadratic and cubic fractals (i.e., Julia and Mandelbrot sets) were presented in detail. We observed the following characteristics of fractals in JSOmhh:

A very small change in the involved parameters caused the drastic change in fractals.

For large values of a_i's, area of the image will be small.

Self-similarity is observed in each image of Julia and Mandelbrot sets. Hence, the visualized complex graphs were the fractals.

In our future research work, we intend to obtain the escape radius for other Jungck-type iterative schemes with (m, h_1, h_2)–convexity. We believe this paper will attract researchers who work on the investigations of different types of fractals [23, 24].

Data Availability

All data required for this paper are included within this paper.

Conflicts of Interest

The authors declare that there are no conflicts of interest.

Authors' Contributions

Zhihua Chen wrote the applications of results in Engineering, enhanced the introduction, and improved the English language. Muhammad Tanveer used the software to generate fractals. Waqas Nazeer proved the main results. Jing Wu wrote the final draft of the paper.

Acknowledgments

The authors are thankful to Professor Yu-Ming Chu for his valuable suggestions and help in witting this paper. This work was supported by the Chinese National Natural Science Foundation under Grant 61876047. This work was sponsored in part by (1) National Natural Science Foundation of China (11501436), (2) Scientific Research Project of Shanxi Provincial Education Department (20JK0963), and (3) Xijing College Fund Project (XJ200102).

References

[1] B. B. Mandelbrot, *The fractal geometry of nature*, W. H. Freeman, New York, NY, 1982.

[2] A. Lakhtakia, V. V. Varadan, R. Messier, and V. K. Varadan, "On the symmetries of the Julia sets for the process z⇒zp+c," *Journal of Physics A: Mathematical and General*, vol. 20, no. 11, pp. 3533–3535, 1987.

[3] P. Blanchard, R. L. Devaney, A. Garijo, and E. D. Russell, "A generalized version of the mcmullen domain," *International Journal of Bifurcation and Chaos*, vol. 18, no. 08, pp. 2309–2318, 2008.

[4] T. Kim, "Quaternion julia set shape optimization," *Computer Graphics Forum*, vol. 34, pp. 167–176, 2015.

[5] V. Drakopoulos, N. Mimikou, and T. Theoharis, "An overview of parallel visualisation methods for mandelbrot and julia sets," *Computers & Graphics*, vol. 27, no. 4, pp. 635–646, 2003.

[6] Y. Sun, L. Chen, R. Xu, and R. Kong, "An image encryption algorithm utilizing julia sets and hilbert curves," *PloS One*, vol. 9, no. 1, p. 655, Article ID e84655, 2014.

[7] M. Rani and V. Kumar, "Superior julia set," *Research in Mathematical Education*, vol. 8, no. 4, pp. 261–277, 2004.

[8] M. Rani and V. Kumar, "Superior mandelbrot set," *Research in Mathematical Education*, vol. 8, no. 4, pp. 279–291, 2004.

[9] M. Rani and R. Agarwal, "Effect of stochastic noise on superior julia sets," *Journal of Mathematical Imaging and Vision*, vol. 36, no. 1, p. 63, 2010.

[10] A. Nagi, M. Rani, and R. Chugh, "Julia sets and mandelbrot sets in noor orbit," *Applied Mathematics and Computation*, vol. 228, pp. 615–631, 2014.
[11] S. M. Kang, A. Rafiq, A. Latif, A. A. Shahid, and Y. C. Kwun, "Tricorns and multicorns of-iteration scheme," *Journal of Function Spaces*, vol. 2015, Article ID 417167, 7 pages, 2015.
[12] K. Goyal and B. Prasad, "Dynamics of iterative schemes for quadratic polynomial," *AIP Conference*, vol. 9, no. 2, pp. 149–153, 2001.
[13] New Julia and Mandelbrot Sets for a New Faster Iterative Process.
[14] M. F. Barnsley, *Fractals Everywhere*, Academic Press, Boston, Massachusetts, 2 edition, 1993.
[15] R. L. Devaney, *A First Course in Chaotic Dynamical Systems: Theory and Experiment*, Addison-Wesley, New York, NY, 1992.
[16] L. Xiangdong, Z. Zhiliang, W. Guangxing, and Z. Weiyong, "Composed accelerated escape time algorithm to construct the general Mandelbrot set," *Fractals*, vol. 9, no. 2, pp. 149–153, 2001.
[17] V. Valery, S. A. Smirnov, S. E. Korepanov, and V. Alexey, Object distance estimation algorithm for real-time fpga-based stereoscopic vision system," *High-Performance Computing in Geoscience and Remote Sensing VIII*, vol. 10792, Article ID 107920A, 2018.
[18] J. Barrallo, Jones, Coloring algorithms for dynamical systems in the complex plane," *Visual Mathematics*, vol. 1, 1999.
[19] O. Khatib, *Real-time obstacle avoidance for manipulators and mobile robots Autonomous Robot Vehicles*, pp. 396–404, Springer, Berlin, Germany, 1986.
[20] N. Hussain, V. Kumar, and M. A. Kutbi, "On rate of convergence of Jungck-type iterative schemes," *Abstract and Applied Analysis*, vol. 2013, Article ID 132626, 15 pages, 2013.
[21] W. Nazeer, S. M. Kang, M. Tanveer, and A. A. Shahid, "Fixed point results in the generation of julia and mandelbrot sets," *Journal of Inequalities and Applications*, vol. 2015, no. 1, p. 298, 2015.
[22] Y. C. Kwun, M. Tanveer, W. Nazeer, M. Abas, and S. M. Kang, "Fractal generation in modified jungck-s orbit," *IEEE Access*, vol. 7, pp. 35060–35071, 2019.
[23] D. Kaur, P. Agarwal, M. Rakshit, and M. Chand, "Fractional calculus involving (p, q)-mathieu type series," *Applied Mathematics and Nonlinear Sciences*, vol. 5, no. 2, pp. 15–34, 2020.
[24] K. A. Touchent, Z. Hammouch, and T. Mekkaoui, "A modified invariant subspace method for solving partial differential equations with non-singular kernel fractional derivatives," *Applied Mathematics and Nonlinear Sciences*, vol. 5, no. 2, pp. 35–48, 2020.

Hindawi
Discrete Dynamics in Nature and Society
Volume 2021, Article ID 6697341, 11 pages
https://doi.org/10.1155/2021/6697341

Research Article

Nonlinear Dynamics of Cournot Duopoly Game: When One Firm Considers Social Welfare

S. S. Askar[1,2] **and A. A. Elsadany**[3]

[1]*Department of Statistics and Operations Research, College of Science, King Saud University, Riyadh, Saudi Arabia*
[2]*Department of Mathematics, Faculty of Science, Mansoura University, Mansoura, Egypt*
[3]*Department of Basic Science, Faculty of Computers and Informatics, Suez Canal University, Ismailia 41522, Egypt*

Correspondence should be addressed to S. S. Askar; s.e.a.askar@hotmail.co.uk

Received 15 December 2020; Revised 12 January 2021; Accepted 15 January 2021; Published 27 January 2021

Academic Editor: Ya Jia

In this paper, we study the competition between two firms whose outputs are quantities. The first firm considers maximization of its profit while the second firm considers maximization of its social welfare. Adopting a gradient-based mechanism, we introduce a nonlinear discrete dynamic map which is used to describe the dynamics of this game. For this map, the fixed points are calculated and their stability conditions are analyzed. This includes investigating some attracting set and chaotic behaviors for the complex dynamics of the map. We have also investigated the types of the preimages that characterize the phase plane of the map and conclude that the game's map is noninvertible of type $Z_4 - Z_2$.

1. Introduction

Because of the appearance of the wealth theory in [1, 2], many studies on Cournot and Bertrand games have been raised. For instance, Singh and Vives introduced a quadratic utility function that has been used to model and study a Cournot duopoly game in [3]. This utility function has been also adopted in different games by many authors such as Askar [4–7], Elsadany [8], Naimzada and Tramontana [9], and Ma and Pu [10]. Modelling such games in a discrete time periods requires some mechanisms such as bounded rationality, Puu's approach, naive expectation, and other adaptive methods.

Several studies have been adopted both bounded rationality and Puu's incomplete information. They are two different mechanisms. For the bounded rationality, the game's players (or firms) are updating their output production depending on discrete time steps and by using a local estimate of their marginal profits. Furthermore, the players do not have to possess a complete knowledge of both demand and cost functions. However, they instead want to discover whether the market responses to small changes in production using an estimation of their marginal profits. For more applications on this mechanism which is sometimes called a myopic mechanism, one can see [11, 12]. The so-called Puu's mechanism has been introduced in [13]. It is characterized by its realistic feature that is the firms do not have to know the profit function in order to get estimation of the commodity produced at the next period of time. The firms only require the commodity and profit at the past two periods of time. There are some other updating mechanisms that have been reported in the literature. For instance, Long and Huang [14], Agiza and Elsadany [15], Kopel [16], Elabbasy et al. [17, 18], Askar and Abouhawwash [19], Hommes [20], Tremblay et al. [21], Ahmed et al. [22], Baiardi and Naimzada [23], Fanti et al. [24], Elsadany and Awad [25], Tremblay and Tremblay [26], Askar and Al-Khedhairi [27], and Gao and Du [28].

The majority of the literature has been analyzed for models of mixed oligopoly on the basis that the game has been in a static case. Liu et al. [29] investigated the static game of endogenous horizontal product differentiation in a mixed duopoly. The relationship between privatization and corporate tax policies has been studied in [30]. Nie [31] has

analyzed the effects of capacity constraints on the mixed duopoly game. The strategy for cost-reduction innovation in the mixed economy has been explored in [32]. All of earlier papers have not discussed the case of a dynamic mixed oligopoly model.

The current paper introduces a dynamic game of Cournot duopoly on which two firms are competing but they are different in optimization process. The first firm focuses on maximizing its profit that depends on a quadratic production cost. The second firm is different and wants to maximize its social welfare using the same quadratic cost form. The main contribution considers introducing such optimization problem and dynamic characteristics emanated from the game's map. Furthermore, the monopolistic case is studied and is shown that each firm behaves monopolistically such as the standard logistic process. In the duopolistic case, the equilibrium points are calculated and their stability conditions are analyzed. Indeed, this includes local and global analysis of the routes by which these equilibrium points can be destabilized. The numerical simulation shows that some attracting sets are born due to both period-doubling and Neimark–Sacker bifurcations. In addition, the nonlinearity and noninvertibility of the game's map give rise to such complex behaviors.

The outline of current paper is divided into the following sections. After the introduction, we give in Section 2 the description of the game represented by a two-dimensional discrete dynamic map. In Section 3, we calculate the game's fixed points and study their stability. Furthermore, we give in this section a detailed discussion on the monopolistic case. In addition, we study by numerical simulation the attracting sets and chaotic behaviors arise due to the dynamics of the duopoly case. Moreover, we investigate the critical curves of the map and categorize the phase plane regions. Finally, we give our conclusion on the obtained results within this paper.

2. Cournot Duopoly Game

The game is constructed based on two competing firms with quantity-based strategies and differentiated products. The quantities produced by the two firms are denoted by q_1 and q_2. Their demand functions are obtained by recalling the following utility function:

$$U(q_1, q_2) = a(q_1 + q_2) - \frac{1}{2}\left(q_1^2 + 2\mathrm{d}qq_2 + q_2^2\right). \quad (1)$$

More information on this utility is given in [3]. Both a and d are constants. Supposing the budget constraint $p_1q_1 + p_2q_2 = M$, we get the following maximization problem:

$$\begin{aligned} &\mathrm{Max}U(q_1, q_2), \\ &s.t. \quad p_1q_1 + p_2q_2 = M. \end{aligned} \quad (2)$$

Solving (2) gives

$$\begin{cases} p_1 = a - q_1 - \mathrm{d}q_2, \\ p_2 = a - q_2 - \mathrm{d}q_1, \end{cases} \quad (3)$$

where p_1 and p_2 denote the retail prices of the two firms' products, respectively. The constants $a > 0$ represent the maximum price while $d \in [-0.5, 1]$ represents the product differentiation. $d = 1$ indicates homogeneous products while $d = 0$ means we have two monopolistic firms. Consider the following cost function:

$$C_i(q_i) = \frac{c}{2}q_i^2, \quad i = 1, 2, \quad (4)$$

where $c > 0$. Now, the profits of the two firms are given by

$$\begin{aligned} \pi_1 &= p_1q_1 - \frac{c}{2}q_1^2 = (1 - q_1 - \mathrm{d}q_2)q_1 - \frac{c}{2}q_1^2, \\ \pi_2 &= (1 - q_2 - \mathrm{d}q_1)q_2 - \frac{c}{2}q_2^2. \end{aligned} \quad (5)$$

The consumer surplus is assumed to be $\mathrm{CS} = (1/2)(q_1^2 + q_2^2 + 2\mathrm{d}q_1q_2)$. The social welfare is defined as the sum of consumer surplus and profits as follows: $W = \mathrm{CS} + \pi_1 + \pi_2$. Now, both firms want to maximize the following payoffs:

$$\begin{aligned} \pi_1 &= (a - q_1 - \mathrm{d}q_2)q_1 - \frac{c}{2}q_1^2, \\ \Pi_2 &= \omega\pi_2 + (1 - \omega)W, \end{aligned} \quad (6)$$

where $\omega \in [0, 1]$. We should highlight that lack of market demand and consumer information bring difficulty for producers. Therefore, producers estimate the market demand by adopting the gradient mechanism defined below:

$$\begin{cases} q_1(t+1) = q_1(t) + \nu_1q_1\dfrac{\partial\pi_1}{\partial q_1}, \\ q_2(t+1) = q_2(t) + \nu_2q_2\dfrac{\partial\Pi_2}{\partial q_2}, \end{cases} \quad (7)$$

where ν_i represents the adjustment speed for the i^{th} firm. Using (6) in (7), we get the map's game:

$$T(q_1, q_2): \begin{cases} q_1(t+1) = q_1(t) + \nu_1q_1[a - (2 + c)q_1 - \mathrm{d}q_2], \\ q_2(t+1) = q_2(t) + \nu_2q_2[a - (1 + \omega + c)q_2 - \mathrm{d}q_1]. \end{cases} \quad (8)$$

This map is a quadratic discrete dynamic map, and it is converted into Fanti's map [24] at $\omega = 1$.

3. Equilibrium Points and Their Stability

Setting $q_i(t+1) = q_i(t) = q_i$, $i = 1, 2$ in (8), one obtains

$$\begin{cases} q_1[a - (2 + c)q_1 - \mathrm{d}q_2] = 0, \\ q_2[a - (1 + \omega + c)q_2 - \mathrm{d}q_1] = 0. \end{cases} \quad (9)$$

Solving algebraically system (9), we get four fixed points as follows:

$$E_0 = (0,0),$$

$$E_1 = \left(\frac{a}{c+2}, 0\right),$$

$$E_2 = \left(0, \frac{a}{c+\omega+1}\right),$$

$$E_* = (q_1^*, q_2^*) = \left(\frac{a + a\omega + ac - a\,d}{3c + 2\omega + c\omega + c^2 - d^2 + 2}, \frac{2a + ac - a\,d}{3c + 2\omega + c\omega + c^2 - d^2 + 2}\right), \tag{10}$$

where E_0, E_1, E_2 are called boundary fixed points while E_* is called a Nash equilibrium point. It should be noted that the equilibrium points E_* become the same as of Fanti's equilibrium point when $\omega = 1$. Studying the stability of these points requires to calculate the Jacobian matrix of the map:

$$J = \begin{bmatrix} 1 + \nu_1[a - 2(2+c)q_1 - \mathrm{d}q_2] & -\nu_1 \mathrm{d} q_1 \\ -\nu_2 \mathrm{d} q_2 & 1 + \nu_2[a - 2(1+\omega+c)q_2 - \mathrm{d}q_1] \end{bmatrix}. \tag{11}$$

It has the following characteristic polynomial:

$$f(\lambda) = \lambda^2 - \mathrm{tr}(J(E))\lambda + \det(J(E)), \tag{12}$$

where $\mathrm{tr}(J)$ and $\det(J)$ represent trace and determinant of (11). They are used in Jury conditions [4]. These conditions are given by

$$\begin{aligned} &f(1) = 1 - \mathrm{tr}(J(E)) + \det(J(E)) > 0, \\ &f(-1) = 1 + \mathrm{tr}(J(E)) + \det(J(E)) > 0, \\ &\det(J) < 1. \end{aligned} \tag{13}$$

The above conditions characterize different types of bifurcations by which the equilibrium points may be unstable. These types are summarized in the following:

(1)Period-doubling bifurcation is raised when $f(-1) = 0$

(2) Transcritical or fold bifurcation is raised when $f(1) = 0$

(3) Neimark–Sacker bifurcation is raised when $\det(J) < 1$

Now, we study the stability of the fixed points.

Theorem 1. *The fixed point E_0 is unstable point.*

Proof. The Jacobian matrix given in (11) at this point becomes

$$J(E_0) = \begin{bmatrix} 1 + \nu_1 a & 0 \\ 0 & 1 + \nu_2 a \end{bmatrix}. \tag{14}$$

It is clear that (15) is a diagonal matrix and hence its eigenvalues become $\lambda_1 = 1 + \nu_1 a$ and $\lambda_2 = 1 + \nu_2 a$. Because of the positivity of the parameters a, ν_1, and ν_2, we have $|\lambda_{1,2}| > 1$ and so E_0 is unstable repelling node. □

Theorem 2. *The fixed point E_1 is saddle point.*

Proof. The Jacobian matrix given in (11) at this point becomes

$$J(E_1) = \begin{bmatrix} 1 - \nu_1 a & \dfrac{\nu_1 d}{c+2} \\ 0 & 1 + \nu_2\left(\dfrac{2a}{c+2}\right) \end{bmatrix}. \tag{15}$$

It is clear that (15) is a triangular matrix and hence its eigenvalues become $\lambda_1 = 1 - \nu_1 a$ and $\lambda_2 = 1 + \nu_2(2a/(c+2))$. It is simple to see $|\lambda_1| < 1$ and $|\lambda_2| > 1$. Therefore, the fixed point E_1 is saddle point. □

Theorem 3. *The fixed point E_2 is saddle point.*

Proof. The Jacobian matrix given in (11) at this point becomes

$$J(E_2) = \begin{bmatrix} 1 + \nu_1\left(\dfrac{a(c+\omega+1-d)}{c+\omega+1}\right) & 0 \\ \dfrac{-\nu_2 a\,d}{c+\omega+1} & 1 - a\nu_2 \end{bmatrix}. \tag{16}$$

It is clear that (16) is a triangular matrix and hence its eigenvalues become $\lambda_1 = 1 + \nu_1((a(c+\omega+1-d))/(c+\omega+1))$ and $\lambda_2 = 1 - a\nu_2$. Because of the positivity of the parameters a, ν_1, ν_2, and $d < 1$, we have $|\lambda_1| > 1$ and $|\lambda_2| < 1$. Therefore, the point E_2 is saddle point.

For Nash equilibrium point, the Jacobian becomes

$$\mathbf{J}(E_*) = \begin{pmatrix} 1 - \dfrac{a(2+c)(1+\omega+c-d)}{2+2\omega+3c-d^2+c\omega+c^2}\nu_1 & -\dfrac{a\,d(1+\omega+c-d)}{2+2\omega+3c-d^2+c\omega+c^2}\nu_1 \\ -\dfrac{a\,d(2+c-d)}{2+2\omega+3c-d^2+c\omega+c^2}\nu_2 & 1 - \dfrac{a(2+c-d)(1+\omega+c)}{2+2\omega+3c-d^2+c\omega+c^2}\nu_2 \end{pmatrix}, \tag{17}$$

whose trace and determinant are given by

$$\operatorname{tr}\left(\mathbf{J}\left(E_*\right)\right) = 2 - \frac{a(2+c)(1+\omega+c-d)\nu_1 + a(1+\omega+c)(2+c-d)\nu_2}{2+2\omega+3c-d^2+c\omega+c^2},$$
$$\operatorname{Det}\left(\mathbf{J}\left(E_*\right)\right) = 1 + \frac{a^2(2+c-d)(1+\omega+c-d)\nu_1\nu_2 - a(1+\omega+c)(2+c-d)\nu_2 - 2a(2+c)(1+\omega+c-d)\nu_1}{2+2\omega+3c-d^2+c\omega+c^2}. \tag{18}$$

The eigenvalues of $\mathbf{J}(E_*)$ have a long analytical form, and instead we discuss the stability of the Nash equilibrium point by using Jury conditions:

$$\begin{cases} 1 - \operatorname{tr}\left(\mathbf{J}\left(E_*\right)\right) + \operatorname{Det}\left(\mathbf{J}\left(E_*\right)\right) > 0, \\ 1 + \operatorname{tr}\left(\mathbf{J}\left(E_*\right)\right) + \operatorname{Det}\left(\mathbf{J}\left(E_*\right)\right) > 0, \\ 1 - \operatorname{Det}\left(\mathbf{J}\left(E_*\right)\right) > 0, \end{cases} \tag{19}$$

which can be rewritten in the form

$$\begin{aligned} &\frac{a^2(2+c-d)(1+\omega+c-d)\nu_1\nu_2}{2+2\omega+3c-d^2+c\omega+c^2} > 0, \\ &4 - \Phi > 0, \\ &\Phi > 0, \\ &\Phi = \frac{a(1+\omega+c)(2+c-d)\nu_2 + 2a(2+c)(1+\omega+c-d)\nu_1 - a^2(2+c-d)(1+\omega+c-d)\nu_1\nu_2}{2+2\omega+3c-d^2+c\omega+c^2}. \end{aligned} \tag{20}$$

It is easy to see that the first condition of (20) is always fulfilled. If the other two conditions are fulfilled, then E_* is locally asymptotically stable provided that $0 < \Phi < 4$. On the other hand, if $\Phi \geq 4$, this means E_* gets unstable due to the coexistence of period-doubling bifurcation. In addition, it becomes unstable due to Neimark–Sacker bifurcation provided that $\Phi \leq 0$. The next section gives some insights about the above analytical analysis. □

3.1. Discussion and Numerical Simulation. Let us now discuss the monopoly case of map (8). It is easy to see that this map is trapped to the point $(0,0)$ which means at $q_1(t) = 0$ or $q_2(t) = 0$, it gives $q_1(t+1) = 0$ or $q_2(t+1) = 0$. Setting $q_1(t) = 0$ or $q_2(t) = 0$ in (8), one gets the following:

$$\begin{aligned} q_1(t+1) &= q_1(t) + \nu_1 q_1(t)\left[a - (2+c)q_1(t)\right], \\ q_2(t+1) &= q_2(t) + \nu_2 q_2(t)\left[a - (1+\omega+c)q_2(t)\right], \end{aligned} \tag{21}$$

which can be simplified to

$$\begin{aligned} q_1(t+1) &= (1+a\nu_1)q_1(t)\left(1 - \frac{\nu_1(2+c)}{1+a\nu_1}q_1(t)\right), \\ q_2(t+1) &= (1+a\nu_2)q_2(t)\left(1 - \frac{\nu_2(1+\omega+c)}{1+a\nu_2}q_2(t)\right). \end{aligned} \tag{22}$$

Separately, each part of (22) conjugates the standard logistic map, $y_j(t+1) = \mu_j y_j(t)(1 - y_j(t))$, $j = 1, 2$. Then, we have the following linear transformations for (22): \openup4

$$\begin{aligned} q_1(t) &= \frac{1+a\nu_1}{\nu_1(2+c)}y_1(t), \\ q_2(t) &= \frac{1+a\nu_2}{\nu_2(1+\omega+c)}y_2(t), \\ \mu_j &= 1 + a\nu_j; \quad j = 1, 2. \end{aligned} \tag{23}$$

This implies that the dynamics of (22) are the same as the logistic map. Each part in (22) is separately a unimodel map. Both have unique critical points $C_{q_1}^{-1}$ and $C_{q_2}^{-1}$ with coordinates given by

$$\begin{aligned} \breve{q}_1 &= \frac{1+a\nu_1}{2\nu_1(2+c)}, \\ \breve{q}_2 &= \frac{1+a\nu_2}{2\nu_2(1+\omega+c)}. \end{aligned} \tag{24}$$

These coordinates conjugate the critical points $y_1 = (1/2)$ and $y_2 = (1/2)$. In addition, system (22) has the following fixed points:

$$q_1^O = 0,$$
$$q_1^{O_1} = \frac{a}{2+c},$$
$$q_2^O = 0,$$
$$q_2^{O_2} = \frac{a}{1+\omega+c}, \tag{25}$$

which conjugate $y_1 = 0$, $y_1 = 1 - (1/\mu_1)$, $y_2 = 0$, and $y_2 = 1 - (1/\mu_2)$ of the logistic map. It is easy to see that $|(\mathrm{d}q_i(t+1))/(\mathrm{d}q_i(t))|_{q_i^O=0} = 1 + a\nu_i > 1, i = 1, 2$ and then $q_i^O, i = 1, 2$ is an unstable repelling point. In addition, we can see that both $q_1^{O_1}$ and $q_2^{O_2}$ are stable attracting points under the condition $0 < a\nu_i < 2, i = 1, 2$. At $a\nu_i > 2, i = 1, 2$, the dynamics of each part in (22) may be a period cycle or a cyclic chaotic attractor. These behaviors are characterized by basins of attraction that are bounded by the repelling points q_1^O or q_2^O and their preimages. These preimages are obtained by setting $q_i(t+1) = 0, i = 1, 2$ in (22) as follows:

$$q_1^{O_{-1}} = \frac{1 + a\nu_1}{\nu_1(2+c)},$$
$$q_2^{O_{-1}} = \frac{1 + a\nu_2}{\nu_2(1+\omega+c)}, \tag{26}$$

which conjugate $y_1 = 1$ and $y_2 = 1$ in the logistic map. Therefore, for the first part of (22), any trajectories starting out of the interval $[0, q_1^{O_{-1}}]$ will be divergent to $-\infty$. The same observation is for the second part of (22). In order to validate the obtained results in the monopoly case, we use numerical simulation by assuming the following parameters' values: $a = 0.5, c = 0.2$. Figure 1(a) shows that $q_1^{O_1}$ is stable for all the values of ν_1 until the parameter reaches the value $\nu_1 = (2/a)$ on where the period-2 cycle arises. At $\nu_1 = 3.88$, Figure 1(b) presents the basins of attraction of the stable point $q_1^{O_1}$. It is also obvious that the basins are bounded by the box defined by $[0, q_1^{O_{-1}}] \times [0, q_1^{O_{-1}}]$. At $k = 5.9$, we give a situation of unstable $q_1^{O_1}$ due to a chaotic attractor behavior. As shown in Figure 1(c), the basins of this chaotic attractor lie within the box $[0, q_1^{O_{-1}}] \times [0, q_1^{O_{-1}}]$. For the second part of (22), we have the same discussions. Figure 1(d) shows that $q_2^{O_2}$ is stable for the values of ν_2 until the parameter reaches $(2/a)$. Reaching this value gives rise to periodic cycle and chaotic attractor. For instance, at the parameters set $a = 0.5, \omega = 0.9, c = 0.2$, and $\nu_2 = 3.88$, the basins of attraction of the stable point $q_2^{O_2}$ are given in Figure 1(e). As ν_2 increases to 5.9, the point $q_2^{O_2}$ gets unstable and chaotic attractor appears. The basins for this chaotic attractor are given in Figure 1(f). We can conclude that as ν_2 increases further, any dynamic behavior will be bounded by the box $[0, q_2^{O_{-1}}] \times [0, q_2^{O_{-1}}]$.

Now, we carry out some numerical simulations in order to investigate and analyze the influences of the parameters ν_1 and ν_2 on the map given in (8). All numerical simulations in this section are performed at the initial datum $(q_1(0), q_2(0)) = (0.11, 0.12)$. Assuming the parameters set, $a = 0.5, c = 0.2, d = 0.35$, and $\omega = 0.45$. This gives $E_* = (0.1853171775, 0.2637205988)$. Assuming $\nu_1 = 3.5$ and $\nu_2 = 4.2$, then (18) becomes

$$\mathbf{J}(E_*) \approx \begin{pmatrix} -0.42694 & -0.22701 \\ -0.38767 & -0.82758 \end{pmatrix}, \tag{27}$$

which has two real eigenvalues, $\lambda_1 \approx -0.26930$ and $\lambda_2 \approx -0.98522$. One can see that $|\lambda_{1,2}| < 1$ and hence E_* is a local stable point. Keeping the parameter set including ν_2 fixed and increasing ν_1 to 3.65, the Jacobian $\mathbf{J}(E_*)$ gets

$$\mathbf{J}(E_*) \approx \begin{pmatrix} -0.48810 & -0.23674 \\ -0.38767 & -0.82758 \end{pmatrix}, \tag{28}$$

and then the real eigenvalues become $\lambda_1 \approx -0.31058$ and $\lambda_2 \approx -1.0051$. This means that E_* is changed into an unstable saddle point. Now, we perform some numerical simulation experiments in order to get more insights on the dynamic of map (8) around the equilibrium point E_*. We start our analysis by investigating the effects of the adjustment parameters ν_1 and ν_2 on the map. In Figures 2(a) and 2(b), we present the bifurcation diagram for the influences of the parameters ν_1 and ν_2 on the quantities q_1 and q_2 at the parameters values, $a = 0.5, c = 0.2, d = 0.35$, and $\omega = 0.45$. They show that the equilibrium point may be destabilized due to period-doubling bifurcation. Figure 2(c) confirms the chaotic behavior of the map by presenting the largest Lyapunov exponent. In Figures 2(d)–2(h), we give some different dynamic situations of the map due to varying the parameter ν_1 and keeping the parameter $\nu_2 = 4.2$. They present the attractive basins of periodic cycles 2, 4, and 8. Besides that, we show in Figures 2(g) and 2(h) two different chaotic attractors for the map around the equilibrium point. We have two disconnected attractors around the equilibrium point given in Figure 2(g) which gather together to form a one chaotic attractor as given in Figure 2(h).

Now, we study another situation when the parameter ν_2 is varied and ν_1 becomes constant at the value 5. Figure 3(a) shows the 1D bifurcation diagram taking ν_1 as the bifurcation parameter and the other parameters are selected to be $a = 0.5, c = 0.2, d = 0.35, \omega = 0.45$, and $\nu_2 = 5$ while Figure 3(b)) depicts the bifurcation diagram with respect to the parameter ν_2 and the other parameters' values are $a = 0.5, c = 0.2, d = 0.35, \omega = 0.45$, and $\nu_1 = 3$. It is clear that the equilibrium point becomes locally asymptotically stable till it reaches the point on where it can be destabilized due to period-doubling bifurcation. Due to a series of period-doubling bifurcated points, the map becomes chaotic and enters the chaos region and this is confirmed in Figure 3(c) which shows the Lyapunov exponent with respect to the variables ν_1 and ν_2. Now, we use some numerical experiments to investigate more the dynamics of the map. Setting the parameters' values to $a = 0.5, c = 0.2, d = 0.35, \omega = 0.45, \nu_1 = 5$, and $\nu_2 = 5$, we get in Figure 3(d)) four closed invariant sets around the equilibrium point. Further increase in ν_2 to 5.2 makes these four sets convert into four disconnected chaotic attractors as shown in Figure 3(e) which turn into two chaotic attractors as ν_2 increases to 5.3 as given in Figure 3(f). At $\nu_2 = 5.4$, a

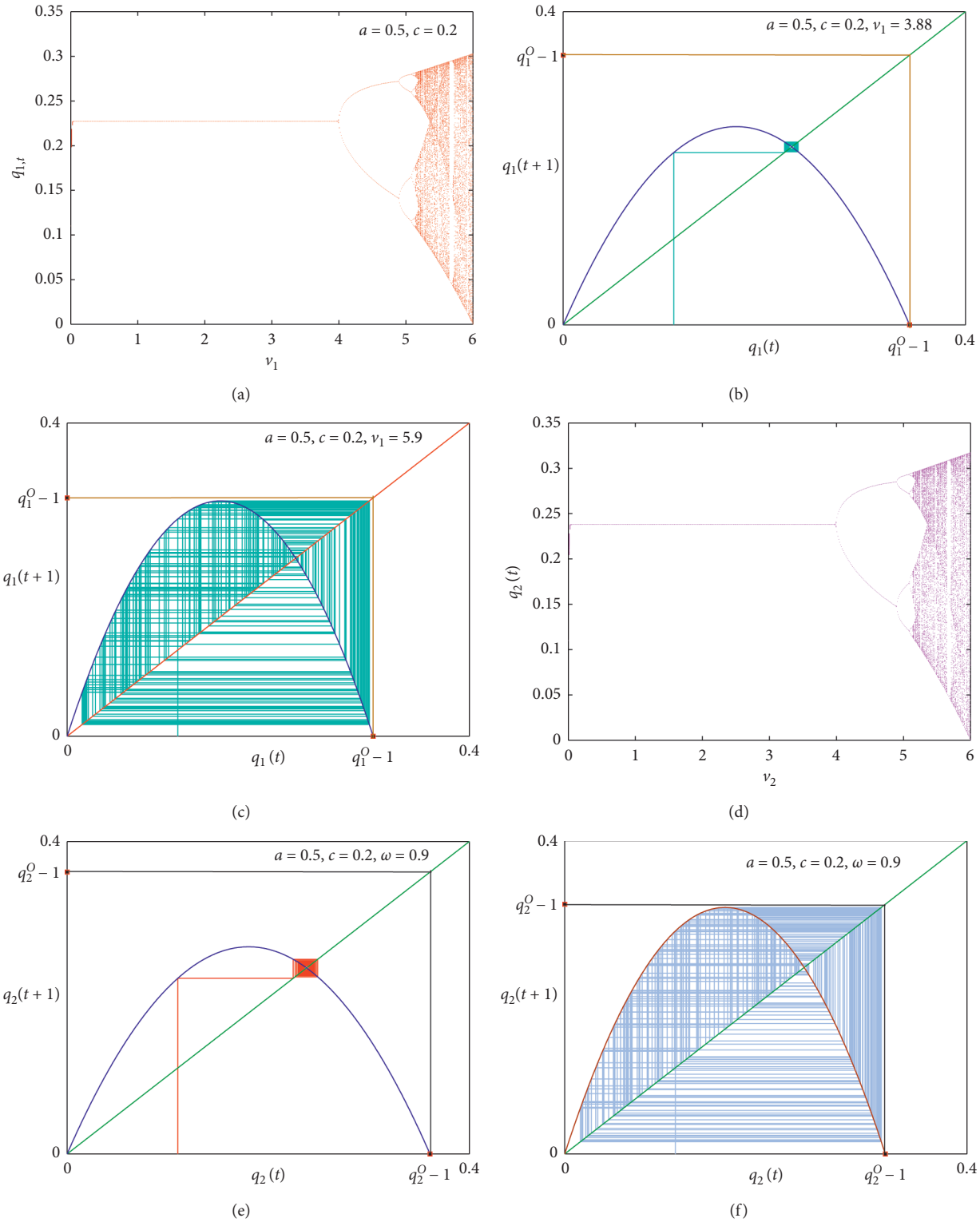

FIGURE 1: (a) Bifurcation diagram in (v_1, q_1) – plane. (b) The basins of attraction of the stable point $q_1^{O_1}$ at $k = 3.88$. (c) The basins of attraction of the stable point $q_1^{O_1}$ at $k = 5.9$. (d) Bifurcation diagram in (v_2, q_2) – plane. (e) The basins of attraction of the stable point $q_2^{O_2}$ at $k = 3.88$. (f) The basins of attraction of the stable point $q_2^{O_2}$ at $k = 5.9$. The other values of the parameters are $a = 0.5$, $c = 0.2$, and $\omega = 0.9$.

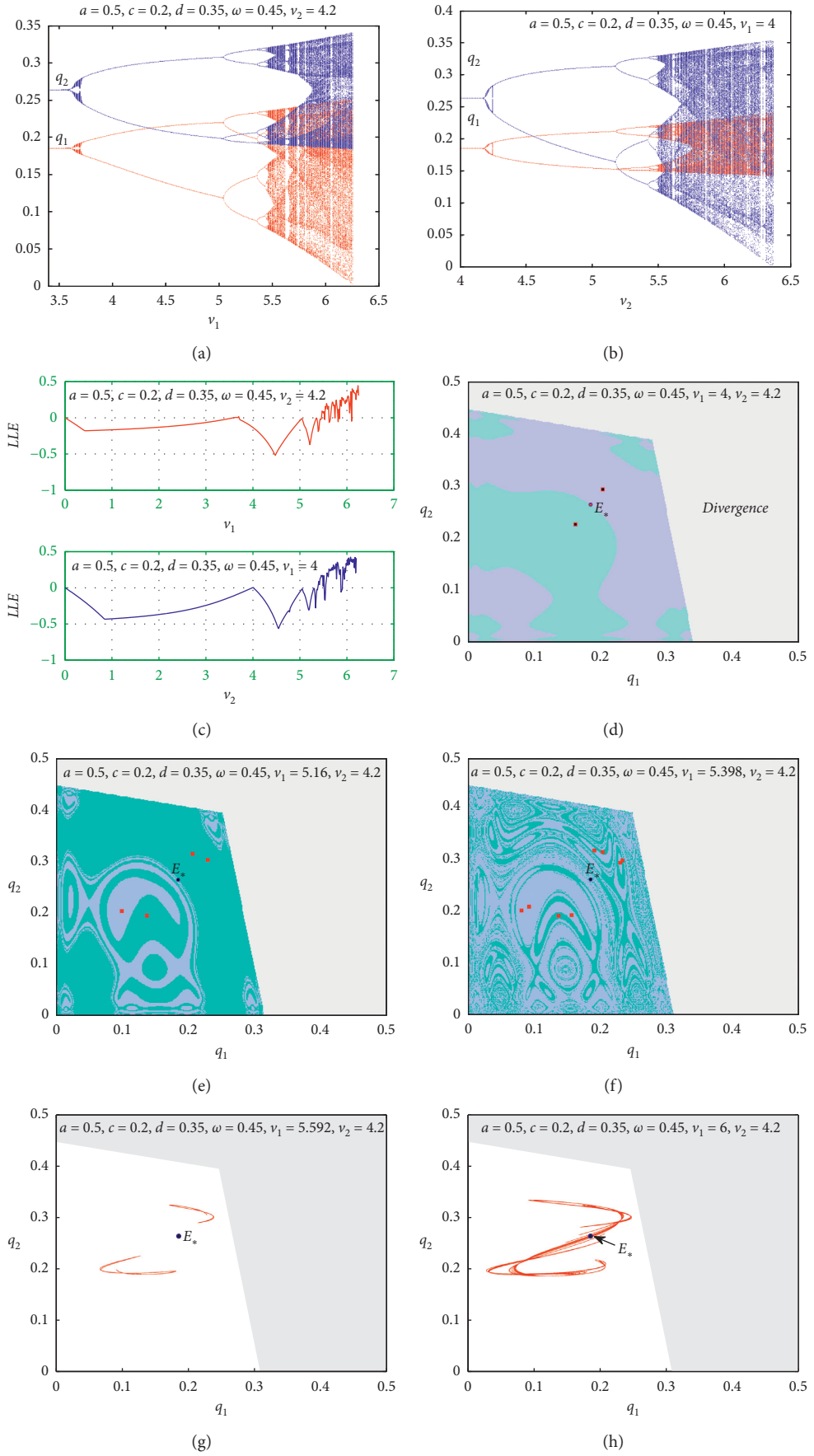

FIGURE 2: (a),(b) Bifurcation diagram with respect to q_1 and q_2 on varying ν_1 and ν_2. (c) Largest Lyapunov exponents with respect to ν_1 and ν_2. Basins of attraction for (d) period-2 cycle at $\nu_1 = 4$ and $\nu_2 = 4.2$. (e) Period-4 cycle at $\nu_1 = 5.16$ and $\nu_2 = 4.2$. (f) Period-8 cycle at $\nu_1 = 5.398$ and $\nu_2 = 4.2$. (g) Two unconnected chaotic attractors at $\nu_1 = 5.592$ and $\nu_2 = 4.2$. (h) One chaotic attractor at $\nu_1 = 6$ and $\nu_2 = 4.2$. Other parameters are $a = 0.5, c = 0.2, d = 0.35$, and $\omega = 0.45$.

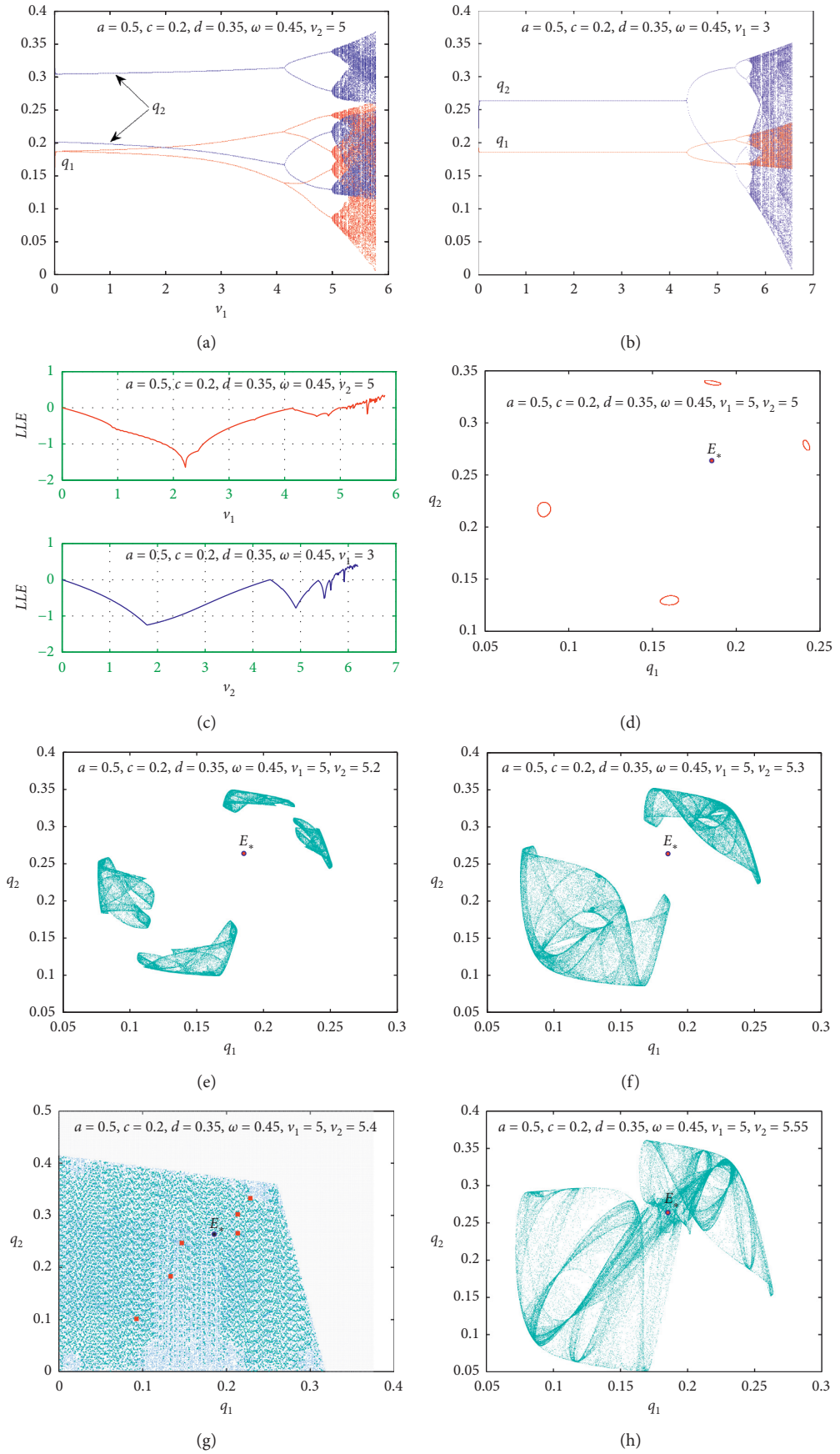

FIGURE 3: (a),(b) Bifurcation diagram with respect to q_1 and q_2 on varying ν_1 and ν_2. (c) Largest Lyapunov exponents with respect to ν_1 and ν_2. Phase plane for (d) four closed invariant sets at $\nu_1 = 5$ and $\nu_2 = 5$. (e) Four chaotic areas at $\nu_1 = 5$ and $\nu_2 = 5.2$. (f) Two chaotic areas at $\nu_1 = 5$ and $\nu_2 = 5.3$. (g) Basins of attraction of period-6 cycle at $\nu_1 = 5$ and $\nu_2 = 5.4$. (h) Phase plane for one chaotic attractor at $\nu_1 = 5$ and $\nu_2 = 5.55$. Other parameters are $a = 0.5, c = 0.2, d = 0.35$, and $\omega = 0.45$.

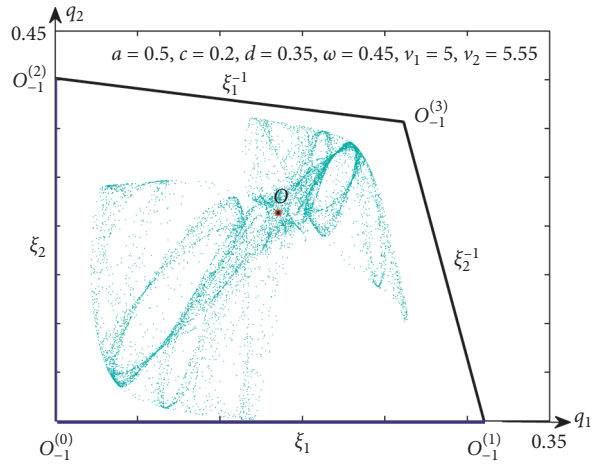

Figure 4: The boundaries of the chaotic attractor given in Figure 3(h).

period-6 cycle is emerged and plotted in Figure 3(g) with its attractive basins. Increasing ν_2 to 5.55, the dynamics of the map become chaotic as depicted in Figure 3(h).

3.2. Noninvertible Map. We have previously discussed that the map T is being trapped in the point $(0,0)$. This means that at $q_1(t) = 0$ or $q_2(t) = 0$, we get $q_1(t+1) = 0$ or $q_2(t+1) = 0$, respectively. So, the point $(0,0)$ is used to calculate basins' boundaries for any attracting set of the map. Doing that requires setting $q_1(t+1) = q_1$ and $q_2(t+1) = q_2$ in (8) as follows:

$$T: \begin{cases} \acute{q}_1 = q_1(t) + \nu_1 q_1[a - (2+c)q_1 - dq_2], \\ \acute{q}_2 = q_2(t) + \nu_2 q_2[a - (1+\omega+c)q_2 - dq_1], \end{cases} \tag{29}$$

where $\prime$ indicates evolution of time. For map (29), if $T^{-1}: (q_1, q_2) \longrightarrow (q_1, q_2)$ gets unique value for each point in the range, then we call T an invertible map and then the point $(q_1, q_2) \in \mathbb{R}^2$ is a rank-1 image while (q_1, q_2) is a rank-1 preimage. If there exist at least two rank-1 preimages for an image (q_1, q_2), then the map T is called a noninvertible map. Now, we calculate the real rank-1 preimages for the point $(0,0)$.

Proposition 4. *The point $O = (0,0)$ possesses four real rank-1 preimages,*

$$\begin{aligned} O_{-1}^{(0)} &= (0,0), \\ O_{-1}^{(1)} &= \left(\frac{1 + a\nu_1}{\nu_1(2+c)}, 0\right), \\ O_{-1}^{(2)} &= \left(0, \frac{1 + a\nu_2}{\nu_2(1+c+\omega)}\right), \\ O_{-1}^{(3)} &= \left(\frac{a\nu_1\nu_2(1+c+\omega-d) + (1+c+\omega)\nu_2 - d\nu_1}{\nu_1\nu_2\left(2+2\omega+3c+c\omega+c^2-d^2\right)}, \frac{a\nu_1\nu_2(2+c-d) + (2+c)\nu_1 - d\nu_2}{\nu_1\nu_2\left(2+2\omega+3c+c\omega+c^2-d^2\right)}\right). \end{aligned} \tag{30}$$

Proof. Setting $\acute{q}_1 = 0$ and $\acute{q}_2 = 0$ in (29) and solving algebraically, we get

This completes the proof. □

The above proposition indicates that any attracting set for map (27) has an attractive basin that is bounded by a quadrilateral shape whose boundaries are defined by the line segments $\xi_1 = OO_{-1}^{(1)}, \xi_2 = OO_{-1}^{(2)}$ and their preimages ξ_1^{-1} and ξ_2^{-1}, respectively. These preimages are given by

$$\begin{aligned} \xi_1^{-1}: q_2 &= \frac{1 + a\nu_2 - d\nu_2 q_1}{\nu_2(1+c+\omega)}, \\ \xi_2^{-1}: q_2 &= \frac{1 + a\nu_1 - \nu_1(2+c)q_1}{d\nu_1}. \end{aligned} \tag{31}$$

Figure 4 displays those line segments and their preimages at the parameters' values: $a = 0.5, c = 0.2, d = 0.35, \omega = 0.45, \nu_1 = 5$, and $\nu_2 = 5.55$.

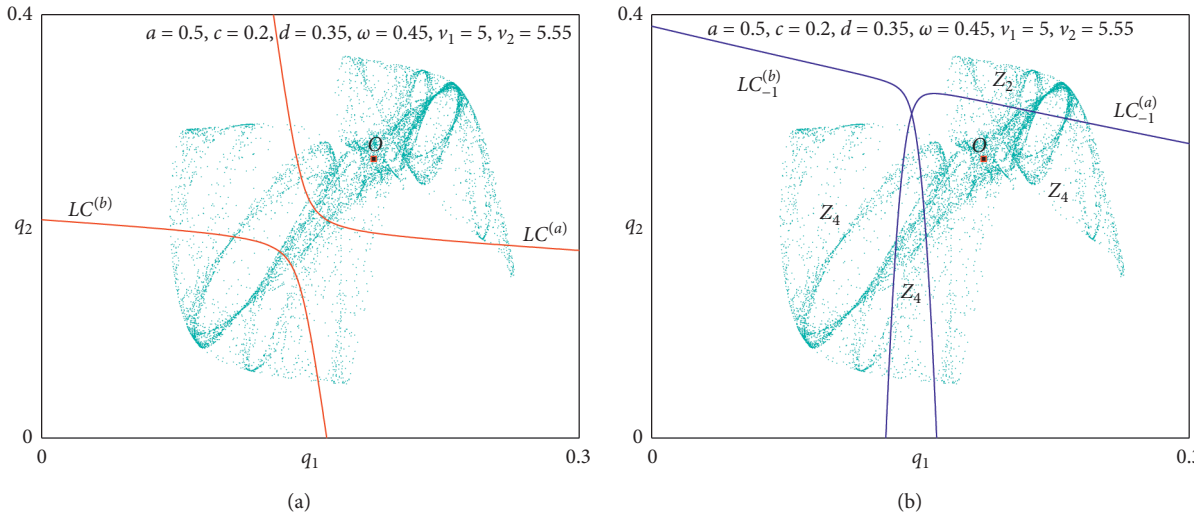

FIGURE 5: (a), (b) The critical curves LC, LC_{-1} and the region, Z_i, $i = 2, 4$ at the parameters' values: $a = 0.5, c = 0.2, d = 0.35, \omega = 0.45, \nu_1 = 5$, and $\nu_2 = 5.55$.

In Figure 5, we plot the critical curves LC and LC_{-1} at the parameters set, $a = 0.5, c = 0.2, d = 0.35, \omega = 0.45, \nu_1 = 5$, and $\nu_2 = 5.55$. It is clear that LC divides the phase plane into the two regions Z_4 and Z_2 as shown in Figures 5(a) and 5(b). Therefore, the map is noninvertible. In addition, the points $(0, 0)$ and the equilibrium point O are belonging to the region Z_4.

4. Conclusion

The current paper has studied a two-dimensional map that has described the competition between two Cournot firms one of which has considered the maximization of social welfare instead of profit. Based on a gradient-based mechanism, the map has been modelled in discrete time steps. It has been analyzed that when the two firms have become monopolistic, their dynamics have turned into just like the standard coupled logistic map. While in the duopolistic case, the map's fixed points have been calculated and their stability conditions have been investigated showing that the Nash equilibrium point may be unstable due to two types of bifurcations. Through some numerical analysis, we have shown some attracting sets with their basins of attraction and other chaotic behaviors of the map around the equilibrium point have been detected. The critical curves of the game's map have been calculated, and the corresponding preimages regions have been identified. We have shown that the map is noninvertible and has belonged to $Z_4 - Z_2$ type. For future studies, we plan to investigate more such adoption of maximization of social welfare on heterogeneous players (or firms). We have shown that the model parameters, in particular the speed of adjustment and the degree of privatization of the second firm, have an effect on the long-term dynamic response of the game, which is important for understanding the functioning of the mixed duopoly game. This result allows players to gain a specific understanding of the mixed oligopoly market and to recognize that the choice of decision criteria would have a certain effect on the system's actions.

Data Availability

The datasets generated during the current study are available from the corresponding author on reasonable request.

Conflicts of Interest

The authors declare that they have no conflicts of interest.

Acknowledgments

This work was supported by King Saud University, Riyadh, Saudi Arabia (research-supporting project number RSP-2020/167).

References

[1] A. A. Cournot, "Researches into the principles of the theory of wealth," in *Classics in Economics*Augustus M Kelley Pubs., New York, NY, USA, 1971.

[2] J. Bertrand, "Theorie mathematique de la richesse sociale," *Journal des Savants*, vol. 67, pp. 499–508, 1883.

[3] N. Singh and X. Vives, "Price and quantity competition in a differentiated duopoly," *The RAND Journal of Economics*, vol. 15, no. 4, pp. 546–554, 1984.

[4] S. S. Askar, "The Influences of asymmetric market information on the dynamics of duopoly game," *Mathematics*, vol. 8, no. 7, p. 1132, 2020.

[5] S. S. Askar and A. Al-Khedhairi, "Dynamic investigations in a duopoly game with price competition based on relative profit and profit maximization," *Journal of Computational and Applied Mathematics*, vol. 367, Article ID 112464, 2020.

[6] S. S. Askar, "Duopolistic Stackelberg game: investigation of complex dynamics and chaos control," *Operational Research*, vol. 20, no. 3, pp. 1685–1699, 2020.

[7] S. S. Askar and A. Al-Khedhairi, "The dynamics of a business game: a 2D-piecewise smooth nonlinear map," *Physica A: Statistical Mechanics and Its Applications*, vol. 537, Article ID 122766, 2020.

[8] A. A. Elsadany, "Dynamics of a Cournot duopoly game with bounded rationality based on relative profit maximization,"

Applied Mathematics and Computation, vol. 294, pp. 253–263, 2017.

[9] A. K. Naimzada and F. Tramontana, "Dynamic properties of a Cournot-Bertrand duopoly game with differentiated products," *Economic Modelling*, vol. 29, no. 4, pp. 1436–1439, 2012.

[10] J. Ma and X. Pu, "The research on Cournot-Bertrand duopoly model with heterogeneous goods and its complex characteristics," *Nonlinear Dynamics*, vol. 72, no. 4, pp. 895–903, 2013.

[11] T. Puu, "Chaos in duopoly pricing," *Chaos, Solitons & Fractals*, vol. 1, no. 6, pp. 573–581, 1991.

[12] J. X. Zhang, D. Q. Zhou, and Y. H. Wang, "Complex dynamics analysis for a Bertrand duopoly model with bounded rationality," in *Proceedings of the 2009 International Conference on Management Science and Engineering*, pp. 190–195, IEEE, Moscow, Russia, September 2009.

[13] T. Puu, "The chaotic monopolist," *Chaos, Solitons & Fractals*, vol. 5, no. 1, pp. 35–44, 1995.

[14] J. Long and H. Huang, "A dynamic stackelberg–cournot duopoly model with heterogeneous strategies through one-way spillovers," *Discrete Dynamics in Nature and Society*, vol. 2020, Article ID 3251609, 11 pages, 2020.

[15] H. N. Agiza and A. A. Elsadany, "Nonlinear dynamics in the Cournot duopoly game with heterogeneous players," *Physica A: Statistical Mechanics and Its Applications*, vol. 320, pp. 512–524, 2003.

[16] M. Kopel, "Simple and complex adjustment dynamics in cournot duopoly models," *Chaos, Solitons & Fractals*, vol. 7, no. 12, pp. 2031–2048, 1996.

[17] E. M. Elabbasy, H. N. Agiza, A. A. Elsadany, and H. EL-Metwally, "The dynamics of triopoly game with heterogeneous players," *International Journal of Nonlinear Science*, vol. 3, no. 2, pp. 83–90, 2007.

[18] E. M. Elabbasy, H. N. Agiza, and A. A. Elsadany, "Analysis of nonlinear triopoly game with heterogeneous players," *Computers & Mathematics with Applications*, vol. 57, no. 3, pp. 488–499, 2009.

[19] S. S. Askar and M. Abouhawwash, "Quantity and price competition in a differentiated triopoly: static and dynamic investigations," *Nonlinear Dynamics*, vol. 91, no. 3, pp. 1963–1975, 2018.

[20] C. Hommes, *Behavioral Rationality and Heterogeneous Expectations in Complex Economic Systems*, Cambridge University Press, Cambridge, EN, UK, 2013.

[21] V. J. Tremblay, C. H. Tremblay, and K. Isariyawongse, "Cournot and Bertrand competition when advertising rotates demand: the case of Honda and Scion," *International Journal of the Economics of Business*, vol. 20, no. 1, pp. 125–141, 2013.

[22] E. Ahmed, M. F. Elettreby, and A. S. Hegazi, "On Puu's incomplete information formulation for the standard and multi-team Bertrand game," *Chaos, Solitons & Fractals*, vol. 30, no. 5, pp. 1180–1184, 2006.

[23] L. C. Baiardi and A. K. Naimzada, "An oligopoly model with rational and imitation rules," *Mathematics and Computers in Simulation*, vol. 156, pp. 254–278, 2019.

[24] L. Fanti, L. Gori, C. Mammana, and E. Michetti, "The dynamics of a Bertrand duopoly with differentiated products: synchronization, intermittency and global dynamics," *Chaos, Solitons & Fractals*, vol. 52, pp. 73–86, 2013.

[25] A. A. Elsadany and A. M. Awad, "Dynamics and chaos control of a duopolistic Bertrand competitions under environmental taxes," *Annals of Operations Research*, vol. 274, no. 1-2, pp. 211–240, 2019.

[26] C. H. Tremblay and V. J. Tremblay, "Oligopoly games and the cournot-bertrand model: a survey," *Journal of Economic Surveys*, vol. 33, no. 5, pp. 1555–1577, 2019.

[27] S. S. Askar and A. Al-Khedhairi, "Analysis of nonlinear duopoly games with product differentiation: stability, global dynamics, and control," *Discrete Dynamics in Nature and Society*, vol. 11, p. 2017, 2017.

[28] B. Gao and Y. Du, "Equilibrium further studied for combined system of cournot and bertrand: a differential approach," *Complexity*, vol. 2020, Article ID 3160658, 11 pages, 2020.

[29] L. Liu, X. H. Wang, and C. Zeng, "Endogenous horizontal product differentiation in a mixed duopoly," *Review of Industrial Organization*, vol. 56, no. 3, pp. 435–462, 2020.

[30] Y. Liu, T. Matsumura, and C. Zeng, "The relationship between privatization and corporate taxation policies," *Journal of Economics*, vol. 132, 2021.

[31] P.-Y. Nie, "Effects of capacity constraints on mixed duopoly," *Journal of Economics*, vol. 112, no. 3, pp. 283–294, 2014.

[32] P. Y. Nie and Y. C. Yang, "Cost-reduction innovation under mixed economy," *Managerial and Decision Economics*, vol. 41, no. 7, p. 1195, 2020.

Hindawi
Discrete Dynamics in Nature and Society
Volume 2020, Article ID 3528684, 9 pages
https://doi.org/10.1155/2020/3528684

Research Article

Chaos on Discrete Neural Network Loops with Self-Feedback

Yuanlong Chen and Xiaoying Wu

Department of Applied Mathematics, GuangDong University of Finance, Guangzhou 510521, China

Correspondence should be addressed to Xiaoying Wu; wxyingyy@163.com

Received 9 June 2020; Revised 23 August 2020; Accepted 15 September 2020; Published 7 December 2020

Academic Editor: Amr Elsonbaty

In this paper, the complex dynamical behaviors in a discrete neural network loop with self-feedback are studied. Specifically, an invariant closed set of the system of neural network loops is built and the subsystem restricted on this invariant closed set is topologically conjugate to a two-sided symbolic dynamical system which has two symbols. In the end, some illustrative numerical examples are given to demonstrate our theoretical results.

1. Introduction

In recent years, researchers have found various chaotic phenomena in the nervous system and that chaotic neural networks play an important role in neural activities. Chaos in neural networks systems have been applied to all kinds of practical problems such as combinatorial optimizations, associative recognition memory, deep learning, and biotechnology (see [1–5]). In fact, some nervous systems consist of large-scale and complex nonlinear dynamics. At present, neuroscience has provided abundant evidence to prove that the central nervous system has complex nonlinear dynamic behavior at all levels [6]. So how to analyze the dynamical behavior of neural networks plays an important role in practical applications. In order to obtain a deep and clear understanding of complex neural networks, there are increasing studies on bifurcations and chaotic behaviors of neural network systems [7].

Recently, Huang and Zou in [8] showed the discrete network system consisting of two identical neurons with a uniform delay demonstrates snapback repeller chaotic behaviors near an equilibrium point. For the Hopfield networks with two different neurons [9–11], the conditions that the systems exhibit chaos are obtained. In [12], Wu et al. analyzed the chaotic behaviors of the parameterized discrete dynamics of recurrent m-neuron networks evoked by external inputs and obtained some conditions which the subsystem is topologically conjugate to symbolic dynamical system. In this paper, we will devote to analysis of the chaotic behaviors of the following discrete neural network loops with multiple delays and self-feedback:

$$\begin{cases} x_1(n+1) = \beta_1 x_1(n) + \alpha_{11} f_1(x_1(n-k_{11})) + \alpha_{1m} f_m(x_m(n-k_{1m})), \\ x_2(n+1) = \beta_2 x_2(n) + \alpha_{21} f_1(x_1(n-k_{21})) + \alpha_{22} f_2(x_2(n-k_{22})), \\ \vdots \\ x_m(n+1) = \beta_m x_m(n) + \alpha_{mm-1} f_{m-1}(x_m(n-k_{mm-1})) + \alpha_{mm} f_m(x_m(n-k_{mm})), \end{cases} \quad n \in \mathbb{Z},\ k_{ij} \geq 1, \tag{1}$$

where $n \in \mathbb{Z}$, for $i = 1, 2, \ldots, m$, $\beta_i \in (0, 1)$ is the internal decay rate of the neurons, α_{ij} is the self-feedback strength or the connection strength of the ith neuron to the next neuron, and the transmission delay $k_{ij} \geq 1$ is a positive integer.

For the case of the neural network with m-identical neurons, Cheng constructed a snapback repeller in [13] and then justified chaos in neural networks. When the discrete neural network with m-different neurons has multiple time delays and self-feedback, it is challenging to rigorously analyze the dynamical behaviors. In this paper, we consider the chaotic behaviors of model (1). To this end, we first rewrite the model (1) as a system of difference equations without delay by a novel way. Especially, this transformation requires a little skill. Then, we find an invariant set for the transformed system by projection and show that the system restricted on this set is topologically conjugate to the full shift map on the symbolic dynamical system. This implies that the system has chaotic behaviors. The obtained results extend the related ones in [10, 11, 13]. Also, we provide some numerical simulations to verify the theoretical results.

2. Invariant Subsystem of Model (1)

Let l_∞ denote the Banach space of bounded sequences of real numbers with the supremum norm defined on it. The norm is denoted by $\|\cdot\|$. Let $\sigma: l_\infty \longrightarrow l_\infty$ be shift map defined by $(\sigma\xi)_n = (\xi)_{n+1}$, $n \in \mathbb{Z}$, for $\xi = (\ldots, \xi_{-n}, \ldots, \xi_{-1}, \widetilde{\xi}_0, \xi_1, \ldots, \xi_n, \ldots) \in l_\infty$. That is,

$$\begin{aligned}\sigma\left(\ldots, \xi_{-n}, \ldots, \xi_{-1}, \widetilde{\xi}_0, \xi_1, \ldots, \xi_n, \ldots\right) \\ = \left(\ldots, \xi_{-n+1}, \ldots, \xi_0, \widetilde{\xi}_1, \xi_2, \ldots, \xi_{n+1}, \ldots\right).\end{aligned} \tag{2}$$

Clearly, the shift map σ on l_∞ is continuously invertible, and its inverse σ^{-1} is being defined by $(\sigma^{-1}\xi)_n = \xi_{n-1}$, $n \in \mathbb{Z}$. The ith iterate of σ, $\overbrace{\sigma \circ \sigma \cdot \circ \sigma}^{i \text{ times}}$, is denoted as σ^i. Let $\Sigma_k = \{(\ldots i_{-1} i_0 i_1 \ldots) | i_n \in \{1, 2, \ldots, k\}, n \in \mathbb{Z}\}$ denote a symbolic space with k symbols. Endowing it with the metric

$$\begin{aligned}d(s,t) = \max\left\{2^{-|n|} | t_n \neq s_n, n \in \mathbb{Z}\right\}, t = \left(\ldots t_{-1} t_0 t_1 \ldots\right), \\ s = \left(\ldots s_{-1} s_0 s_1 \ldots\right) \in \Sigma_k,\end{aligned} \tag{3}$$

Σ_k becomes a compact and totally disconnected metric space. The shift map $\sigma: \Sigma_k \longrightarrow \Sigma_k$ is defined by $(\sigma t)_n = t_{n+1}$. Then, (Σ_k, σ) is a two-sided symbolic system. To proceed, let $m, l \geq 2, i, j$ be positive integers.

Lemma 1. *Let $q \leq m$ be a positive integer. $a_{q_1}, a_{q_2}, \ldots, a_{q_l}$ are l different real numbers with $l \geq 2$ and a_i is a real number with $1 \leq i \neq q \leq m$. $\Lambda = \left\{(\xi_n) \in l_\infty | \xi_{mn+i} = a_i, \xi_{mn+q} = a_{q_j}\right\}$ be a subset of l_∞. Then, (Λ, σ^m) is topological conjugate to (Σ_l, σ).*

Proof. Define $g: \Lambda \longrightarrow \Sigma_l$ by $g(\xi) = (\ldots, \xi_{-mn+q}, \ldots, \xi_{-m+q}, \xi_q, \ldots, \xi_{mn+q}, \ldots)$, for $\xi = (\xi_n) \in \Lambda$. In fact, $g(\xi)$ is defined by deleting the elements whose indexes are congruent i modulo m in W, where $1 \leq i \neq q \leq m$. It is not difficult to see that g is a homeomorphism. By definition of g, we have $g \circ \sigma^m = \sigma \circ g$. So (Λ, σ^m) and (Σ_l, σ) are topological conjugacy. □

Lemma 2 (see [14]). *Let X and Y be Banach spaces, L is an invertible linear map from X to Y, and S is a bounded linear map from X to Y. If $\|S\| < \|L^{-1}\|^{-1}$, then $L + S$ is an invertible linear map from X to Y.*

Lemma 3 (see [15]). *Let (Λ, d) be a metric space, Y and X be Banach spaces, and $U \subset \Lambda \times Y$ be open. Suppose that $F: U \longrightarrow X$ is a continuous map and that there exists a point $(\lambda_0, y_0) \in U$ with the following conditions:*

(i) $F(\lambda_0, y_0) = 0$.

(ii) $DF_y(\lambda, y)$ is continuous at (λ_0, y_0), where $DF_y(\lambda, y)$ is Frechet partial derivative of $F(\lambda, y)$ with respect to y.

(iii) $DF_y(\lambda_0, y_0): Y \longrightarrow X$ is an invertible linear map.

Then, there exist open balls $B_{\delta_0}(y_0) = \{y: \|y - y_0\| < \delta_0\}$ and $B_{r_0}(\lambda_0) = \{\lambda: d(\lambda, \lambda_0) < r_0\}$, where $\delta_0 > 0, r_0 > 0$ such that, for any $\lambda \in B_{r_0}(\lambda_0)$, the equation $F(\lambda, y) = 0$ has a unique continuous solution $y = h(\lambda) \in B_{\delta_0}(y_0)$ with $h(\lambda_0) = y_0$.

For convenience, we set $i - 1 = m$ when $i - 1 = 0$. Let $\alpha = \alpha_{11}, C_{ij} = (\alpha_{ij}/\alpha)(i \in \{1, 2, \ldots, m\}, j = i - 1 \text{ or } i)$. Without losing generality, we may suppose that $k_{mm} \geq k_{1m} \geq k_{m-1m-1} \geq k_{mm-1} \cdots \geq k_{22} \geq k_{32} \geq k_{11} \geq k_{21}$. In the other cases, we can discuss it in a similar way. The activation functions $f_i (i = 1, \ldots, m)$ have the following conditions (G1):

(G1) For every $i \in \{1, 2, \ldots, m\}$, f_i is a continuously differentiable function from $\mathbb{R}$ to $\mathbb{R}$. f_1 has two distinct zero points $\widehat{x}^{q1}, \widehat{x}^{q2}$, satisfying $f_1(\widehat{x}^{q1}) = f_1(\widehat{x}^{q2}) = 0$, $f_1'(\widehat{x}^{q1}) \neq 0$, and $f_1'(\widehat{x}^{q2}) \neq 0$, and $f_i (i \in \{2, \ldots, m\})$ has a zero point $\overline{x}^i$,satisfying $f_i(\overline{x}^i) = 0$ and $f_i'(\overline{x}^i) \neq 0$.

Let $p_1 = mk_{11}, p_l = mk_{11} + \sum_{i=2}^{l} (m - i + 1)(k_{ii} - k_{i-1i-1})$, $2 \leq l \leq m$, $p = p_m + m$ and define $\eta(n) = (\eta_1(n), \ldots, \eta_p(n))$, where

$$\begin{cases} \eta_{mj+i}(n) = x_i(n - k_{ii} + j), \quad 0 \le j \le k_{11},\ 1 \le i \le m, \\ \eta_{p_1+j(m-1)+i}(n) = x_i(n - k_{ii} + k_{11} + j), \quad 1 \le j \le k_{22} - k_{11},\ 2 \le i \le m, \\ \eta_{p_2+j(m-2)+i}(n) = x_i(n - k_{ii} + k_{22} + j), \quad 1 \le j \le k_{33} - k_{22},\ 3 \le i \le m, \qquad \forall n \in \mathbb{Z}. \\ \vdots \\ \eta_{p_{m-1}+m+j}(n) = x_i(n - k_{ii} + k_{m-1m-1} + j), \quad 1 \le j \le k_{mm} - k_{m-1m-1},\ i = m. \end{cases} \tag{4}$$

For any $1 \le i \le m$, there exists $1 \le l_i \le m-1$ such that $k_{l_i l_i} < k_{i-1i-1} - k_{ii-1} \le k_{l_i+1 l_i+1}$. Then, we transform system (1) into the discrete dynamical system without delays on $\mathbb{R}^p$:

$$\eta(n+1) = F_\alpha(\eta(n)), \quad n \in \mathbb{Z}, \tag{5}$$

where $F_\alpha: \mathbb{R}^p \longrightarrow \mathbb{R}^p$ is defined as

$$F_\alpha\begin{pmatrix} \eta_1(n) \\ \eta_2(n) \\ \vdots \\ \eta_{p_1+1}(n) \\ \eta_{p_1+2}(n) \\ \vdots \\ \eta_{p_i+i}(n) \\ \eta_{p_i+i+1}(n) \\ \vdots \\ \eta_{p-1}(n) \\ \eta_p(n) \end{pmatrix} = \begin{pmatrix} \eta_{m+1}(n) \\ \eta_{m+2}(n) \\ \vdots \\ \beta_1\eta_{p_1+1}(n) + C_{11}\alpha f_{11}(\eta_1(n)) + C_{1m}\alpha f_{1m}\left(\eta_{p_{l_1}+\left(k_{mm}-k_{1m}-k_{l_1l_1}\right)(m-l_1)+m}(n)\right) \\ \eta_{p_1+m+1}(n) \\ \vdots \\ \beta_i\eta_{p_i+i}(n) + C_{ii-1}\alpha f_{ii-1}\left(\eta_{\widetilde{p}_{l_i}}(n)\right) + C_{ii}\alpha f_{ii}(\eta_i(n)) \\ \eta_{p_i+m+1}(n) \\ \vdots \\ \eta_p(n) \\ \beta_m\eta_p(n) + C_{mm-1}\alpha f_{mm-1}\left(\eta_{\widetilde{p}_{l_m}}(n)\right) + C_{mm}\alpha f_{mm}((\eta_m)(n)) \end{pmatrix}, \tag{6}$$

where $\widetilde{p}_{l_i} = p_{l_i} + (k_{i-1i-1} - k_{ii-1} - k_{l_i l_i})(m - l_i) + i - 1$, $2 \le i \le m$.

To investigate chaos in System (1), we only consider the chaotic behavior of the system $(\mathbb{R}^p, F_\alpha)$. Next, by the projection approach, we are going to find the invariant set Λ_α of F_α such that the subsystem $(F_\alpha, \Lambda_\alpha)$ has chaotic behavior for α being sufficiently large.

We consider a family of maps $\Phi(\lambda, \cdot): l_\infty \longrightarrow l_\infty$ depending on a parameter $\lambda \in \mathbb{R}$, and the class of maps is defined by

$$\begin{cases} \Phi(\lambda,\xi)_{m(n+1)+1} = \lambda\left(-\xi_{m(n+1)+1} + \beta_1\xi_{mn+1}\right) + C_{11}f_1\left(\xi_{(m(n-k_{11}))+1}\right) + C_{1m}f_m\left(\xi_{(m(n-k_{1m}))+m}\right), \\ \vdots \qquad\qquad \forall \xi = (\xi_n) \in l_\infty,\ 2 \le i \le m. \\ \Phi(\lambda,\xi)_{m(n+1)+i} = \lambda\left(-\xi_{m(n+1)+i} + \beta_i\xi_{mn+i}\right) + C_{ii-1}f_{i-1}\left(\xi_{m\left(n-k_{ii-1}\right)+i-1}\right) + C_{ii}f_i\left(\xi_{m\left(n-k_{ii}\right)+i}\right), \end{cases} \tag{7}$$

It is easy to see that if $\xi = \{\xi_n\}_{n\in\mathbb{Z}} \in l_\infty$ satisfies $\Phi(1/\alpha, \xi) = 0$, then the sequence $\{x_1(n), x_2(n), \ldots, x_m(n)\}_{n\in\mathbb{Z}}$ with $x_i(n) = \xi_{mn+i}$ satisfies (1). On the contrary, if the sequence $\{x_1(n), x_2(n), \ldots, x_m(n)\}_{n\in\mathbb{Z}}$ satisfies (1), then $\xi = \{\xi_n\}_{n\in\mathbb{Z}} \in l_\infty$ with $\xi_{mn+i} = x_i(n)$ satisfies $\Phi(1/\alpha, \xi) = 0$.

Let

$$\begin{aligned}
\Gamma &= \left\{\xi = (\xi_n) \in l_\infty | \xi_{mn+i} = \overline{x}^i, \xi_{mn+1} = \widehat{x}^{q1} \text{ or } \widehat{x}^{q2}, \quad 2 \le i \le m,\ n \in \mathbb{Z}\right\},\\
b_{11} &= |C_{11} \max\left\{\left|f_1'\left(\widehat{x}^{q1}\right)\right|, \left|f_1'\left(\widehat{x}^{q1}\right)\right|\right\},\\
b_{21} &= \left|C_{21}\right| \min\left\{\left|f_1'\left(\widehat{x}^{q1}\right)\right|, \left|f_1'\left(\widehat{x}^{q2}\right)\right|\right\},\\
b_{ii} &= \left|C_{ii} f_i'\left(\overline{x}^i\right)\right|, \ (i \in \{2, \ldots, m\}),\\
b_{ii-1} &= \left|C_{ii-1} f_{i-1}'\left(\overline{x}^i\right)\right|, \ (i \in \{1, 3, 4, \ldots, m\}),\\
b &\triangleq \frac{1}{\max\left\{b_{11}^{-1}, b_{ii}^{-1} + b_{ii}^{-1} b_{ii-1} b_{i-1i-1}^{-1} + \cdots + b_{ii}^{-1} b_{ii-1} b_{i-1i-1}^{-1} \ldots b_{21} b_{11}^{-1}, \quad \forall 2 \le i \le m\right\}}.
\end{aligned} \tag{8}$$

Lemma 4. *Under the assumption* (*G*1)*, if* $b_{11} > b_{1m}$ *and* $b_{ii} > b_{1m} + b_{ii-1}$ $(2 \le i \le m)$*, then we have the following:*

(i) There exist positive real numbers r_0 *and* δ_0 *such that, for any* $\overline{\xi} \in \Gamma$ *and* $-r_0 \le \lambda \le r_0$*, there exists a unique point* $\xi(\lambda) \in B_{\delta_0}(\overline{\xi})$*, satisfying* $\Phi(\lambda, \xi(\lambda)) = 0$.

(ii) For every $0 < \delta < \delta_0$*, there exists* $0 < r < r_0$ *such that, for any* $-r \le \lambda \le r$ *and* $\overline{\xi} \in \Gamma$*, there is a unique point* $\xi(\lambda)$*, satisfying* $\|\xi(\lambda) - \overline{\xi}\| \le \delta$ *and* $\Phi(\lambda, \xi(\lambda)) = 0$.

$B_{\delta_0}(\overline{\xi})$ is the open ball in l_∞ centered at $\overline{\xi}$ with radius δ_0.

Proof. For a given sequence $\overline{\xi} \in \Gamma$, we have $\Phi(0, \overline{\xi}) = 0$. By the assumption (*G*1) and the definition of $\Phi(\lambda, \xi)$, this can ensure the continuous differentiability of $\Phi(\lambda, \xi)$. The Fréchet derivative of $\Phi(0, \xi)$ with respect to ξ at the point $(0, \overline{\xi})$ be denoted as $D\Phi_\xi(0, \overline{\xi})$ which is represented as

$$\begin{cases}
\left(D\Phi_\xi(0, \overline{\xi})\xi\right)_{m(n+1)+1} = C_{11} f_1'\left(\overline{\xi}_{m\left(n-k_{11}\right)+1}\right)\xi_{m\left(n-k_{11}\right)+1} + C_{1m} f_m'\left(\overline{\xi}_{m\left(n-k_{1m}\right)+m}\right)\xi_{m\left(n-k_{1m}\right)+m},\\
\left(D\Phi_\xi(0, \overline{\xi})\xi\right)_{m(n+1)+i} = C_{ii-1} f_{i-1}'\left(\overline{\xi}_{m\left(n-k_{ii-1}\right)+i-1}\right)\xi_{m\left(n-k_{ii-1}\right)+i-1} + C_{ii} f_i'\left(\overline{\xi}_{m\left(n-k_{ii}\right)+i}\right)\xi_{m\left(n-k_{ii}\right)+i},
\end{cases} \quad n \in \mathbb{Z},\ 2 \le i \le m. \tag{9}$$

Firstly, we have to show the invertibility of $D\Phi_\xi(0, \overline{\xi})$. We denote that $D\Phi_\xi(0, \overline{\xi}) = L_1(\overline{\xi}) + L_2(\overline{\xi})$, where

$$\begin{cases}
\left(L_1(\overline{\xi})\xi\right)_{m(n+1)+1} = C_{11} f_1'\left(\overline{\xi}_{m\left(n-k_{11}\right)+1}\right)\xi_{m\left(n-k_{11}\right)+1},\\
\left(L_1(\overline{\xi})\xi\right)_{m(n+1)+i} = C_{ii-1} f_{i-1}'\left(\overline{\xi}_{m\left(n-k_{ii-1}\right)+i-1}\right)\xi_{m\left(n-k_{ii-1}\right)+i-1} + C_{ii} f_i'\left(\overline{\xi}_{m\left(n-k_{ii}\right)+i}\right)\xi_{m\left(n-k_{ii}\right)+i},
\end{cases} \quad n \in \mathbb{Z},\ 2 \le i \le m,$$

$$\begin{cases}
\left(L_2(\overline{\xi})\xi\right)_{m(n+1)+1} = C_{1m} f_m'\left(\overline{\xi}_{m\left(n-k_{1m}\right)+m}\right)\xi_{m\left(n-k_{1m}\right)+m},\\
\left(L_2(\overline{\xi})\xi\right)_{m(n+1)+i} = 0,
\end{cases} \quad n \in \mathbb{Z}. \tag{10}$$

Let

$$\begin{aligned}
a_{ii-1}^l &= C_{i-l+1i-l} f_{i-l}'\left(\overline{\xi}_{m\left(n+k_{ii}-k_{ii-1}+\cdots+k_{i-l+1i-l+1}-k_{i-li-l-1}+i-l-1\right)}\right)(0 \le l \le i-1),\\
a_{ii}^l &= C_{i-li-l} f_{i-l}'\left(\overline{\xi}_{m\left(n+k_{ii}-k_{ii-1}+k_{i-1i-1}-\cdots+k_{i-li-l}+i-l\right)}\right)(0 \le l \le i-1).
\end{aligned} \tag{11}$$

It follows from (G1) that the linear operator $L_1(\bar{\xi})$ is invertible. By directing calculation, the inverse operator $L_1(\bar{\xi})^{-1}$ is

$$\begin{cases} \left(L_1(\bar{\xi})^{-1}\xi\right)_{m(n-1)+1} = \dfrac{1}{a_{11}^0}\xi_{m(n+k_{11})+1}, \\ \left(L_1(\bar{\xi})^{-1}\xi\right)_{m(n-1)+i} = \dfrac{1}{a_{ii}^0}\xi_{m(n+k_{ii})+i} - \dfrac{1}{a_{ii}^0}a_{ii-1}^0\dfrac{1}{a_{ii}^1}\xi_{m(n+k_{ii}-k_{ii-1}+k_{i-1i-1})+i-1} + \\ \cdots + (-1)^{i-1}\dfrac{1}{a_{ii}^0}a_{ii-1}^0\dfrac{1}{a_{ii}^1}, \ldots, a_{ii-1}^{i-2}\dfrac{1}{a_{ii}^{i-1}}\xi_{m(n+k_{ii}-k_{ii-1}+\cdots-k_{21}+k_{11})+1}. \end{cases} \quad n \in \mathbb{Z},\ 2 \le i \le m. \tag{12}$$

Since $\bar{\xi} \in \Gamma$, $\bar{\xi}_{mn+1} = \hat{x}^{q1}$ or $\hat{x}^{q2}$, $\bar{\xi}_{mn+i} = \bar{x}^i$, $2 \le i \le m$. This implies that

$$\begin{aligned} \left\|L_1(\bar{\xi})^{-1}\right\| &\le \frac{1}{b}, \\ \left\|L_2(\bar{\xi})\right\| &= b_{1m}, \end{aligned} \tag{13}$$

so

$$\left\|L_1(\bar{\xi})^{-1}\right\|^{-1} > \left\|L_2(\bar{\xi})\right\|, \tag{14}$$

by the fact that $b_{11} > b_{1m}$ and $b_{ii} > b_{1m} + b_{ii-1}$ $(2 \le i \le m)$. This shows the invertibility of $D\Phi_\xi(0, \bar{\xi})$ by Lemma 2.

Therefore, according the implicit function theorem, there exist positive constants $r_{\bar{\xi}}, \delta_{\bar{\xi}}$ such that, for every $-r_{\bar{\xi}} \le \lambda \le r_{\bar{\xi}}$, there is a unique point $\xi = \xi(\lambda) \in B_{\delta_{\bar{\xi}}}(\bar{\xi})$ with $\Phi(\lambda, \xi(\lambda)) = 0$.

To complete the proof of (i), it only needs to prove that there exist two positive constants r_0, δ_0 which are independent of $\bar{\xi} \in \Gamma$ such that the conclusion is satisfied in (i). From the proof of the implicit function theorem, for the given $\bar{\xi} \in \Gamma$, the constants $r_{\bar{\xi}}$ and $\delta_{\bar{\xi}}$ above are chosen such that, for $-r_{\bar{\xi}} \le \lambda \le r_{\bar{\xi}}$ and $\xi \in B_{\delta_{\bar{\xi}}}(\bar{\xi})$, we have

$$\begin{aligned} \left\|\left(D\Phi_\xi(\lambda, \xi)\right) - \left(D\Phi_\xi(0, \bar{\xi})\right)\right\| &\le \frac{1}{2M_{\bar{\xi}}}, \\ \left\|\Phi(\lambda, \bar{\xi})\right\| &\le \frac{\delta_{\bar{\xi}}}{2M_{\bar{\xi}}}. \end{aligned} \tag{15}$$

Here, $M_{\bar{\xi}}$ is the constant such that $\left\|\left(D\Phi_\xi(0, \bar{\xi})\right)^{-1}\right\| \le M_{\bar{\xi}}$.

We now give the above estimates which are independent of $\bar{\xi} \in \Gamma$. Firstly, we have, for any $\bar{\xi} \in \Gamma$,

$$\left\|\left(D\Phi_\xi(0, \bar{\xi})\right)^{-1}\right\| \le \frac{1}{\left\|L_1(\bar{\xi})^{-1}\right\|^{-1} - \left\|L_2(\bar{\xi})\right\|} \le \frac{1}{b - b_{1m}} \triangleq M, \tag{16}$$

where b is given by (8). Secondly, by assumption $(G1)$, there exists δ_1 such that

$$\max\left\{\left|C_{11}\right|, \left|C_{21}\right|\right\}\left|f_1'(x) - f_1'\left(\hat{x}^{q1}\right)\right| \le \frac{1}{8M}, \tag{17}$$

for $x \in B_{\delta_1}(\hat{x}^{q1})$,

$$\max\left\{\left|C_{11}\right|, \left|C_{21}\right|\right\}\left|f_1'(x) - f_1'\left(\hat{x}^{q2}\right)\right| \le \frac{1}{8M}, \tag{18}$$

for $x \in B_{\delta_1}(\hat{x}^{q2})$, and

$$\max\left\{\left|c_{ii-1}\right|, \left|c_{i-1i-1}\right|\right\}\left|f_{i-1}'(x) - f_{i-1}'\left(\bar{x}^{i-1}\right)\right| \le \frac{1}{4M}, \tag{19}$$

for $x \in B_{\delta_1}(\bar{x}^{i-1})$, $1 \le i \ne 2 \le m$. Note that

$$\begin{cases} \left(D\Phi_\xi(\lambda, \xi) - D\Phi_\xi(0, \bar{\xi})\xi\right)_{m(n+1)+1} \\ \quad = \lambda\left(-\xi_{m(n+1)+1} + \beta_1\xi_{m(n+1)+1}\right) \\ + C_{11}\left(f_1'\left(\xi_{m(n-k_{11})+1}\right) - f_1'\left(\bar{\xi}_{m(n-k_{11})+1}\right)\xi_{m(n-k_{11})+1}\right) \\ + C_{1m}\left(f_m'\left(\xi_{m(n-k_{1m})+m}\right) - f_m'\left(\bar{\xi}_{m(n-k_{1m})+m}\right)\xi_{m(n-k_{1m})+m}\right), \\ \left(D\Phi_\xi(\lambda, \xi) - D\Phi_\xi(0, \bar{\xi})\xi\right)_{m(n+1)+i} \\ \quad = \lambda\left(-\xi_{m(n+1)+i} + \beta_i\xi_{m(n+1)+i}\right) \\ + C_{ii-1}\left(f_{i-1}'\left(\xi_{m((n-k_{ii-1})+i-1}\right) - f_1'\left(\bar{\xi}_{m((n)-k_{ii-1})+i-1}\right)\right. \\ \quad \left.\xi_{m((n-k_{ii-1})+i-1}\right) \\ + C_{ii}\left(f_i'\left(\xi_{m(n-k_{ii})+i}\right) - f_i'\left(\bar{\xi}_{m(n-k_{ii})+i}\right)\right)\xi_{m(n-k_{ii})+i}, \quad 2 \le i \le m. \end{cases} \tag{20}$$

Taking $\delta_0 = \delta_1, r_1 = (1/4M(1+a))$, where $a \triangleq \max\{\beta_i | i = 1, 2, \ldots, m\}$, we have that, for $\bar{\xi} \in \Gamma$, $\xi \in l_\infty$ with $\|\xi - \bar{\xi}\| \le \delta_0$ and $|\lambda| \le r_1$:

$$\left\|D\Phi_\xi(\lambda, \xi) - D\Phi_\xi(0, \bar{\xi})\right\| \le |\lambda|(1+a) + \frac{1}{4M} \le \frac{1}{2M}. \tag{21}$$

On the contrary, let $r_2 = (\delta_0/2M(1+a))$, and it follows from the definition of $\Phi(\lambda, \cdot)$ that

$$\left\|\Phi(\lambda, \bar{\xi})\right\| \le |\lambda|(1+b) \le \frac{\delta_0}{2M}, \tag{22}$$

when $|\lambda| \le r_2$.

Finally, take $r_0 = \min\{r_1, r_2\}$ and then the constants r_0 and δ_0 satisfy (i).

For every $0 < \delta < \delta_0$, (ii) follows by taking $r = \min\{(1/4M(1+a)), (\delta/2M(1+a))\} (< r_0)$ and the proof of (i). □

3. Chaos in System (1)

In this section, we shall show that the system (1) exists chaotic behaviors. By Lemma 4, for sufficiently large $\alpha > 0$, we define the map T_α from Γ to l_∞ by

$$T_\alpha(\overline{\xi}) = \xi\left(\frac{1}{\alpha}\right), \tag{23}$$

where $\xi(1/\alpha)$ is the unique solution of $\Phi((1/\alpha), \xi) = 0$, satisfying $\|\xi(1/\alpha) - \overline{\xi}\| \le \delta$. Then, we have the following proposition.

Proposition 1. *For sufficiently large $\alpha > 0$, let $\Gamma_\alpha = T_\alpha(\Gamma)$, then the map T_α and the shift map σ^m are commutative, i.e.,*

$$\sigma^m \circ T_\alpha = T_\alpha \circ \sigma^m. \tag{24}$$

Moreover, $\sigma^m(\Gamma_\alpha) = \Gamma_\alpha$.

Proof. Note that if ξ is a solution of $\Phi((1/\alpha), \xi) = 0$ so is $\sigma^m(\xi)$. Thus, for any $\overline{\xi} \in \Gamma$, $\sigma^m \circ T_\alpha(\overline{\xi}) = \sigma^m(\xi(1/\alpha))$ is a solution of $\Phi((1/\alpha), \xi) = 0$. On the contrary, $\|\xi(1/\alpha) - \overline{\xi}\| \le \delta$ by Lemma 4, which leads to $\|\sigma^m(T_\alpha(\overline{\xi}) - \sigma^m(\overline{\xi}))\| = \|\sigma^m(\xi(1/\alpha)) - \sigma^m(\overline{\xi})\| = \|\xi(1/\alpha) - \overline{\xi}\| \le \delta$. Hence, by the uniqueness of $\xi(\lambda)$ in Lemma 4, we have $\sigma^m(T_\alpha(\overline{\xi})) = T_\alpha(\sigma^m(\overline{\xi}))$. Note that $\sigma^m(\Gamma) = \Gamma$, it follows that $\sigma^m(\Gamma_\alpha) = \Gamma_\alpha$.

For every $k \in \mathbb{Z}$, we define the projection Π_k: $l_\infty \longrightarrow \mathbb{R}^p$ by

$$\Pi_k(\xi) = \eta(k), \quad \forall \xi \in l_\infty, \tag{25}$$

where for $\xi = (\xi_n) \in l_\infty$, $\eta(k) = (\eta_1(k), \ldots, \eta_p(k)) \in \mathbb{R}^p$ is given by

$$\begin{aligned}
\eta_{mj+i}(k) &= \xi_{m\left(k-k_{ii}+j\right)+i}, \quad 0 \le j \le k_{11},\ 1 \le i \le m,\\
\eta_{p_1+j(m-1)+i}(k) &= \xi_{m\left(k-k_{ii}+k_{11}+j\right)+i}, \quad 1 \le j \le k_{22}-k_{11},\ 2 \le i \le m,\\
\eta_{p_2+j(m-2)+i}(k) &= \xi_{m\left(k-k_{ii}+k_{22}+j\right)+i}, \quad 1 \le j \le k_{33}-k_{22},\ 3 \le i \le m,\\
&\vdots\\
\eta_{p_{m-1}+m+j}(k) &= \xi_{m\left(k-k_{mm}+k_{m-1m-1}+j\right)+m}, \quad 1 \le j \le k_{mm}-k_{m-1m-1}.
\end{aligned} \tag{26}$$

□

Proposition 2. *Let $\Lambda_\alpha = \Pi_0(\Gamma_\alpha)$, then Λ_α is invariant for F_α.*

Proof. For each $\eta(0) \in \Lambda_\alpha$, then there exists $\xi \in \Gamma_\alpha$ such that $\Pi_0(\xi) = \eta(0)$. Therefore,

$$F_\alpha(\eta(0)) = \eta(1) = \Pi_0\left(\sigma^m(\xi)\right) \in \Pi_0\left(\sigma^m(\Gamma_\alpha)\right) = \Pi_0(\Gamma_\alpha) = \Lambda_\alpha. \tag{27}$$

This proves $F_\alpha(\Lambda_\alpha) \subset \Lambda_\alpha$.

On the contrary, by Proposition 1, we have $\sigma^m(\Gamma_\alpha) = \Gamma_\alpha$. Thus, there exists $\xi' \in \Gamma_\alpha$ such that $\xi = \sigma^m(\xi')$. Thus,

$$\begin{aligned}
\eta(0) = \Pi_0(\xi) &= \Pi_0\left(\sigma^m(\xi')\right) = \eta'(1) = F_\alpha(\eta'(0))\\
&= F_\alpha(\Pi_0(\xi')) \in F_\alpha(\Lambda_\alpha),
\end{aligned} \tag{28}$$

which shows that $\Lambda_\alpha \subset F_\alpha(\Lambda_\alpha)$. Therefore, $F_\alpha(\Lambda_\alpha) = \Lambda_\alpha$. □

Theorem 1. *Under the assumption of (G1), if $b_{11} > b_{1m}$ and $b_{ii} > b_{1m} + b_{ii-1}$ $(2 \le i \le m)$, then there exists $\alpha_0 > 0$ such that, for any $\alpha > \alpha_0$, $(\Lambda_\alpha, F_\alpha)$ is topologically conjugate to the full shift map (Σ_2, σ), and therefore, the system is chaotic in the sense of Devaney.*

Proof. Note that (Γ, σ^m) is an invariant subsystem. By Lemma 1 and Proposition 1, we only need to prove that there is $\alpha_0 > 0$ such that, for any $\alpha > \alpha_0$, $(\Lambda_\alpha, F_\alpha)$ is topological conjugate to (Γ, σ^m).

Let $\Omega = \Pi_0(\Gamma)$, then Ω is a set in $\mathbb{R}^p$ consisting of $2^{k_{11}+1}$ elements, denoted by

$$\Omega = \{b_1, b_2, \ldots, b_{2^{k_{11}+1}}\}. \tag{29}$$

Let δ_0 and r_0 be given as in Lemma 4, and let $\delta \in (0, \delta_0)$ be small enough such that the family of closed balls $\{A_i = \overline{B}(b_i, \delta)\}_{i=1}^{2^{k_{11}+1}}$ in $\mathbb{R}^p$ is piecewise disjoint.

For the given δ and any $\overline{\xi} = (\overline{\xi}_n) \in \Gamma$, by (ii) in Lemma 4, there exists an $\alpha_0 = (1/r) > 0$ such that, for every $\alpha > \alpha_0$, there exists a unique $T_\alpha(\overline{\xi}) = \xi(1/\alpha)$ satisfying $\|\xi(1/\alpha) - \overline{\xi}\| \le \delta$ and $\Phi((1/\alpha), \xi(1/\alpha)) = 0$. By the definition of the projections Π_k and Γ, we have $\Pi_k(\Gamma) = \Pi_0(\Gamma) = \Omega$. So we let

$$\begin{aligned}
S = \Big\{ & s = (\ldots, s_{-1}, s_0, s_1, \ldots) | s_i \in \left\{1, 2, \ldots, 2^{k_{11}+1}\right\},\\
& \xi_{s_i} = \Pi_i(\overline{\xi}), \quad \text{for some } \overline{\xi} \in \Gamma \Big\}.
\end{aligned} \tag{30}$$

The set S is a subset of $\Sigma_{2^{k_{11}+1}}$. For every $s = (\ldots, s_{-1}, s_0, s_1, \ldots) \in S$, for all $i, j > 0$, we set

$$\begin{aligned}
V_{s_{-i}\ldots s_0 \ldots s_j} &= F_\alpha^{-j}\left(A_{s_j}\right) \cap \cdots \cap A_{s_0} \cap \cdots \cap F_\alpha^{i}\left(A_{s_i}\right),\\
V_s &= \bigcap_{i>0, j>0} V_{s_{-i}\ldots s_0 \ldots s_j}.
\end{aligned} \tag{31}$$

We claim the following:

(1) For every $s \in S$, V_s contains a unique point.

(2) $\cup_{s\in S} V_s = \Lambda_\alpha$.

In fact, for each $s \in S$, we note that

$$V_{s_{-i}\ldots s_0 \ldots s_j} = \left\{\eta \in \mathbb{R}^p | F_\alpha^{-i}(\eta) \in A_{s_i}, \ldots, F_\alpha^{j}(\eta) \in A_{s_j}\right\}. \tag{32}$$

Therefore, there exists a unique $\overline{\xi} \in \Gamma$ such that, for all $i \in \mathbb{Z}$, $\Pi_i(\overline{\xi}) = \xi_{s_i} \in \Omega$. Then, by the definition of T_α and Lemma 4, there exists a unique $T_\alpha(\overline{\xi}) = \xi(1/\alpha)$, satisfying $\|\xi(1/\alpha) - \overline{\xi}\| \le \delta$ and $\Phi((1/\alpha), \xi(1/\alpha)) = 0$. So $\{\Pi_n(\xi(1/\alpha)) = \eta(n)\}_{n\in\mathbb{Z}}$ is a bounded orbit of F_α, that is, $\eta(n) = F_\alpha^n(\eta(0)) \in A_{s_n}$, $\forall n \in \mathbb{Z}$. Therefore, $\eta(0) \in V_s$, which implies V_s is nonempty.

On the contrary, for any $\eta' \in V_s$, for all $n \in \mathbb{Z}$, there are $F_\alpha^n(\eta') \in A_{s_n}$. Thus, $\{F_\alpha^n(\eta')\}_{n\in\mathbb{Z}}$ is a bounded orbit of F_α. Then, there exists $\xi \in l_\infty$ such that $\Pi_n(\xi) = F_\alpha^n(\eta')$. So $\|\xi - \overline{\xi}\| \le \delta$, and $\Phi((1/\alpha), \xi) = 0$. Again by Lemma 4 (ii), there is $\xi = T_\alpha(\overline{\xi})$, and hence, $\eta' = \eta(0)$. Claim (1) holds.

For Claim (2), let $\eta \in \Lambda_\alpha$. Then, there exists a $\overline{\xi} \in \Gamma$ such that $\eta = \Pi_0(T_\alpha(\overline{\xi}))$ Let $s = (\ldots s_{-1}, s_0, s_1 \ldots) \in S$ be the corresponding sequence of $\overline{\xi}$. Similar to the above argument, we have $\eta \in V_s$. Therefore,

$$\Lambda_\alpha \subset \bigcup_{s\in S} V_s. \tag{33}$$

From Claim (1), each V_s contains a unique point which belongs to Λ_α, so the converse inclusion holds. This proves Claim (2).

For every $\alpha > \alpha_0$, define a map $h\colon \Gamma \longrightarrow \Lambda_\alpha$ by $h = \Pi_0 \circ T_\alpha$. We claim that h is a conjugacy from σ^m to F_α. To prove this, we need to show that both h and h^{-1} are continuous and

$$h \circ \sigma^m = F_\alpha \circ h, \quad \text{on } \Gamma. \tag{34}$$

By Claim (2) and the definition of h, it is easy see that h is surjective. From Claim (1) and Lemma 4, it follows that h is injective. Therefore, h is bijective. Since h is a map from a compact metric space Γ to a Hausdorff space Λ_α, to prove that h is homeomorphic, we just need to show the continuity of h. Let the corresponding subindex sequence of $\overline{\xi} \in \Gamma$ be $\overline{s} = (\ldots s_{-1}, s_0, s_1 \ldots) \in S$. It follows from Claim (1) that

$$\lim_{i,j\longrightarrow+\infty} \operatorname{diam}\left(V_{s_{-i}\ldots s_0\ldots s_j}\right) = 0, \tag{35}$$

where $\operatorname{diam}(V_{s_{-i}\ldots s_0\ldots s_j})$ denotes the diameter of the set $V_{s_{-i}\ldots s_0\ldots s_j}$. Thus, for any $\varepsilon > 0$, there exists a positive integer n such that $\operatorname{diam}(V_{\overline{s}_{-n}\ldots\overline{s}_0\ldots\overline{s}_n}) < \varepsilon$. Take $\delta_1 = (1/2^{m(n+k_{mm}+1)})$. Then, for any $\widetilde{\xi} \in \Gamma$ with $d(\widetilde{\xi}, \overline{\xi}) < \delta_1$, it follows that $\widetilde{\xi}$ agrees with $\overline{\xi}$ in those terms with lower indices from $i = -m(n + k_{mm} + 1)$ to $i = m(n + k_{mm} + 1)$. Let $\widehat{s}, \overline{s} \in S$ be the symbolic sequences corresponding to $\widehat{\xi}$ and $\overline{\xi}$, respectively. We have $\widehat{s}$ agrees with $\overline{s}$ in those terms with subscripts from $i = -n$ to $i = n + k_{mm} + 1$. Thus, $h(\widehat{\xi}), h(\overline{\xi}) \in V_{\overline{s}_{-n}\ldots\overline{s}_0\ldots\overline{s}_n}$ and $\|h(\widehat{\xi}) - h(\xi)\| < \varepsilon$. This shows the continuity of h. Hence, we conclude that h is a homeomorphism.

Finally, for any $\overline{\xi} \in \Gamma$, we have

$$h(\overline{\xi}) = \Pi_0 \circ T_\alpha(\overline{\xi}) = \eta(0) = \left(\eta_1(0), \ldots, \eta_q(0)\right)^T. \tag{36}$$

Thus,

$$\begin{aligned} F_\alpha(h(\overline{\xi})) &= \left(\eta_1(1), \eta_2(1), \ldots, \eta_q(1)\right)^T \\ &= \Pi_0 \circ \sigma^m \circ T_\alpha(\overline{\xi}) \text{ by (1)} \\ &= \Pi_0 \circ T_\alpha \circ \sigma^m(\overline{\xi}), \text{ by Proposition 1} \\ &= h \circ \sigma^m(\overline{\xi}). \end{aligned} \tag{37}$$

The Theorem 1 holds. □

4. Some Simulations

In this section, we will give some numerical simulation results to verify our theoretical results. We choose $\beta_1 = \beta_3 = (1/4), \beta_2 = \beta_4 = (3/4)3/4, f_1(t) = \sin(t), f_2(t) = \tanh(t), f_3(t) = \cos(t), f_4(t) = \tanh(t), \alpha_{11} = 0.5\alpha, \alpha_{14} = \alpha, \alpha_{21} = -0.4\alpha, \alpha_{22} = 2\alpha, k_{11} = 1, k_{21} = 2, k_{14} = 3, k_{22} = 4, k_{32} = 3, k_{33} = 1, k_{43} = 2,$ and $k_{44} = 4$. In this case, system (1) becomes

$$\begin{cases} x_1(n+1) = \dfrac{1}{4}x_1(n) + 1.5\alpha \sin\left(x_1(n-1)\right) + \alpha \tanh\left(x_4(n-3)\right), \\ x_2(n+1) = \dfrac{3}{4}x_2(n) - 0.4\alpha \sin\left(x_1(n-2)\right) + 2\alpha \tanh\left(x_2(n-4)\right), \\ x_3(n+1) = \dfrac{1}{4}x_3(n) + \alpha \tanh\left(x_2(n-3)\right) + 1.5\alpha \cos\left(x_3(n-1)\right), \\ x_4(n+1) = \dfrac{3}{4}x_4(n) - 0.4\alpha \cos\left(x_3(n-2)\right) + 2\alpha \tanh\left(x_4(n-4)\right), \end{cases} \quad \forall n \ge 5. \tag{38}$$

In Figure 1, for every α value, the initial values were reset to $x_1(1) = -0.1, x_1(2) = 0.1, x_1(3) = 0.12, x_1(4) = -0.2, x_1(5) = 0.9, x_2(1) = 0.11, x_2(2) = -0.2, x_2(3) = -0.1, x_2(4) = 0.2, x_2(5) = 0.1, x_3(1) = 0.12, x_3(2) = 0.15, x_3(3) = -0.2, x_3(4) = 0.22, x_3(5) = 1.1,$ and $x_4(1) = -0.1, x_4(2) = -0.23, x_4(3) = -0.1, x_4(4) = 0.2, x_4(5) = 0.11$. After 10^4 time steps being iterated, we plot the data consisting of 500 points for per α value. The plotting is for x_1, x_3 vs the parameter α. The bifurcation figures illustrate that the fixed point of x_1 loses stability and period bifurcation occurs when $\alpha \approx 0.95$, and the fixed point of x_3 loses stability and period bifurcation occurs when $\alpha \approx 1.1$. Making the bifurcation figures of the x_2 vs α and the x_4 vs α similar, they are omitted.

In Figure 2, we show the largest Lyapunov exponent diagram for $\alpha \in [0, 6]$. For every α value, the initial values were the same as Figure 1. From the simulation results in Figure 2, we can find that the largest Lyapunov exponent is negative when $\alpha \in (0, 1)$ and is positive when $\alpha > 2.8$. Thus,

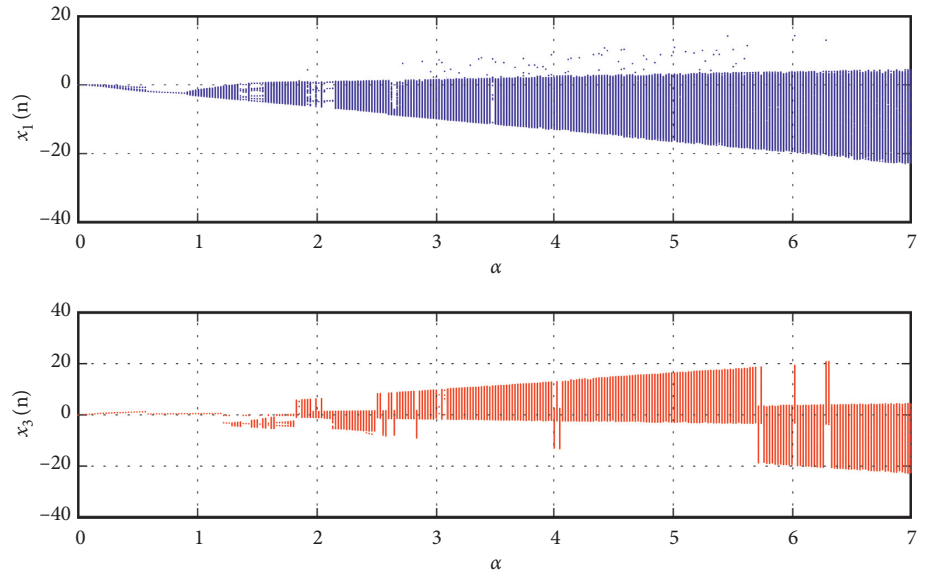

Figure 1: Bifurcation diagram.

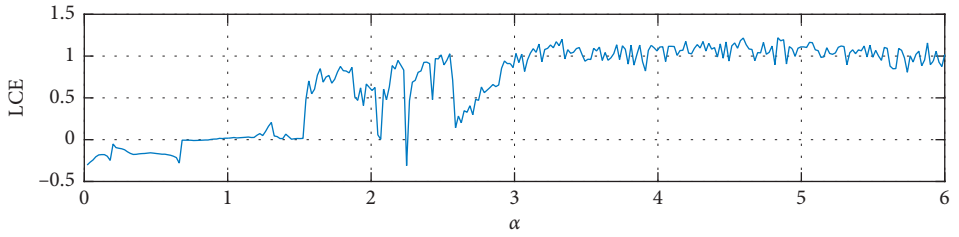

Figure 2: Largest Lyapunov exponents diagram.

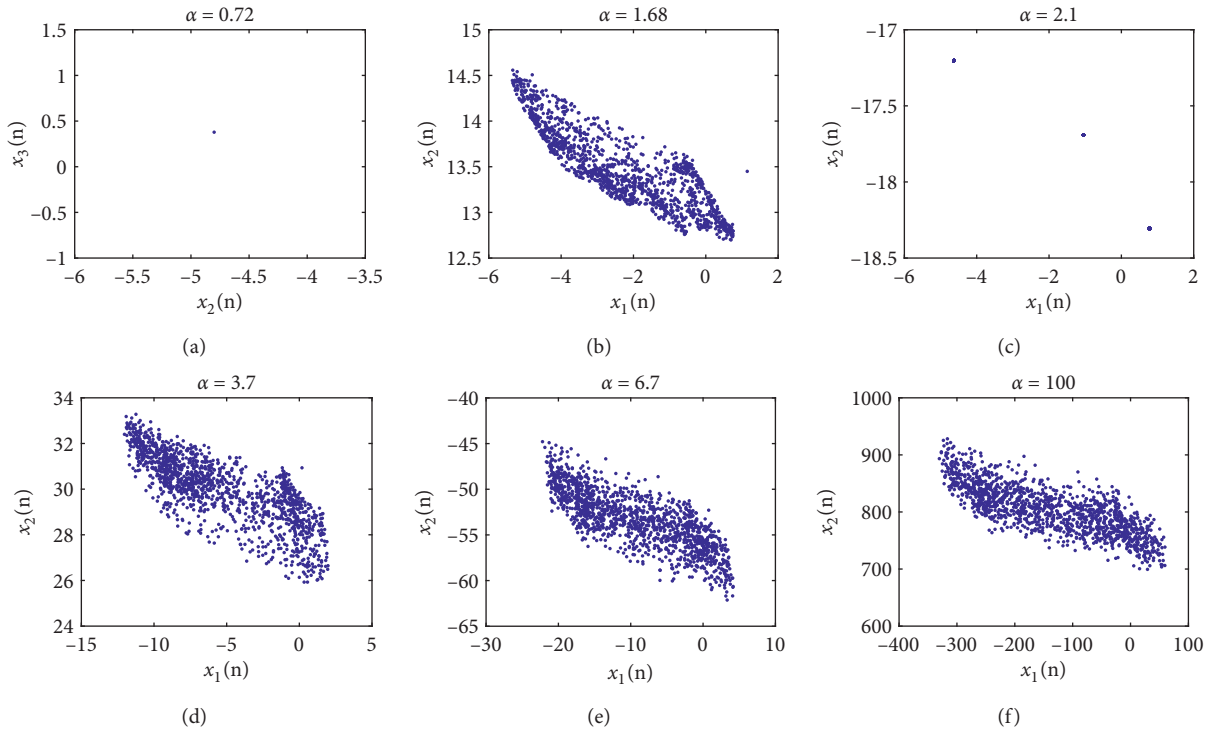

Figure 3: Continued.

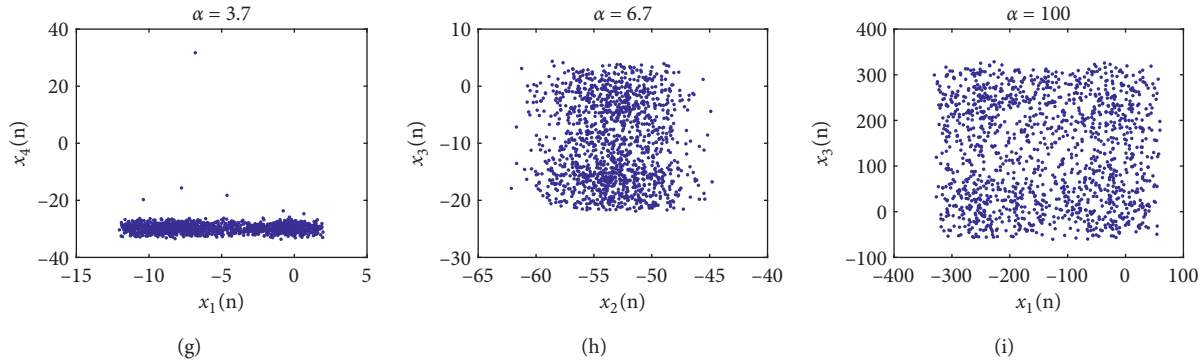

Figure 3: Chaos diagram.

the figures illustrate that the system (38) has chaotic behaviors when α is large enough.

In Figure 3, we show the chaotic figures. For each α value, after 6×10^5 time steps being iterated, plot the 6000 data points. The figure illustrates that there are no chaos for small α (e.g., $\alpha = 0.72, 2.1$) and chaotic behavior occurs when α is larger (e.g., $\alpha = 1.68, 3.0, 6.7, 100$). Those numerical simulations support the theoretical results in Section 2.

5. Conclusion

In this paper, the chaos of a discrete neural network loops with self-feedback is studied. The discrete neural network loops with multiple delays and self-feedback can demonstrate chaotic behavior when the interconnection strengths are large enough. Numerical simulations support the theoretical results. The theoretical results are to provide some new methods for the design of chaotic neural networks.

Data Availability

No data were used to support this study.

Conflicts of Interest

The authors declare that there are no conflicts of interest regarding the publication of this paper.

Acknowledgments

This study was supported in part by the National Natural Science Foundation of P. R. China (11671410) and Natural Science Foundation of Guangdong Province (2017A030313037).

References

[1] M. Adachi and K. Aihara, "Associative dynamics in a chaotic neural network," *Neural Networks*, vol. 10, no. 1, pp. 83–98, 1997.

[2] K. Aihara, T. Takabe, and M. Toyoda, "Chaotic neural networks," *Physics Letters A*, vol. 144, no. 6-7, pp. 333–340, 1990.

[3] L. Chen and K. Aihara, "Chaotic simulated annealing by a neural network model with transient chaos," *Neural Networks*, vol. 8, no. 6, pp. 915–930, 1995.

[4] L. Chen and K. Aihara, "Chaotic dynamics of neural networks and its application to combinatorial optimization," *Differential Equations and Dynamical Systems*, vol. 9, pp. 139–168, 2001.

[5] I. Tokuda, T. Nagashima, and K. Aihara, "Global bifurcation structure of chaotic neural networks and its application to traveling salesman problems," *Neural Networks*, vol. 10, no. 9, pp. 1673–1690, 1997.

[6] E. E. Basar, *Chaos in Brain Function*, Springer Berlin Heidelberg, Berlin, China, 1990.

[7] J. J. Hopfield, "Neural networks and physical systems with emergent collective computational abilities," *Proceedings of the National Academy of Sciences*, vol. 79, no. 8, pp. 2554–2558, 1982.

[8] Y. Huang and X. Zou, "Co-existence of chaos and stable Periodic orbits in a simple discrete neural network," *Journal of Nonlinear Science*, vol. 15, no. 5, pp. 291–303, 2005.

[9] Y. Chen, Y. Huang, and X. Zou, "Chaotic invariant sets of a delayed discrete neural network of two non-identical neurons," *Science China Mathematics*, vol. 56, no. 9, pp. 1869–1878, 2013.

[10] Y. Chen, T. Huang, and Yu Huang, "Complex dynamics of a delayed discrete neural network of two nonidentical neurons," *Chaos*, vol. 24, no. 1, 2014.

[11] E. Kaslik and Ş. Balint, "Chaotic dynamics of a delayed discrete-time Hopfield network of two nonidentical neurons with no self-connections," *Journal of Nonlinear Science*, vol. 18, no. 4, pp. 415–432, 2008.

[12] X. Wu, Y. Chen, J. Tian, and L. Li, "Chaotic dynamics of discrete multiple-time delayed neural networks of ring architecture evoked by external inputs," *International Journal of Bifurcation and Chaos*, vol. 26, no. 11, Article ID 1650179, 2016.

[13] C.-Y. Cheng, "Coexistence of multistability and chaos in a ring of discrete neural network with delays," *International Journal of Bifurcation and Chaos*, vol. 20, no. 04, pp. 1119–1136, 2010.

[14] Z. Zhang, *Principles of Differentiable Dynamical Systems*, Science Press, Beijing, China, 2003, in Chinese.

[15] Y. L. Chen, Y. Huang, and L. L. Li, "The persistence of snap-back repellers under small C^1 perturbations in Banach spaces," *International Journal of Bifurcation and Chaos*, vol. 21, no. 3, pp. 1–8, 2011.

Hindawi
Discrete Dynamics in Nature and Society
Volume 2020, Article ID 8825694, 10 pages
https://doi.org/10.1155/2020/8825694

Research Article

Fractional Grassi–Miller Map Based on the Caputo *h*-Difference Operator: Linear Methods for Chaos Control and Synchronization

Ibtissem Talbi,[1] Adel Ouannas,[2] Giuseppe Grassi,[3] Amina-Aicha Khennaoui,[4] Viet-Thanh Pham,[5] and Dumitru Baleanu[6,7,8]

[1]*Department of Mathematics, Constantine University, Constantine 25000, Algeria*
[2]*Department of Mathematics and Computer Science, University of Larbi Ben M'hidi, Oum El Bouaghi, Algeria*
[3]*Universita del Salento, Dipartimento Ingegneria Innovazione, Lecce 73100, Italy*
[4]*Laboratory of Dynamical System and Control, University of Larbi Ben M'hidi, Oum El Bouaghi, Algeria*
[5]*Nonlinear Systems and Applications, Faculty of Electrical and Electronics Engineering, Ton Duc Thang University, Ho Chi Minh City, Vietnam*
[6]*Cankaya University, Ankara, Turkey*
[7]*China Medical University, Taichung, Taiwan*
[8]*Institute of Space Sciences, Magurele-Bucharest, Romania*

Correspondence should be addressed to Amina-Aicha Khennaoui; kamina_aicha@yahoo.fr

Received 7 August 2020; Revised 3 November 2020; Accepted 16 November 2020; Published 26 November 2020

Academic Editor: Qamar Din

Investigating dynamic properties of discrete chaotic systems with fractional order has been receiving much attention recently. This paper provides a contribution to the topic by presenting a novel version of the fractional Grassi–Miller map, along with improved schemes for controlling and synchronizing its dynamics. By exploiting the Caputo *h*-difference operator, at first, the chaotic dynamics of the map are analyzed via bifurcation diagrams and phase plots. Then, a novel theorem is proved in order to stabilize the dynamics of the map at the origin by linear control laws. Additionally, two chaotic fractional Grassi–Miller maps are synchronized via linear controllers by utilizing a novel theorem based on a suitable Lyapunov function. Finally, simulation results are reported to show the effectiveness of the approach developed herein.

1. Introduction

Nonlinear dynamics, chaos control, and chaos synchronization represent important research topics [1–27]. In particular, referring to synchronization and control, new advances have been recently reported, for both integer-order systems and fractional-order systems [28, 29]. In particular, referring to continuous-time systems described by fractional derivative, some interesting techniques involving adaptive synchronization have been recently illustrated in [28, 29]. However, there is a remarkable difference in fractional calculus regarding continuous-time and discrete-time systems. Namely, while fractional derivatives made their first appearance in a letter that Gottfried Wilhelm Leibniz wrote to Guillaume de l'Hopital in 1695, discrete fractional calculus has been introduced by Diaz and Olser only in 1974 [6]. Indeed, the authors of [6] presented the first definition of a discrete fractional operator, obtained by discretizing a continuous-time fractional operator. Over the years, several types of difference operators have been introduced in the field of discrete fractional calculus [3, 7, 8]. In particular, a number of fractional *h*-difference operators, which represent generalizations of the fractional difference operators, have been investigated in [7].

Based on fractional difference equations, in recent years some chaotic discrete-time systems have been studied [10, 25–27]. These systems are fractional-order maps, which show complex unpredictable behaviors due to the nonlinearities included in their difference equations [7]. With the introduction of fractional chaotic maps, attention has been

also focused on the issues related to the synchronization and control of these systems [12]. For example, in [26] the fractional logistic map and its chaotic behaviors have been illustrated, whereas in [27] the presence of chaos in fractional sine and standard maps has been discussed. In [10], discrete chaos in the fractional Hénon map is reported, whereas in [25] the chaotic dynamics of the fractional delayed logistic map are analyzed in detail. In [12], three different discrete-time systems, namely, the fractional Lozi map, the fractional Lorenz map, and the fractional flow map, have been studied, along with the control laws for stabilizing and synchronizing these three maps. In [23], the fractional generalized hyperchaotic Hénon map has been introduced, whereas in [20], the dynamics of the Ikeda map have been investigated via phase plots and bifurcation diagrams. In [13], three fractional chaotic maps, namely, the Stefanski map, the Rossler map, and the Wang map have been studied, along with the synchronization properties of these systems. In [16], dynamics and control of the fractional version of the discrete double-scroll hyperchaotic map are investigated in detail. In [18], bifurcations, entropy, and control of a quadratic fractional map without equilibrium points are analyzed, whereas in [9] the dynamics of fractional maps with fixed points located on closed curves are studied.

A challenging topic in discrete fractional calculus is to study dynamics, synchronization, and control of very complex systems, such as the chaotic three-dimensional (3D) maps [8]. Namely, by computing the approximate entropy, it can be shown that 3D maps highlight a higher degree of complexity with respect to one-dimensional (1D) or two-dimensional (2D) fractional maps [5,21]. Since the increased complexity can enhance the applicability of 3D maps in pseudo-random number generators and image encryption techniques [22], it is important to analyze their dynamics as well as conceive improved synchronization and control schemes for these maps. In this regard, some interesting results have been recently published [11, 17, 19]. In [11], synchronization and control schemes for a new 3D generalized Hénon map have been proposed, whereas in [19] control and synchronization properties of a 3D fractional map without equilibria have been analyzed in detail. In [17], the fractional form of the Grassi–Miller map has been introduced using the ν-Caputo delta difference. In particular, phase portraits and bifurcation diagrams have been illustrated in [17], with the aim of deriving the fractional-order range for which the system is chaotic. In addition, two nonlinear control laws have been proposed in [17], one for stabilizing the system dynamics and the other for synchronizing a master-slave pair of maps. Although the methods developed in [11, 17, 19] are interesting, a drawback is represented by the fact that very complex control laws have been exploited for controlling and synchronizing the corresponding 3D fractional maps. For example, in [11], synchronization and control in the 3D generalized Hénon maps have been achieved using nonlinear control laws. Moreover, in [19], the 3D fractional maps with hidden attractors have been synchronized and controlled via nonlinear control laws that include several nonlinear terms. We would observe that it might be difficult to implement very complex control laws in practical applications of fractional maps. This drawback also regards the Grassi–Miller map in [17], since its introduction via the Caputo delta difference has led to complex nonlinear control laws to achieve synchronization and control of its chaotic dynamics.

Inspired by the mentioned above considerations, this paper provides a further contribution to the topic of dynamics, control, and synchronization of fractional 3D maps by presenting a novel version of the Grassi–Miller map, along with improved schemes for controlling and synchronizing its dynamics. The structure of the article is as follows. In Section 2, definition of the fractional Caputo h-difference operator [7] and a novel fractional Grassi–Miller map is proposed, along with its chaotic dynamic behavior. In Section 3 linear control laws are proposed to stabilize the dynamics of the map at the origin. In particular, a novel theorem is proved, which assures the stability condition via a suitable Lyapunov function. In Section 4, a master-slave system based on two chaotic Grassi–Miller maps is synchronized using linear controllers. The objective is achieved by exploiting a novel theorem involving a Lyapunov-based approach. Note that this paper makes an attempt to overcome the weakness and the difficulties encountered in [11, 17, 19]. Namely, on one hand, this paper focuses on a novel 3D map, with the aim of exploiting the potentials deriving from the higher degree of complexity of 3D maps with respect to simpler 1D and 2D maps. On the other hand, the paper proposes simple linear control laws (with respected to the complex control laws developed [11, 17, 19]), with the aim of making feasible their implementation for potential applications of 3D maps in pseudo-random number generators and image encryption techniques. In addition to these improvements, note that, by virtue of the linearity of the control laws developed herein, the proposed control and synchronization schemes require less control effort with respect to the nonlinear approaches illustrated in [17]. Finally, simulation results are reported to show the effectiveness of the control and synchronization methods developed herein. All the results developed thorough the manuscript clearly highlight the novelty of the conceived approach, consisting in the following: (i) the introduction of a new 3D fractional map characterized by complex dynamics; (ii) the proof of a novel theorem for stabilizing the map via a linear control law; (iii) the proof of a novel theorem for synchronizing the map via linear control law; (iv) comparisons for illustrating the better performances of our method if compared to recent published articles where complex nonlinear control laws have been used.

2. Fractional Grassi–Miller Map Based on the Caputo h-Difference Operator

In this section, a novel version of the fractional Grassi–Miller map is presented. To this purpose, some concepts related to the Caputo h-difference operator are briefly summarized.

Throughout the rest of the paper, we assume that $(h\mathbb{N})_a = \{a, a + h, a + 2h, \ldots\}$, where h is a positive real and

$a \in \mathbb{R}$. The forward h-difference operator of a function X defined on $(h\mathbb{N})_a$ is defined as

$$\Delta_h X(t) = \frac{X(t+h) - X(t)}{h}. \tag{1}$$

Definition 1 (see [2]). Let X: $(h\mathbb{N})_a \longrightarrow \mathbb{R}$. The fractional h-sum of positive fractional order ν is defined by

$${}_h\Delta_a^{-\nu} X(t) = \frac{h}{\Gamma(\nu)} \sum_{s=(a/h)}^{(t/h)-\nu} (t - \sigma(sh))_h^{(\nu-1)} X(sh), \tag{2}$$

where $\sigma(sh) = (s+1)h$, $a \in \mathbb{R}$, and $t \in (h\mathbb{N})_{a+\nu h}$. $t_h^{(\nu)}$ is the h-falling fractional function with two real numbers t, h that can be written in the form

$$t_h^{(\nu)} = \frac{h^\nu \Gamma((t/h)+1)}{\Gamma((t/h)+1-\nu)}. \tag{3}$$

Definition 2 (see [1]). For $X(t)$ defined on $(h\mathbb{N})_a$ and a real order $0 < \nu \le 1$, the Caputo fractional h-difference operator is given by

$${}_h^C\Delta_a^\nu X(t) = \Delta_a^{-(n-\nu)} \Delta^n X(t), \quad t \in (h\mathbb{N})_{a+(n-\nu)h}, \tag{4}$$

in which $n = \lceil \nu \rceil + 1$.

Now, a theorem reported in [4] is briefly illustrated, with the aim to identify the stability conditions of the zero equilibrium point for the fractional nonlinear difference system written in the form

$${}_h^C\Delta_a^\nu = F(t + \nu h, X(t + \nu h)). \tag{5}$$

Theorem 1. *The fractional nonlinear discrete system (5) is asymptotically stable if there exists a positive definite and decreasing scalar function $V(t, X(t))$ for the equilibrium point $x = 0$, such that $V(t, X(t)) \le 0$.*

Lemma 1. *For every $t \in (h\mathbb{N})_{a+(n-\nu)h}$, the following inequality holds:*

$${}_h^C\Delta_a^\nu X^2(t) \le 2X(t + \nu h)\,{}_h^C\Delta_a^\nu X(t), \quad 0 < \nu \le 1. \tag{6}$$

All the details regarding the proof of Lemma 1 can be found in [4].

Referring to the fractional Grassi–Miller map, it was introduced in [17] using the ν-Caputo delta difference operator. The fractional map, which proved to be chaotic for proper values of the system parameters (α, β) and of the fractional order $\nu \in (0, 1]$, possesses only a nonlinear term [17].

Herein, the fractional Caputo h-difference operator is considered, in order to derive a different mathematical model of the 3D Grassi–Miller map. Namely, the following equations are proposed:

$$\left\{ {}_h^C\Delta_a^\nu x(t) = \alpha - y^2(t + \nu h) - \beta z(t + \nu h) - x(t + \nu h), {}_h^C\Delta_a^\nu y(t) = x(t + \nu h) - y(t + \nu h), {}_h^C\Delta_a^\nu z(t) = y(t + \nu h) - z(t + \nu h), \right. \tag{7}$$

where ${}_h^C\Delta_a^\nu$ denotes the fractional h-difference operator, $t \in (h\mathbb{N})_{a+(n-\nu)h}$, a is the starting point, and (α, β) are system parameters. The fractional map (7) can be considered a generalized model of the map introduced in [17].

The solution of the fractional Grassi–Miller map (7) is obtained by introducing the fractional h-sum operator. According to [15], the equivalent implicit discrete formula can be written in the form

$$\begin{cases} x(n+1) = x(0) + \dfrac{h^\nu}{\Gamma(\nu)} \displaystyle\sum_{j=0}^{n} \frac{\Gamma(n-j+\nu)}{\Gamma(n-j+1)} \Big(\alpha - y^2(j+1) - \beta z(j+1) - x(j+1)\Big), \\ y(n+1) = y(0) + \dfrac{h^\nu}{\Gamma(\nu)} \displaystyle\sum_{j=0}^{n} \frac{\Gamma(n-j+\nu)}{\Gamma(n-j+1)} (x(j+1) - y(j+1)), \\ z(n+1) = z(0) + \dfrac{h^\nu}{\Gamma(\nu)} \displaystyle\sum_{j=0}^{n} \frac{\Gamma(n-j+\nu)}{\Gamma(n-j+1)} (y(j+1) - z(j+1)), \end{cases} \tag{8}$$

where $x(0)$, $y(0)$, and $z(0)$ are the initial state values. Based on predictor-corrector method [14], the implicit equation (8) is transformed into its explicit form, which can be used for investigating the dynamic behavior of the Grassi–Miller map (7). By taking the initial state values $x(0) = 1$, $y(0) = 0.1$, and $z(0) = 0$, with the fractional order value $\nu = 0.999$ and the system parameters $\alpha = 1$, $\beta = 0.5$, it can be shown that map (7) displays the attractor reported in Figure 1. The computation of the bifurcation diagram and of the largest Lyapunov exponent, both reported in Figure 2 as a

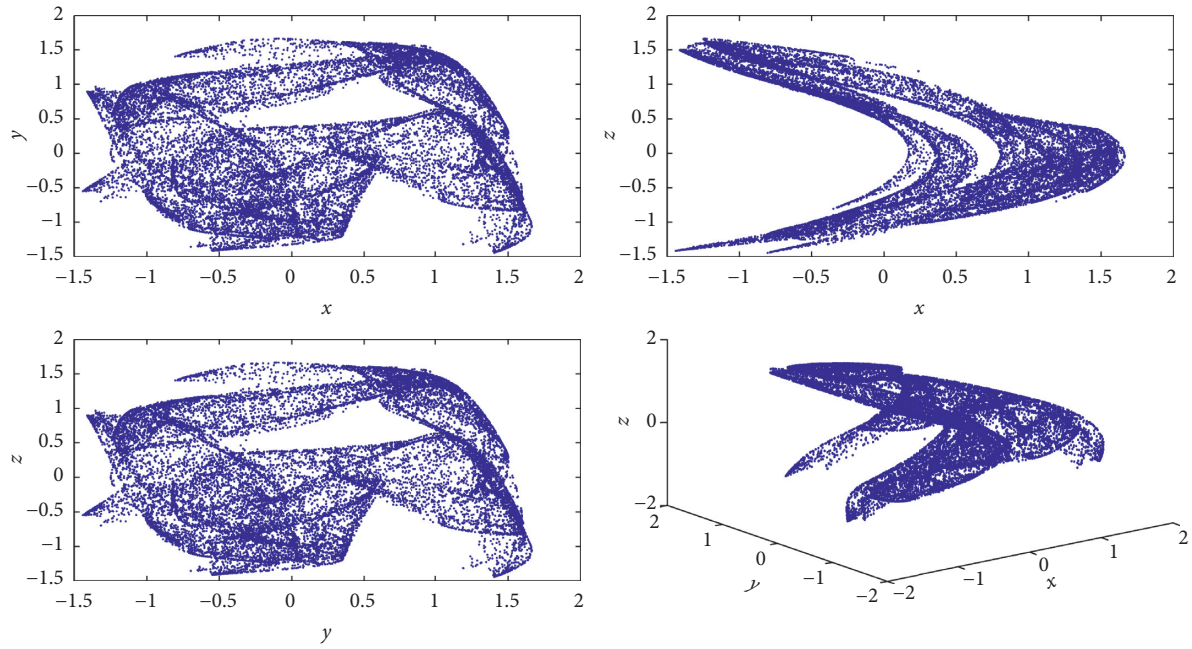

Figure 1: Chaotic attractor of the fractional order Grassi–Miller map for $\alpha = 1$, $\beta = 0.5$, and order $\nu = 0.999$.

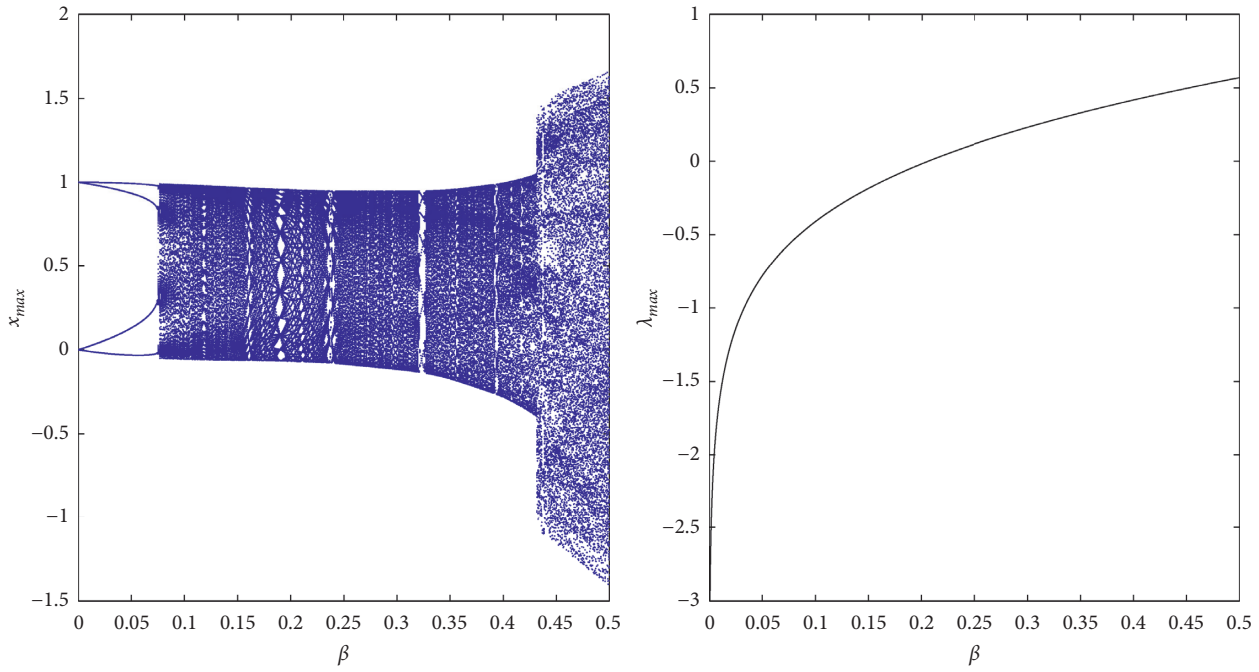

Figure 2: Bifurcation and largest Lyapunov exponent plots versus system parameter β for fractional order $\nu = 0.999$.

function of the system parameter β, clearly highlights the chaotic behavior of the fractional Grassi–Miller map (7) for $\alpha = 1$, $\beta = 0.5$, and $\nu = 0.999$. Regarding the bifurcation diagram reported in Figure 2, it can be noted that the map oscillates when β assumes values around 0.05. When β approaches the value of 0.1, more complex dynamic regimes appear, until β approaches the value of 0.45, when chaotic behaviours are reached. Note that the presence of chaos for $0.45 < \beta < 0.5$ is also confirmed by the positive values assumed by the maximum Lyapunov exponents (see Figure 2). Note that the evolution of states of the fractional map (7), which involves the adoption of the Caputo h-difference operator, is different from those of the map reported in [17], the latter being based on the ν-Caputo delta difference operator. This can be clearly seen by comparing the shapes of the chaotic attractors reported in Figure 1 with those of the attractors reported in [17]. Namely, the adoption of two different fractional operators has led to different shapes in

the chaotic attractors as well as different parameter values for generating chaos (see [17]), indicating that the proposed Grassi–Miller map (7) provides a contribution to the topic of 3D discrete-time fractional systems.

Referring to potential applications of the proposed model (7), it should first be noted that 3D maps highlight a higher degree of complexity with respect to 1D and 2D maps [5, 21]. Thus, the applicability of the conceived 3D map (7) would mainly be in pseudo-random number generators and image encryption techniques. This makes perceive the importance of developing simple and feasible control methods, given that master-slave synchronization schemes based on model (7), in combination with encryption algorithms, might be used for experimentally generating and recovering the secret keys.

3. Chaos Control of the New Version of the Grassi–Miller Map

Here, a controller is presented in order to stabilize at zero the chaotic trajectories of the state-variables in the Grassi–Miller map (7) with fractional order. The objective is achieved by adding two linear terms into both first and second equations of the map. Namely, the controlled fractional Grassi–Miller chaotic map is described by

$$\begin{cases} {}_h^C\Delta_a^{\nu} x(t) = \alpha - y^2(t+\nu h) - \beta z(t+\nu h) - x(t+\nu h) + \mathbf{C}_1(t+\nu h), \\ {}_h^C\Delta_a^{\nu} y(t) = x(t+\nu h) - y(t+\nu h) + \mathbf{C}_2(t+\nu h), \\ {}_h^C\Delta_a^{\nu} z(t) = y(t+\nu h) - z(t+\nu h), \end{cases} \tag{9}$$

where $\mathbf{C}_1$ and $\mathbf{C}_2$ are suitable controllers to be determined. To this purpose, a theorem is now given for rigorously assuring that the dynamics of (9) can be stabilized at zero.

Theorem 2. *The three-dimensional fractional Grassi–Miller map (9) is controlled at the origin under the following control laws:*

$$\begin{cases} \mathbf{C}_1(t) = -\alpha + \beta z(t) - y(t), \\ \mathbf{C}_2(t) = -b_1 y(t) - z(t), \end{cases} \tag{10}$$

where $|x(t)| \le b_1$, $\forall t \in (h\mathbb{N})_{a+(n-\nu)h}$.

Proof of Theorem 2. By subtracting (10) into system (9), we get the following fractional difference equations:

$$\begin{cases} {}_h^C\Delta_a^{\nu} x(t) = -y^2(t+\nu h) - x(t+\nu h) - y(t+\nu h), \\ {}_h^C\Delta_a^{\nu} y(t) = x(t+\nu h) - (1+b_1) y(t+\nu h) - z(t+\nu h), \\ {}_h^C\Delta_a^{\nu} z(t) = y(t+\nu h) - z(t+\nu h). \end{cases} \tag{11}$$

By taking a Lyapunov function in the form $V = (1/2)(x^2(t) + y^2(t) + z^2(t))$, the adoption of the Caputo h-difference operator implies that

$${}_h^C\Delta_a^{\nu} V = \frac{1}{2} {}_h^C\Delta_a^{\nu} x x^2(t) + \frac{1}{2} {}_h^C\Delta_a^{\nu} x y^2(t) + \frac{1}{2} {}_h^C\Delta_a^{\nu} x z^2(t). \tag{12}$$

By using Lemma 1, it follows that

$$\begin{aligned} {}_h^C\Delta_a^{\nu} V &\le x(t+\nu h) {}_h^C\Delta_a^{\nu} x(t) + y(t+\nu h) {}_h^C\Delta_a^{\nu} y(t) + z(t+\nu h) {}_h^C\Delta_a^{\nu} z(t) \\ &= -x(t+\nu h) y^2(t+\nu h) - x^2(t+\nu h) - x(t+\nu h) y(t+\nu h) + y(t+\nu h) x(t+\nu h) \\ &\quad - (1+b_1) y^2(t+\nu h) - y(t+\nu h) z(t+\nu h) + z(t+\nu h) y(t+\nu h) - z^2(t+\nu h) \\ &\le |x(t+\nu h)| y^2(t+\nu h) - x^2(t+\nu h) - (1+b_1) y^2(t+\nu h) - z^2(t+\nu h) \\ &\le b_1 y^2(t+\nu h) - x^2(t+\nu h) - (1+b_1) y^2(t+\nu h) - z^2(t+\nu h) \\ &= -x^2(t+\nu h) - y^2(t+\nu h) - z^2(t+\nu h) < 0. \end{aligned} \tag{13}$$

From Theorem 1, it can be concluded that the zero equilibrium of (9) is asymptotically stable. As a consequence, it is proved that the dynamics of the proposed 3D Grassi–Miller map (7) are stabilized at the origin by the linear control laws (10). □

Remark 1. Since all the chaotic states of map (9) are bounded, it can be deduced that it is easy to find a parameter b_1 larger than the absolute value of the state variable $x(t)$, as requested by the proof of Theorem 2. Namely, the existence of b_1 is intrinsically justified by the property of boundedness of the state $x(t)$. Thus, the value of b_1 can be easily found by looking at the plots reported in Figure 1, from which it is clear that $-1.6 < x(t) < 1.6$ for any t. Through the paper, the value of b_1 has been selected as $b_1 = 1.7$. Note that the value of b_1 does not significantly affect the time for stabilizing the map dynamics.

Now, we give the numerical simulation to prove the above theory. We select $\alpha = 1$ and $\beta = 0.5$, and we give the evolution of the states and the phase-space plots as shown in Figure 3 for $\nu = 0.999$. These plots clearly show that the new fractional map (7) is driven to the origin by linear control laws in the form (10).

Now comparisons are carried out with recent results regarding 3D fractional maps, with the aim to confirm the effectiveness of the conceived approach when comparing control strategies for maps of similar degree of complexity. For example, the results in [11] show that the 3D fractional map proposed therein is stabilized after more than 20 steps, whereas the map illustrated herein is stabilized in at most 3 steps. On the other hand, the results in [19] highlight that the 3D fractional map proposed therein is stabilized in the same number of steps taken by our method. However, the control law adopted in [19] is complex, since it involves some nonlinear terms, whereas the proposed control strategies is simple and involves only linear terms. Finally, the results in [4] show that the 3D fractional Grassi–Miller map proposed therein, based on the-Caputo delta difference, is stabilized after more than 20 steps, whereas the map illustrated herein, based on the Caputo h-difference operator, is stabilized in at most 3 steps. These comparisons make us perceive the effectiveness of the proposed control strategy with respect to 3D fractional maps of similar complexity published in recent literature.

3.1. Synchronization of the Fractional Grassi–Miller Map. In this paragraph, a master-slave system, based on two identical chaotic fractional Grassi–Miller maps, is synchronized using linear controllers. The dynamics of the master system can be written as follows:

$$\begin{cases} {}_h^C\Delta_a^{\nu} x_m(t) = \alpha - y_m^2(t+\nu h) - \beta z_m(t+\nu h) - x_m(t+\nu h), \\ {}_h^C\Delta_a^{\nu} y_m(t) = x_m(t+\nu h) - y_m(t+\nu h), \\ {}_h^C\Delta_a^{\nu} z_m(t) = y_m(t+\nu h) - z_m(t+\nu h), \end{cases} \tag{14}$$

where $x_m(t)$, $y_m(t)$, and $z_m(t)$ are the system states. The equations of the slave system are given by

$$\begin{cases} {}_h^C\Delta_a^{\nu} x_s(t) = \alpha - y_s^2(t+\nu h) - \beta z_s(t+\nu h) - x_s(t+\nu h) + \mathbf{L}_1(t+\nu h), \\ {}_h^C\Delta_a^{\nu} y_s(t) = x_s(t+\nu h) - y_s(t+\nu h), \\ {}_h^C\Delta_a^{\nu} z_s(t) = y_s(t+\nu h) - z_s(t+\nu h) + \mathbf{L}_2(t+\nu h), \end{cases} \tag{15}$$

where $x_s(t)$, $y_s(t)$, and $z_s(t)$ are the system states, whereas $\mathbf{L}_1$ and $\mathbf{L}_2$ are suitable linear controllers to be determined.

We subtract master system (14) from the slave system (15) to get the error system as

$$\left(e_1(t), e_2(t), e_3(t)\right)^T = \left(x_s(t), y_s(t), z_s(t)\right)^T - \left(x_m(t), y_m(t), z_m(t)\right)^T. \tag{16}$$

Now a theorem involving a Lyapunov-based approach is proved, with the aim of synchronizing the master-slave (14) and (15) via linear controllers $\mathbf{L}_1$ and $\mathbf{L}_2$.

Theorem 3. *The master system (14) and the slave system (15) achieve synchronized dynamics, provided that the linear control laws* $\mathbf{L}_1$ *and* $\mathbf{L}_2$ *are selected as*

$$\begin{cases} \mathbf{L}_1(t) = \left(1 - \left(b_2 + \dfrac{1}{2}\right)^2\right) e_1(t), \\ \mathbf{L}_2(t) = \beta e_1(t) - e_2(t), \end{cases} \tag{17}$$

where $|y_m(t)| = |y_s(t)| \le b_2$, $t \in (h\mathbb{N})_{a+(n-\nu)h}$.

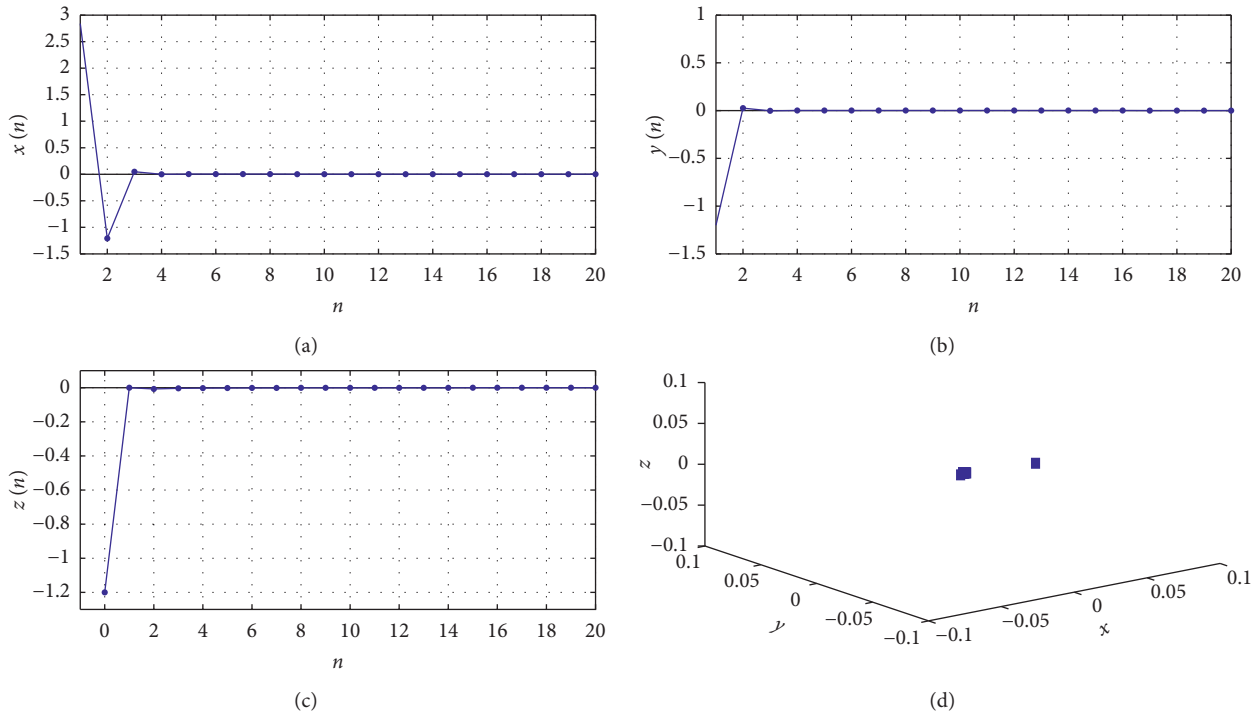

Figure 3: Stabilized states of the controlled fractional Grassi–Miller map (9) via linear control laws (10) with $\alpha = 1$, $\beta = 0.5$, and fractional order $\nu = 0.999$.

Proof of Theorem 3. By taking into account (16), the dynamics of the error system can be written as

$$\begin{aligned}\left\{ {}_{h}^{C}\Delta_{a}^{\nu} e_1(t) = y_m^2(t+\nu h) - y_s^2(t+\nu h) - \beta e_3(t+\nu h) - e_1(t+\nu h) + \mathbf{L}_1(t+\nu h), {}_{h}^{C}\Delta_{a}^{\nu} e_2(t)\right. \\ \left. = e_1(t+\nu h) - e_2(t+\nu h), {}_{h}^{C}\Delta_{a}^{\nu} e_3(t) = e_2(t+\nu h) - e_3(t+\nu h) + \mathbf{L}_2(t+\nu h).\right.\end{aligned} \tag{18}$$

By substituting the control law (17) into error system (18), we get

$$\begin{aligned}\left\{ {}_{h}^{C}\Delta_{a}^{\nu} e_1(t) = -\left(y_m(t+\nu h) + y_s(t+\nu h)\right)e_2(t+\nu h) - \beta e_3(t+\nu h) - \left(b_2 + \frac{1}{2}\right)^2 e_1(t+\nu h), {}_{h}^{C}\Delta_{a}^{\nu} e_2(t)\right. \\ \left. = e_1(t+\nu h) - e_2(t+\nu h), {}_{h}^{C}\Delta_{a}^{\nu} e_3(t) = \beta e_1(t+\nu h) - e_3(t+\nu h).\right.\end{aligned} \tag{19}$$

Now, by taking a Lyapunov function in the form $V = (1/2)(e_1^2(t) + e_2^2(t) + e_3^2(t))$ and by exploiting Lemma 1, it follows that

$$
\begin{aligned}
{}_h^C\Delta_a^{\nu} V &\le e_1(t+\nu h)\,{}_h^C\Delta_a^{\nu} e_1(t) + e_2(t+\nu h)\,{}_h^C\Delta_a^{\nu} e_2(t) + e_3(t+\nu h)\,{}_h^C\Delta_a^{\nu} e_3(t) \\
&= -\left(b_2 + \frac{1}{2}\right)^2 e_1^2(t+\nu h) - \left(y_m(t+\nu h) + y_s(t+\nu h)\right) e_1(t+\nu h) e_2(t+\nu h) \\
&\quad - \beta e_1(t+\nu h) e_3(t+\nu h) + e_2(t+\nu h) e_1(t+\nu h) - e_2^2(t+\nu h) + \beta e_1(t+\nu h) e_3(t+\nu h) - e_3^2(t+\nu h) \\
&\le -\left(b_2 + \frac{1}{2}\right)^2 e_1^2(t+\nu h) + \left(1 + \left|y_m(t+\nu h) + y_s(t+\nu h)\right|\right) \\
&\quad \left|e_1(t+\nu h)\right|\left\|e_2(t+\nu h)\right| - e_2^2(t+\nu h) - e_3^2(t+\nu h) \\
&\le -\left(b_2 + \frac{1}{2}\right)^2 e_1^2(t+\nu h) + (1+2b_2)\left|e_1(t+\nu h)\right|\left\|e_2(t+\nu h)\right| - e_2^2(t+\nu h) - e_3^2(t+\nu h) \\
&= -\left(\left(b_2 + \frac{1}{2}\right) e_1(t+\nu h) - e_2(t+\nu h)\right)^2 - e_3(t+\nu h) \le 0.
\end{aligned}
\tag{20}
$$

From Theorem 1, it can be concluded that the dynamics of the error system (18) are stabilized at the origin. As a consequence, it is proved that the master system (14) and the slave system (15) achieve synchronized dynamics via linear control laws in the form (17). □

Remark 2. It is easy to find a parameter b_2 larger than the absolute value of the variables $y_m(t) = y_s(t)$, as requested by the proof of Theorem 3. Namely, the existence of b_2 is intrinsically justified by the property of boundedness of the chaotic states of map (9). Thus, the value of b_2 can be easily found by looking at the plots reported in Figure 1, from which it is clear that $-1.6 < y(t) < 1.6$ for any t. Herein, in order to achieve synchronization, the value of b_2 has been selected as $b_2 = 2$. Note that the value of b_2 does not significantly affect the time for synchronizing the master-slave pair.

In order to show the effectiveness of the proposed approach, Figure 4 displays the chaotic dynamics of the master system states (blue color) and of the slave system states (red color) when $\alpha = 1, \beta = 0.5$, and $\nu = 0.999$. These plots clearly show that two identical Grassi–Miller maps achieve chaos synchronization via linear controllers. Note that, through the manuscript, all the simulation results and the related figures have been obtained using the software MATLAB.

Now, we would discuss the issue regarding the complexity of the proposed method. We would observe that the approach proposed herein is simpler than similar methods reported in literature. For example, the techniques developed in [11, 17, 19] present the drawback that very complex control laws have been exploited for controlling and synchronizing the corresponding 3D fractional maps. For example, in [11, 19] synchronization and control have been achieved using nonlinear control laws that include several nonlinear terms. This drawback also regards the Grassi–Miller map in [17], since complex nonlinear control laws have been used to achieve synchronization and control of its chaotic dynamics. Since it might be difficult to implement very complex control laws in practical applications of fractional maps, this paper has provided a contribution to the topic by developing simple linear control laws for stabilizing and synchronizing 3D fractional maps.

Referring to synchronization issues, now comparisons are carried out with recent results regarding 3D fractional maps. The objective is to highlight the effectiveness of the conceived approach when synchronization involves 3D maps with similar degree of complexity. For example, the results in [11] show that synchronization for the 3D fractional map proposed therein is achieved after more than 10 steps, whereas the map illustrated herein can be synchronized in at most 3 steps. On the other hand, the results in [19] show that synchronization for the 3D fractional map proposed therein is achieved in the same number of steps taken by our method. However, [19] exploits a complex control law that involves some nonlinear terms, whereas the proposed synchronization technique is simple and involves only linear terms. Finally, the results in [17] show that synchronization for 3D fractional Grassi–Miller map proposed therein, based on the ν-Caputo delta difference, is achieved after more than 20 steps, whereas the map illustrated herein, based on the Caputo h-difference operator, achieves synchronized dynamics in at most 3 steps. These comparisons make us perceive the effectiveness of the proposed synchronization strategy with respect to 3D fractional maps of similar complexity published in recent literature.

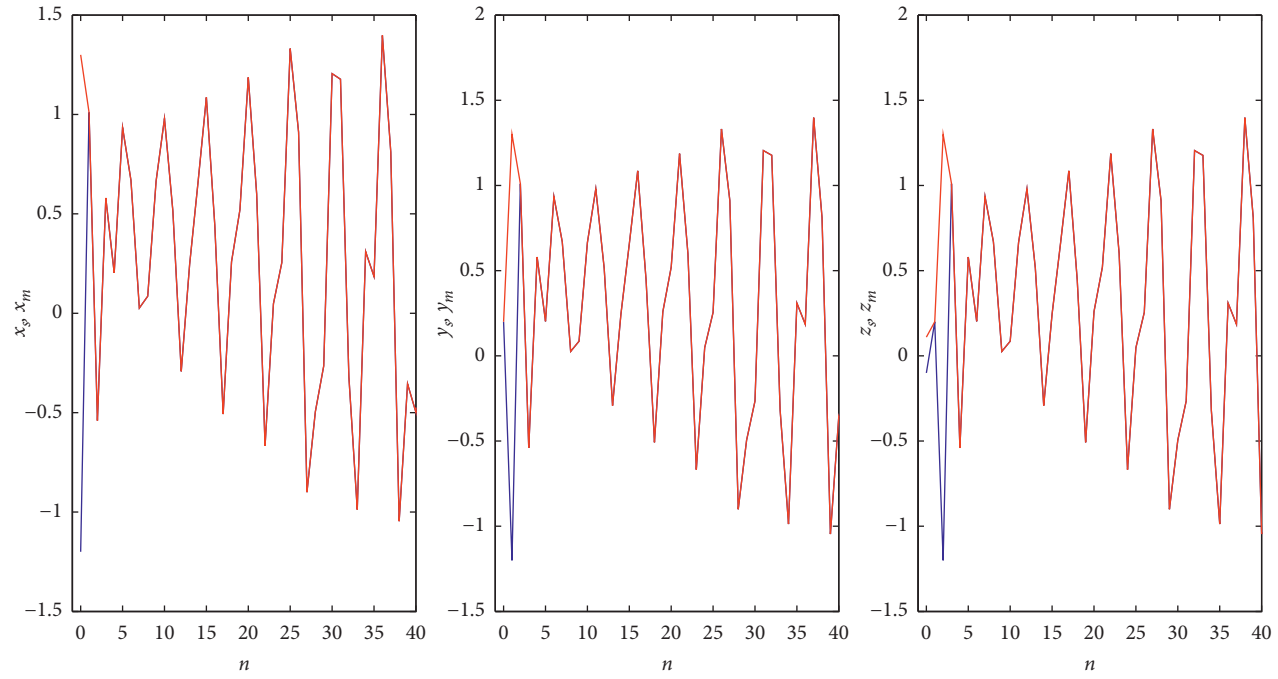

FIGURE 4: Synchronization of two identical Grassi–Miller map with $\alpha = 1$, $\beta = 0.5$, and $\nu = 0.999$: evolutions of the master system states (blue color) and of the slave system states (red color).

Finally, we would briefly discuss the potential applications of the conceived approach in real world. As any 3D map, the Grassi–Miller map highlights a higher degree of complexity with respect to 1D or 2D fractional maps. This increased complexity can be very useful for pseudo-random number generators in chaos-based communications systems. Moreover, since the production of images is increasing day by day in real life, confidentiality and privacy are becoming key issues when transmitting digital images using portable devices. Thus, referring to secure image transmission, the proposed discrete-time synchronization scheme could be utilized for retrieving the secrets keys at the receiver side in chaos-based image encryption systems.

4. Conclusions and Future Work

By including Grassi as a coauthor, this paper has presented a novel version of the chaotic fractional Grassi–Miller map, based on the Caputo h-difference operator. Two novel theorems have been proved, with the aim of deriving improved schemes (with respect to those presented in [17]) for controlling and synchronizing the dynamics of the map. Namely, while synchronization and control in [17] are achieved via more complex nonlinear control laws, herein, simple linear controllers have been conceived. Finally, simulation results have been carried out to highlight the effectiveness of the proposed method. Referring to future improvements of the conceived approach, our plan is to make an attempt to further simplify the control laws developed herein. Specifically, the objective is to reduce the control law (10) to just one term $C(t)$, instead of having two terms $C_1(t)$ and $C_2(t)$. Furthermore, regarding synchronization, we will try to reduce the control law (17) to just one term $L(t)$, instead of having two terms $L_1(t)$ and $L_2(t)$.

By exploiting the results achieved herein, our future work will focus on two main steps. At first, we will implement the proposed Grassi–Miller map using an Arduino board, with the aim of experimentally showing the high degree of complexity generated by fractional 3D maps. Then, the second step will consist in applying the conceived linear controllers to image encryption. Namely, our plan is to implement in hardware the proposed master-slave synchronization scheme, which will be used in combination with an encryption algorithm to experimentally generate and recover the secret keys.

Data Availability

The data used to support the findings of this study are included within the article.

Conflicts of Interest

The authors declare that they have no conflicts of interest.

Acknowledgments

The author Adel Ouannas thanks the Directorate General for Scientific Research and Technological Development in Algeria who supported the research to be at hand.

References

[1] T. Abdeljawad, "On Riemann and Caputo fractional differences," *Computers & Mathematics with Applications*, vol. 62, no. 3, pp. 1602–1611, 2011.

[2] F. Atici and P. Eloe, "Initial value problems in discrete fractional calculus," *Proceedings of the American Mathematical Society*, vol. 137, no. 3, pp. 981–989, 2009.

[3] F. M. Atici and P. W. Eloe, "A transform method in discrete fractional calculus," *International Journal of Differential Equations*, vol. 2, pp. 165–176, 2007.

[4] D. Baleanu, G. C. Wu, Y. R. Bai, and F. L. Chen, "Stability analysis of Caputo-like discrete fractional systems," *Communications in Nonlinear Science and Numerical Simulation*, vol. 48, pp. 520–530, 2017.

[5] S. Bendoukha, A. Ouannas, X. Wang et al., "The co-existence of different synchronization types in fractional-order discrete-time chaotic systems with non–identical dimensions and orders," *Entropy*, vol. 20, no. 9, 2018.

[6] J. B. Diaz and T. J. Osler, "Differences of fractional order," *Mathematics of Computation*, vol. 28, no. 125, pp. 185–202, 1974.

[7] M. Edelman, E. E. Macau, and M. A. Sanjuan, Eds., *Chaotic, Fractional, and Complex Dynamics: New Insights and Perspectives*, Springer International Publishing, Berlin, Germany, 2018.

[8] C. Goodrich and A. C. Peterson, *Discrete Fractional Calculus*, Springer, Berlin, Germany, 2015.

[9] F. Hadjabi, A. Ouannas, N. Shawagfeh, A.-A. Khennaoui, and G. Grassi, "On two-dimensional fractional chaotic maps with symmetries," *Symmetry*, vol. 12, no. 5, p. 756, 2020.

[10] T. Hu, "Discrete chaos in fractional Henon map," *Applied Mathematics*, vol. 05, no. 15, pp. 2243–2248, 2014.

[11] L. Jouini, A. Ouannas, A. A. Khennaoui, X. Wang, G. Grassi, and V. T. Pham, "The fractional form of a new three-dimensional generalized Hénon map," *Advances in Difference Equations*, vol. 122, no. 1, 2019.

[12] A.-A. Khennaoui, A. Ouannas, S. Bendoukha, G. Grassi, R. P. Lozi, and V.-T. Pham, "On fractional-order discrete-time systems: chaos, stabilization and synchronization," *Chaos, Solitons & Fractals*, vol. 119, pp. 150–162, 2019.

[13] A. A. Khennaoui, A. Ouannas, S. Bendoukha et al., "Chaos, control, and synchronization in some fractional-order difference equations," *Advances in Difference Equations*, vol. 412, no. 1, pp. 1–23, 2019.

[14] Y. Li, C. Sun, H. Ling, A. Lu, and Y. Liu, "Oligopolies price game in fractional order system," *Chaos, Solitons & Fractals*, vol. 132, Article ID 109583, 2020.

[15] D. Mozyrska and E. Girejko, "Overview of fractional h-difference operators," in *Advances in Harmonic Analysis and Operator Theory*, pp. 253–268, Birkhuser, Basel, Switzerland, 2013.

[16] A. Ouannas, A. A. Khennaoui, S. Bendoukha, and G. Grassi, "On the dynamics and control of a fractional form of the discrete double scroll," *International Journal of Bifurcation and Chaos*, vol. 29, no. 06, 2019.

[17] A. Ouannas, A.-A. Khennaoui, G. Grassi, and S. Bendoukha, "On chaos in the fractional-order Grassi-Miller map and its control," *Journal of Computational and Applied Mathematics*, vol. 358, pp. 293–305, 2019.

[18] A. Ouannas, A.-A. Khennaoui, S. Momani et al., "A quadratic fractional map without equilibria: bifurcation, 0-1 test, complexity, entropy, and control," *Electronics*, vol. 9, no. 5, p. 748, 2020.

[19] A. Ouannas, A. A. Khennaoui, S. Momani, G. Grassi, and V. T. Pham, "Chaos and control of a three-dimensional fractional order discrete-time system with no equilibrium and its synchronization," *AIP Advances*, vol. 10, no. 4, 2020.

[20] A. Ouannas, A.-A. Khennaoui, Z. Odibat, V.-T. Pham, and G. Grassi, "On the dynamics, control and synchronization of fractional-order Ikeda map," *Chaos, Solitons & Fractals*, vol. 123, pp. 108–115, 2019.

[21] S. Pincus, "Approximate entropy (ApEn) as a complexity measure," *Chaos: An Interdisciplinary Journal of Nonlinear Science*, vol. 5, no. 1, pp. 110–117, 1995.

[22] P. Ostalczyk, *Discrete Fractional Calculus: Applications in Control and Image Processing*, World Scientific, Switzerland, 2016.

[23] M. K. Shukla and B. B. Sharma, "Investigation of chaos in fractional order generalized hyperchaotic Henon map," *AEU-International Journal of Electronics and Communications*, vol. 78, pp. 265–273, 2017.

[24] S. H. Strogatz, *Nonlinear Dynamics and Chaos with Student Solutions Manual: With Applications to Physics, Biology, Chemistry, and Engineering*, CRC Press, Boca Raton, FL, USA, 2018.

[25] G.-C. Wu and D. Baleanu, "Discrete chaos in fractional delayed logistic maps," *Nonlinear Dynamics*, vol. 80, no. 4, pp. 1697–1703, 2015.

[26] G.-C. Wu and D. Baleanu, "Discrete fractional logistic map and its chaos," *Nonlinear Dynamics*, vol. 75, no. 1-2, pp. 283–287, 2014.

[27] G.-C. Wu, D. Baleanu, and S.-D. Zeng, "Discrete chaos in fractional sine and standard maps," *Physics Letters A*, vol. 378, no. 5-6, pp. 484–487, 2014.

[28] A. Modiri and S. Mobayen, "Adaptive terminal sliding mode control scheme for synchronization of fractional-order uncertain chaotic systems," *ISA Transactions*, vol. 105, 2020.

[29] O. Mofid and S. Mobayen, "Adaptive synchronization of fractional-order quadratic chaotic flows with non hyperbolic equilibrium," *Journal of Vibration and Control*, vol. 24, no. 21, pp. 4971–4987, 2018.